OPTIMAL ENERGY DISPATCH OF ICE-HARVEST SYSTEM

OPTIMAL ENERGY DISPATCH OF INTEGRATED COMMUNITY ENERGY AND HARVESTING (ICE-HARVEST) SYSTEM

By ALIREZA LORESTANI, MSc

A Thesis Submitted to the School of Graduate Studies in Partial Fulfillment of the Requirements for the Degree PhD of Applied Science

McMaster University

PHD OF APPLIED SCIENCE (2023)

Hamilton, Ontario, Canada (Mechanical Engineering Department)

TITLE:	Optimal Energy Dispatch of Integrated Community Energy and Harvesting (ICE-HARVEST) System
AUTHOR:	Alireza Lorestani MSc (Electrical Engineering), Amirkabir University of Technology, Tehran, Iran
SUPERVISOR:	Dr. James S. Cotton, Dr. Mehdi Narimani
NUMBER OF PAGES:	xxii, 149

Lay Abstract

This dissertation aims to develop an energy management system for an integrated smart energy system, called integrated community energy and harvesting (ICE-Harvest). The ICE-Harvest system is envisioned as the future of energy systems for dense communities in cold climates. This system comprises a single-pipe variable-temperature micro-thermal network, a micro-electrical network, and distributed energy resources. The goal is to coordinate all the variables and assets so that the system's capabilities in harvesting waste energy to offset the community's thermal demands, performing demand management without affecting occupants' comfort, and realizing energy arbitrage are realized. For this aim, a hierarchical decision-making framework is developed in which three sequential layers are integrated. The three layers determine the long-term, short-term, and ultra-short-term optimal operation of the ICE-Harvest system. The layers are differentiated by their objective, planning horizon, time resolution, and optimization models.

Abstract

This dissertation presents a comprehensive investigation into the performance optimization of a smart energy system called the Integrated Community Energy and Harvesting (ICE-Harvest) system, designed to optimize energy utilization in dense communities in cold climates. This system comprises a single-pipe variable-temperature micro-thermal network, a micro-electrical network, and distributed energy resources such as combined heat and power units, boilers, heat pumps, short-term storage systems, and long-term storage system. The objective of this research is to develop an optimal operation strategy for the system, considering the coordination of its components to realize its full potential including achieving demand management while ensuring occupants' comfort, harvesting and sharing waste energy, and facilitating energy arbitrage and taking advantage of energy price fluctuations, among other benefits. For this aim, the study begins by formulating precise quasi-dynamic mathematical representations of the system, considering the physical and operational limitations to capture the system's intricacies. The resultant optimization problem is a mixed integer nonlinear programming model that commercial solvers could not solve. To make the nonlinear models more tractable and solvable, various mathematical techniques are employed to linearize them. It is worth noting that many of these formulations are original contributions to the field. Given the specific configuration of

the system with components requiring short-term and long-term operation scheduling and the large-scale nature of the optimization problem, a decomposition algorithm is proposed that breaks down the problem into three sequential layers: long-term, short-term, and ultra-short-term. Each layer addresses specific planning horizons, time resolutions, and optimization models, enabling effective optimization of the system's operation. The proposed optimization algorithm offers an effective framework for planning and optimizing ICE-Harvest operation at various time horizons and resolutions. It demonstrates the system's flexibility in performing waste energy harvesting and sharing, demand management, and dynamic switching between energy carriers based on real-time prices.

Dedication

This dissertation is dedicated to the following special people in my life:

To Elahe and Vania,

This dissertation is dedicated to you, both the anchors of my life and the driving forces behind my pursuit of knowledge. Your unwavering love, support, and belief in me have been my driving force. Elahe, your belief in my abilities and sacrifices have been the bedrock of my success. Vania, your presence in my life has brought immeasurable happiness and purpose. Your joy and curiosity have reminded me of the purpose behind my pursuit of knowledge. This dissertation is dedicated to both of you, my pillars of strength.

To my Parents,

I want to express my heartfelt appreciation to my parents. Your unconditional love, unwavering support, and constant encouragement have been the foundation of my achievements. You have sacrificed so much to provide me with the opportunities and resources necessary to pursue my dreams. I am forever grateful.

Acknowledgements

I would like to express my heartfelt gratitude to my supervisors, Dr. Cotton and Dr. Narimani. Your guidance and mentorship have been absolutely invaluable on my journey. Dr. Cotton, your critical and systematic approach throughout my Ph.D. has played a pivotal role in shaping the work into its current form. Your leadership and insightful suggestions have not only motivated me but also sparked fruitful discussions. And Dr. Narimani, I cannot thank you enough for your constant guidance and unwavering support. Without the mentorship of both of you, I would not have achieved the level of success I have attained today.

I would also like to extend my gratitude to my supervisory committee members, Dr. Emadi and Dr. Sirouspour, and my external examiner, Dr. Jose A. Romagnoli, for their valuable suggestions and comments.

A special mention goes to my dear friend, Jorge Chebeir. Your unwavering support, intellectual discussions, and friendship have been an immense source of strength throughout this challenging journey. Whenever I've asked for help, you've gone above and beyond to assist, making things easier for me. I will never forget you, "my bro".

And thank you to Mechanical Engineering Department administrators- Nicole, Diane, Lily, and Leslie - I am truly grateful for your prompt and dedicated assistance whenever I've reached out. You've made everything so much easier for all of us.

Table of Contents

Lay Abstract **iii**

Abstract **iv**

Dedication **vi**

Acknowledgements **vii**

Notation, Definitions, and Abbreviations **xv**

Declaration of Academic Achievement **xxiii**

1 Introduction **1**

1.1 Motivation and Background 1

1.2 Integrated Community Energy and Harvesting System 5

1.3 Energy Management System (EMS) 8

1.4 Research Contributions 9

2 Literature Review **13**

2.1 Literature Review 14

2.2 Summary 19

3 Day-ahead Scheduling of a Building Microgrid **23**

3.1 Mathematical Model 24

3.2 Simulation Studies and Discussions 32

3.3 Summary 35

4 Day-ahead Optimal Dispatch of ICE-Harvest System **37**

4.1 Mathematical Model 38

4.2 Optimization and Problem Decomposition 54

4.3 Simulation Studies and Discussions 60

4.4 Summary 77

5 Multi-objective Operation-Aware Optimal Design of ICE-Harvest System **80**

5.1 Mathematical Formulation 81

5.2 Optimization Problem 86

5.3 Simulation Studies and Discussions 91

5.4 Summary 95

6 Long-Term Operation Optimization of ICE-Harvest System **97**

6.1 Mathematical Model 98

6.2 Optimization 109

6.3 Simulation Studies and Discussions 113

6.4 Summary 128

7 Conclusion and Future Work **131**

7.1 Conclusion 131

7.2 Future Work 134

A Verificaiton Study **137**

List of Figures

1.1 ICE-Harvest Conceptual Outline 6

1.2 Micro-thermal Network in ICE-Harvest 7

1.3 Three Stage Decision Making Framework 11

3.1 Schematic Representation of the Thermal Section of the BMG. 24

3.2 Schematic Representation of the Electrical Section of the BMG. . . . 25

3.3 Optimal Operation of the BMG-Electrical Section 33

3.4 Optimal Operation of the BMG-Thermal Section. 34

3.5 Variation of Mass Flow Rates in the System 35

3.6 Temperature in Different Sections of the Main Loop. 36

4.1 Schematic Representation of the Micro-Thermal Network of ICE-Harvest. 38

4.2 Schematic Representation of the Micro-Electrical Network of ICE-Harvest. 39

4.3 Schematic Representation of CHP. 40

4.4 Schematic Representation of SHWT. 41

4.5 Schematic Representation of HEX. 44

4.6 Schematic Representation of Two Consecutive Branches (one segment). 45

4.7 Schematic Representation of CT. 50

4.8 Proposed Framework for the Decomposition of the Optimization Problem. 55

4.9 Plugin Electrical Demand, Heating Demand, Cooling Demand, and HEP. 61
4.10 Overall Performance of (a) Electrical and (b) Thermal DERs in EGC. 62
4.11 Thermal power flow in ICE-Harvest. 64
4.12 Breakdown of electrical loads in ICE-Harvest. 65
4.13 Flow of the harvested energy from the buildings in ICE-Harvest. . . . 66
4.14 Energy Arbitrage in ICE-Harvest 67
4.15 Temperatures and Mass Flow Rate in USPN Under Different Strategies 70
4.16 Electricity Demand of ICE-Harvest Under Different Optimal Dispatch Strategies. 74
4.17 Dumped Power in the CT in BAU vs. ICE-Harvest Under Different Dispatch Strategies. 75
5.1 Pareto front (top) and the corresponding capacities of the components (bottom) relative to the GHG emission level. 92
5.2 ICE-Harvest system's operation in each design day. 95
6.1 Schematic representation of the micro-thermal network of ICE-Harvest. 98
6.2 Schematic representation of the ETSs in a building 100
6.3 Schematic representation of the GBF. 103
6.4 3D plot for the fitted regression of GBF's COP 107
6.5 Instantaneous Energy Demands in ICE-Harvest System 114
6.6 Time-of-Use Electricity Price 115
6.7 The Cumulative Heating and Cooling Demands. 116
6.8 The Breakdown of Sources of Harvested Heat from Cooling Process . 117
6.9 The Breakdown of Utilization of Harvested Heat from Cooling Process. 118
6.10 Monthly Network Temperature Over the Year 119

6.11 Monthly Electrical Power of CHP 120
6.12 Monthly Surplus Heat Energy of CHP 121
6.13 Distribution of Electricity Consumption in the ICE-Harvest System . 121
6.14 Electricity Consumption Analysis of Cooling HPs Based on Time-of-Use 122
6.15 Breakdown of Energy Sources Contributing to GBF Charging 123
6.16 State-of Charge of the GBF 124
6.17 Distribution of Imported Power of ICE-Harvest System Vs. Business-as-Usual 125
6.18 Distribution of Electricity Generation of CHP 126
6.19 Imported Power and CHP Generation between ICE-Harvest and BAU 127
6.20 The Range of Network Temperature Variations Across the Scenarios . 128
6.21 CHP Power Generation across Price Ranges and Scenarios 129
6.22 Imported Power Variation across Price Ranges and Scenarios 129
A.1 Total Imported Electricity and Natural Gas of BAU Vs ICE-Harvest System 139
A.2 On-Peak Imported Electricity by BAU Vs ICE-Harvest System 140

List of Tables

2.1 Summary of studies on the operation of 5G-DESs in the literature . . 20

4.1 Comparison of Different Dispatch Strategies 68

4.2 Results of the Operating Strategies vs. BAU 76

5.1 Simulation Parameters 91

Notation, Definitions, and Abbreviations

Subscripts and Superscripts

act	actual
$HR2ST$	Recovered heat sent to the GBF
sc/sh	Supply cooling/heating
t	Time period
w	Water
MU	CT's make-up Water
$BD/E/DR$	Blow-down/Evaporation/drift water in CT
g	Distributed energy resources
WP	Water pump
WB	Wet bulb temperature

$elec$	Electrical or electricity
GBF	Geothermal borehole field
max/min	Maximum/Minimum
rec	Recovery
$loss$	Energy losses
Tot	Total
JW/EX	Jacket water/Exhaust gas
h/c	Hot or heating/Cold or cooling
mix	Mixing layer
CHP	Combined heat and power unit
$SHWT$	Stratified hot water tank
NGB	Natural gas boiler
BES	Battery energy storage
HEX	Heat exchanger
HP	Heat pump
$USPN$	Unidirectional single pipeline
ch/dch	Charging/Discharging
CT	Cooling tower

CW	Circulating water in CT's closed loop
PCC	Point of common coupling
$O\&M$	Operation and maintenance
imp/exp	Imported/Exported
rej	Injected heat from USPN to building for heating
Hrv	Harvested energy from cooling processes
amb	Ambient
ref	Refrigeration
$plugin$	Plugin load of building
$load$	load
Rng	Range
b	Set of branches
s	Set of segments
B	Set of building
BP	Bypass coefficient of flow rate

Simulation Parameters

$\Delta\tau$	Time step (hr)

a, b, c	CHP parameters
η_0	Reference efficiency
cp	Water's specific heat capacity (kWh/Kg°C)
k	Constant factor within [0,1]
β	Additional factor of thermal losses
ρ	Density (kg/m^3)
R^e	Soil thermal resistance
L	Pipeline length (m)
N^s	Number of segments in USPN
N^B	Number of buildings in USPN
N^{cycles}	Number of concentration cycles
d^{in}/d^{ex}	Internal/external pipeline diameter (m)
λ^b	Thermal conductivity of insulation material
λ^{exp}	Expansion rate of mixing layer in SHWT
ϵ	Effectiveness coefficient of HEX
$Cfan$	Fan coefficient (kW/m^3)
cf	Air to water factor (kg air/kg water)
Pr	Price

Ts	Building's supply temperature
ϕ	Phase angle
ΔT	Temperature difference (°C)
M	Water mass (kg)/ Big number
RR	Ramp rate coefficient

Simulation Variables

Pl	CHP's Partial load
η	CHP's electrical efficiency
F	Fuel consumption (kWh)
H/C	Heating/cooling power (kW)
P/Q	Active/reactive power (kW)
CS	Cost (CA$)
U	Binary variables for On/off state
SOC	State of charge (kWh)
POC	Inverse of COP
COP	Coefficient of performance
W	Volume of the water in each layer (m^3)

$\dot{m}$	Mass flow rate (kg/hr)
A	Auxiliary variable: $U \cdot \Delta T$
To/Ti	Outlet/inlet temperature (°C)
Tav	Average of temperatures in the pipeline (°C)
ΔPS	Pressure loss (kPa/m)
SU/SD	Start-up/shut-down state binary variable

Definitions

Challenge With respect to video games, a challenge is a set of goals presented to the player that they are tasks with completing; challenges can test a variety of player skills, including accuracy, logical reasoning, and creative problem solving

Abbreviations

5G-DES	5th-generation district energy systems
BAU	Business-as-usual
BES	Battery Energy Storage
BLTN	Bidirectional low-temperature network
BMG	Building microgrid

CHP	Combined heat and power
COP	Coefficient of performance
CT	Cooling tower
DER	Distributed energy resources
DES	District energy system
DHCN	District heating and cooling network
DRC	Direct cooling
DRH	Direct Heating
EGC	Energy generation center
EMS	Energy management system
ETS	Energy transfer station
GHG	Greenhouse gas emission
HEP	Hourly electricity price
HEX	Heat exchange
HP	Heat pump
GBF	Geothermal borehole field
ICE-Harvest	Integrated Community Energy and Harvesting
MILP	Mixed integer linear programming

MINLP	Mixed integer non-linear programming
NGB	Natural gas boiler
NGPP	Natural gas power plant
PCC	Point of common coupling
SHWT	Stratified hot water tank
USPN	Unidirectional single-pipe network
WP	Water pump

Declaration of Academic Achievement

I, Alireza Lorestani, hereby declare that the research presented in this Ph.D. thesis, titled Optimal Energy Dispatch of ICE-Harvest system, is my original work conducted at McMaster University under the supervision of Dr. Cotton and Dr. Narimani. This thesis has not been submitted for any other degree, and all sources used have been appropriately acknowledged. The experiments, analyses, and conclusions presented in this thesis adhere to rigorous scientific methods and ethical guidelines. I take full responsibility for the content of this work and understand the consequences of academic misconduct.

Chapter 1

Introduction

1.1 Motivation and Background

Concerns over climate change have driven a global effort to explore new effective energy provisions to decarbonize the energy sectors and curb greenhouse gas emissions (GHG). Building operations are estimated to account for 27% of all GHG emissions in 2021, according to the IEA [1]. A total of 8% of that was emitted directly by buildings, while 19% was from generating electricity and heat utilized in those structures. Aside from this, residential and non-residential buildings represented 21.2% and 8.8% of the final energy consumption in the same year, respectively. Therefore, holistic generation and demand-side management measures can significantly facilitate the reduction of emissions and the reduction of carbon emissions in the building sector.

Renewable energy technologies and integrating multiple energy carriers (electricity, heating, and cooling) have been considered promising to decarbonize the residential and commercial sectors and reduce GHG emissions. In this regard, wind, photovoltaic, and solar thermal, along with electrifying heating via electric boilers or

heat pumps (HPs), have been studied by many studies, and their advantages have been showcased [2].

A cold climate can, however, present challenges when it comes to utilizing renewable energy technologies, primarily because solar generation is out of phase with the heating demand. Furthermore, in these regions, the peak of electric heating demand during the winter can exceed five times that of the summer [3], posing significant challenges for the power grid in terms of balancing and flexibility. For example, in Ontario, Canada, wind power is curtailed for thousands of hours during the fall and spring seasons due to relatively low heating and cooling demands, while conventional natural gas power plants (NGPPs) are used as peaking power plants to respond to load fluctuations and renewable energy generator intermittency [4]. Furthermore, replacing an 80% efficient natural gas boiler (NGB) with an electric boiler simply because the electric boiler emits zero site emissions may increase the region's emissions if the electric boiler uses NGPP's electricity. Therefore, electrification of heating may not only fail to offset emissions in this case but may increase them. These examples emphasize the importance of holistic measures in optimizing building sector energy management, considering regional rather than local emissions in analyses.

Harvesting waste heat has always been one of the cornerstones of decarbonizing heating and cooling. An NGPP converts 42% of natural gas heating value into electricity, and the rest is wasted [3]. This waste energy in Ontario, Canada, is more than 10 TWh, accounting for 5% of the total natural gas used for heating loads in the province [3]. Decentralized combined heat and power (CHP) units can capture this high-grade heat and facilitate optimal energy management by integrating the electricity and thermal sectors, which will reduce GHG emissions.

A further area of harvesting waste heat that has yet to be fully explored is capturing and utilizing thermal energy from cooling processes normally wasted in communities via cooling towers (CTs). It is estimated that 21 TWh of thermal energy was wasted in the cooling processes of data centers, grocery stores, and other community buildings in Ontario, Canada, in 2017 [5]. Harvesting this waste energy can offset the building's or surrounding buildings' heating demand, resulting in significant reductions in GHG emissions and energy consumption.

The most recent technology in this direction is 5th-generation district energy systems (5G-DESs). 5G-DES puts forward two new concepts: first, the buildings can provide thermal energy to their communities by harvesting and sharing their residual energy, and second, cooling and heating demands have mutual benefits [6].

In 5G-DESs, the heating supply temperature is typically lower than the buildings' heating requirements, and the cooling supply temperature is usually higher than the cooling requirements. Water-source HPs and chillers are needed to obtain appropriate temperatures for heating and cooling. Using water-based HPs and chillers results in partial electrification of heating and cooling as well.

5G-DESs can have one or two pipelines instead of four, as in conventional DESs. The single-pipeline network is usually called a unidirectional single-pipe network (USPN) and consists of a single pipeline connecting community buildings in series. The cooling demand in a building is met by water flowing from the network to the chiller, and the warmed water is returned to the pipeline. To meet the heating demand, water flows to the HP, and the cooled water is returned to the pipeline. A two-pipeline system is comprised of a warm and a cold pipeline. Cooling and heating processes are accomplished similarly to USPNs, with the exception that HPs and

chillers of the buildings are connected to separate pipelines [7]. The two-pipeline system is sometimes called a bidirectional thermal network (BDTN).

5G-DESs have lower heat losses and higher efficiency. Thus, they are anticipated to be the future energy systems, while their adoption entails an in-depth analysis focusing on economic feasibility and environmental concerns. One of the challenges with 5G-DESs is that they use significantly more electricity than conventional DESs. However, 5G-DESs, especially USPNs, can be designed so that in each building, the HP and the chiller are paralleled with a heat exchanger (HEX). As a result, if the network temperature is higher than the supply heating temperature, direct heating (DRH) can be enabled through the HEX, or if the network temperature is lower, direct cooling (DRC) can be enabled by bypassing the chiller. This allows for arbitrage between different energy sources so that the high electricity consumption of USPNs can be managed during peak and off-peak hours.

Recent state-of-the-art studies have conceptualized the future energy systems as decentralized low-temperature micro-thermal networks coupled to micro-electrical networks and on-site distributed energy resources (DERs). These systems are called smart energy systems and are controlled by intelligent central controllers coordinating supplies and demands so that costs and/or carbon emissions are minimized [8]. Their micro-thermal networks are constituted by the 5G-DESs, so the heat losses are reduced, and the residual/wasted heat of the cooling processes is harvested to offset the thermal demand of the building or surrounding buildings. [9].

The main objective of this study is to investigate these capabilities for a smart energy system equipped with a USPN, named Integrated Community Energy and

Harvesting (ICE-Harvest) System system. For this aim, an energy management system (EMS) for ICE-Harvest is developed to administrate the system and determine the real-time optimal operating set-points for downstream controllers so that the system's performance aligns with desired results.

1.2 Integrated Community Energy and Harvesting System

ICE-Harvest project is a collaborative research project between academia and industry, aiming to minimize GHG emissions in the energy sector while maximizing energy efficiency[10]. The conceptual outline of the ICE-Harvest system is illustrated in Fig.1.1. The system is envisioned as the next generation of district heating and cooling networks (DHCNs) for service-dense community areas, such as institutional campuses or downtown cores, especially in colder climates with massive heating demand [11]. The ICE-Harvest system comprises an energy generation center (EGC), a micro-thermal network, and a micro-electrical network. In the EGC, electrical and thermal DERs are placed. The (USPN)comprises a group of buildings as well as a centralized CT. The micro-electrical network constitutes the electrical section of the system, including the distribution network and loads.

DERs are a battery energy storage (BES), a CHP, a stratified hot water tank (SHWT), an NGB, and a geothermal borehole field (GBF). In the EGC, the thermal DERs are connected in series to an HEX via a high-temperature header (see Fig.1.2). The GBF is also connected to a mid-temperature header, linked to the high-temperature header via an HP. In EGC, CHP and NGB provide means of responding

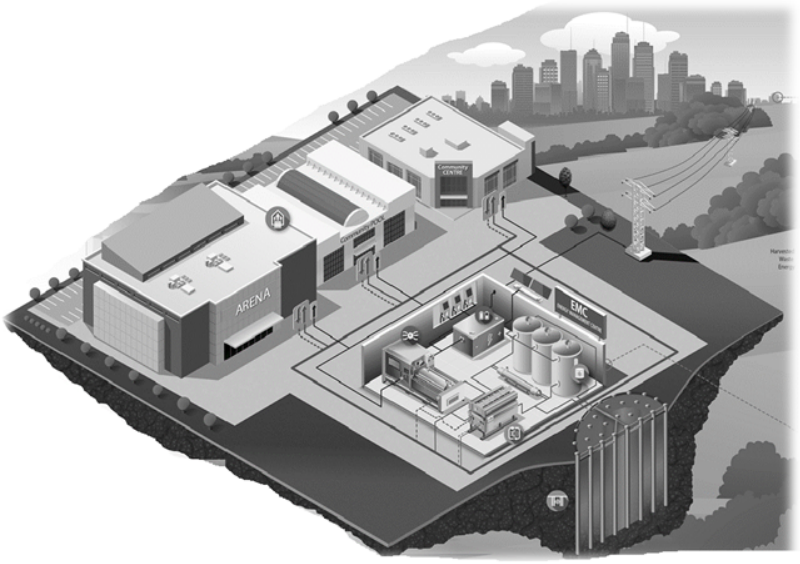

Figure 1.1: ICE-Harvest Conceptual Outline

to real-time electricity and natural gas prices and arbitraging between them. CHP can offset peak-time fossil fuel power plants while recovering thermal energy usually wasted. The GBF, as the long-term energy storage, and SHWT and BES, as short-term thermal energy storage systems, are utilized simultaneously. SHWT and BES aim to alleviate the daily mismatch between the energy generations and demands, whereas GBF deals with seasonal variability by storing excess thermal energy during the summer and spring and releasing it during the winter and fall.

In the USPN, a group of buildings, as well as a centralized CT, are connected in series to the HEX via the pipeline. Each building has one heating energy transfer station (ETS) and one cooling ETS, each constituting a HEX and an HP (or chiller). HPs that electrify the thermal demand in the USPN help harvest the residual/wasted heat of the cooling processes to offset the thermal demand of the building or surrounding buildings. HEXs at the buildings facilitate direct heating (DRH) or direct cooling (DRC) by bypassing the HPs. That is, if the network temperature is higher than the

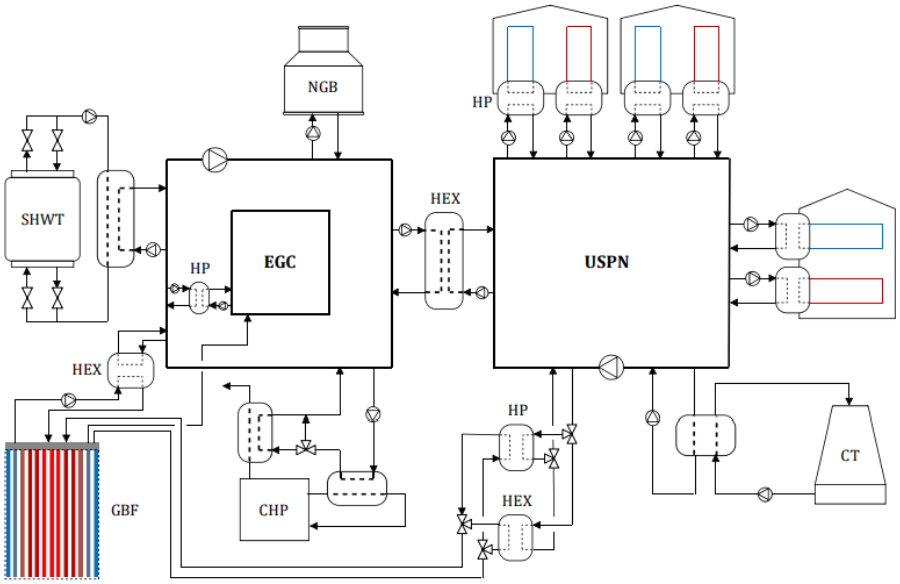

Figure 1.2: Schematic Representation of the Micro-thermal Network of the ICE-Harvest System

supply heating temperature, DRH is carried out through the HEX, or if the network temperature is lower, DRC is realized by bypassing the chiller. There is also a path that connects the USPN to the GBF so that the excessively harvested energy can be stored in the GBF.

In the micro-electrical network, two general categories of electrical loads can be defined: controllable and uncontrollable. The first one includes plugin loads and air conditioning of the buildings, and the latter one consists of HPs, water pumps (WPs), and the CT. The controllable loads and the CHP tie the micro-thermal and micro-electrical networks and facilitate the energy arbitrage and demand management in the system.

It is anticipated that the ICE-Harvest system operation can benefit the upstream power network by minimizing the curtailment of renewable energies. This can be realized since, in ICE-Harvest, the thermal and electrical sectors are interconnected

through CHP, HPs, and chillers, allowing for managing electrical and thermal loads simultaneously. For instance, during surplus-based load generation in the grid, ICE-Harvest can potentially come into play and levelize its electricity consumption. It can consume less/zero natural gas and more electricity to meet its onsite thermal demands. On the other hand, during peak hours when 40% efficient NGPPs are utilized, ICE-Harvest, by manipulating the USPN's temperature and reducing its electricity demand along with utilizing onsite BES and CHP with more than 65% efficiency, can minimize its electricity import from the grid to zero. These features not only decrease/eliminate the curtailment of renewable energies but also mitigate GHG emissions and contribute to reducing the penetration of natural gas-fired power plants in the power grid.

1.3 Energy Management System (EMS)

EMS is a decision-making tool that supervises the system by determining the optimal operating setpoints for local controllers. To determine these setpoints, EMS solves an optimization problem in which the system is modeled as a set of constraints. This model is a quasi-steady-state representation of the system at each discrete time step. The results of this optimization problem are the optimal setpoints (dispatch) of every single component by which the system's operation aligns with what would be desired.

This optimization problem is generally subject to equality constraints (such as g) and inequality constraints (such as h), which must be satisfied. Additionally, there is a set of dynamic equation (such as $Z_{t+1} = m$) that relates the variables at time t to

the variables at time $t+1$, as illustrated below:

$$min : \sum_{t} F(X_t, Z_t, U_t, P_t) \tag{1.3.1}$$

$$g(X_t, Z_t, U_t, P_t) = 0 \tag{1.3.2}$$

$$h(X_t, Z_t, U_t, P_t) \leq 0 \tag{1.3.3}$$

$$Z_{t+1} = m(X_t, Z_t, U_t, P_t) \tag{1.3.4}$$

where X_t, Z_t, U_t, and P_t represent different sets of parameters or variables involved in the problem. The objective is to find values for these variables that minimize the objective function while satisfying the given constraints and dynamic equation.

1.4 Research Contributions

This dissertation contributes to the field by conducting a thorough exploration of the optimization and performance analysis of the ICE-Harvest system. It delves into the intricate details of the system by considering all the nonlinear physical and practical limitations, offering a more profound understanding of the system. In pursuit of this goal, an optimized operational strategy that represents the EMS of the ICE-Harvest system is developed to effectively coordinate the system's components, enabling the realization of its full potential in various aspects. It is worth noting that many of these formulations are original contributions to the field.

The following research questions are addressed in this study:

- What benefits are achieved by a non-convex variable-temperature variable-flow rate model compared to simpler models?

- How short-term and long-term energy storage systems be utilized simultaneously to alleviate the daily and seasonal energy mismatch?
- How can energy harvesting and sharing be optimized?
- How can energy arbitrage between natural gas and electricity from the grid be realized within the framework of an integrated energy system?
- What is the impact of dispatch strategies on energy harvesting and sharing and the economics of the system?
- How is thermal and electrical power switching practiced in the HPs in accordance with the real-time energy carriers' prices?
- How does the thermal storage capacity of the network contribute to the heating and cooling demand balancing and economics of the system?

1.4.1 Methodological Approach: Hierarchical Decision-Making Framework

A novel quasi-dynamic model for optimal dispatch of ICE-Harvest is put forward, taking all the thermal and electrical characteristics into account. The proposed optimal dispatch model is a variable-temperature variable-flow rate model accounting for heat transfer, hydraulics constraints, and thermal mass of the pipeline. Moreover, the constraints associated with the micro-electrical network, such as power flow equations, part-load limitations and efficiencies, and ramping of DERs, are included in the optimization model.

These formulations capture the system's intricacies and are the foundation for the EMS. The resultant optimization problem is a mixed integer nonlinear programming model that commercial solvers could not solve. To make the nonlinear models more tractable and solvable, various mathematical techniques are employed to linearize them.

Given the specific configuration of the system with components requiring short-term and long-term operation scheduling and the large-scale nature of the optimization problem, the optimization model is decomposed into three sequential layers, as illustrated in Fig. 1.3. . In the second layer, using the operation state of seasonal

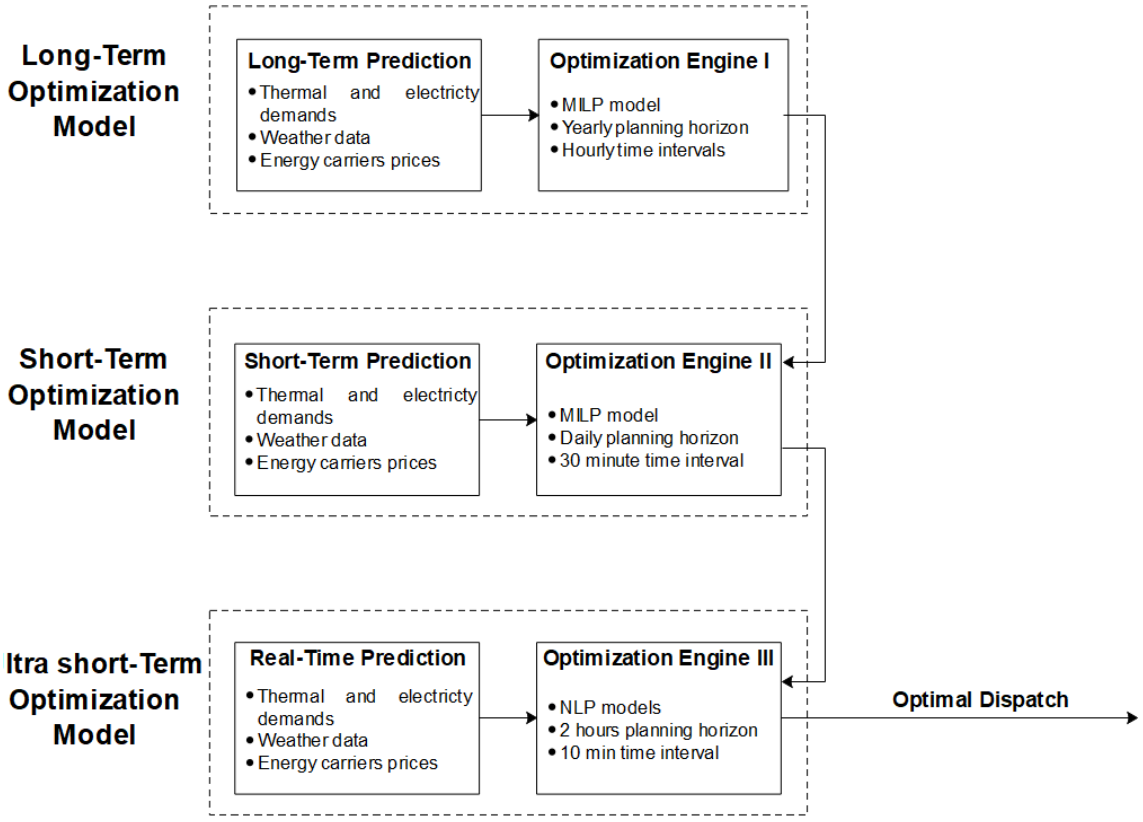

Figure 1.3: Three Stage Decision Making Framework Proposed for the ICE-Harvest System's Operation Optimization

storage as an input, the optimal operating state of CHP, SHWT, and NGB and the direction of the power transaction with the grid are determined. The scheduling horizon is daily, and the time stamp is 30 minutes. After all, in the real-time or ultra-short-term stage, the optimal dispatch of all the components is determined.

In the first layer, a year-ahead variable temperature-based optimization problem is developed for the ICE-Harvest system. The time resolution of the problem is one-hour, while this granularity is not suitable for changing the charging/discharging operation state of the GBF. As a result, the GBF's power can fluctuate hourly while its operational state remains fixed throughout the day. This layer is primarily responsible for determining the daily charging/discharging state of the GBF. Furthermore, the values obtained for other variables, such as network temperature and output powers of DERs, are utilized as starting points for the second layer.

Moving onto the second layer, this optimization model is employed for day-ahead operation planning of the system, and the time stamp is 30 minutes. This model is a linear relaxation of the original problem and takes the operating state of the GBF for the simulation day from the first layer. The main objective is to determine the binary variables representing the operational states of the remaining DERs for the upcoming day. The optimization model in this layer accounts for variable temperature and variable-flowrate considerations.

Taking the binary variables and the starting point from the first and second layers, this layer determines the optimal dispatch for the ICE-Harvest. This optimization model is nonlinear and includes all model details and non-linearities.

Chapter 2

Literature Review

In North America, residential and commercial buildings comprise a significant amount of the total energy consumption. In the United States, these sectors account for roughly 40% of total energy consumption [12]; in Canada, they account for approximately 26% of the total end-use demand[13]. Recent studies have enlightened the potentiality of integrating district energy systems (DESs) with electrical grids to achieve mutual benefits and an optimal solution for overall energy consumption [14, 15].

In this regard, some studies have showcased the opportunities in energy-saving and electrical load profile alteration in DESs by integration of heat pumps (HPs) [16, 17] and electric boilers [18]. The utilization of surplus renewable energy generated in the electrical grid for heating purposes [19, 2] and high-efficiency energy provisioning units such as combined heat and power (CHP) units have also been explored [20–22].

Although these solutions provide a more effective method of managing energy demands, conventional DESs have certain inherent drawbacks which cannot be alleviated simply by them. For instance, distribution temperature in conventional DESs is high for heating and low for cooling, which leads to increased energy losses to the

surroundings [23]. Further, they cannot harvest waste heat from cooling processes [24]. In addition, their long pipelines limit the system's flexibility and controllability. To overcome these limitations, redesigning the conventional structure of energy systems is indispensable [25].

2.1 Literature Review

Recent state-of-the-art studies have conceptualized the future energy systems as decentralized low-temperature micro-thermal networks coupled to micro-electrical networks and on-site distributed energy resources (DERs). These smart energy systems are controlled by intelligent central controllers coordinating on-site supplies and demands so that costs and/or carbon emissions are minimized [8].

Micro-thermal networks are analogous to the concept of microgrids but in thermal systems. A microgrid is a localized energy system that integrates various DERs and enables the generation, distribution, and consumption of electricity in a smaller, localized area. It operates autonomously or in conjunction with the main grid, allowing for enhanced energy management and resilience. The smart energy system complements the electrical aspect of a microgrid by providing heating and cooling services by the micro-thermal network. In a microgrid scenario, while the electrical grid handles the supply and demand of electricity, the micro-thermal network manages the thermal energy requirements of the buildings or facilities within the smart energy system. Integrating electrical and thermal systems creates a comprehensive and efficient energy infrastructure.

Micro-thermal networks are constituted by the fifth generation of DESs (5G-DESs)

that runs near ambient temperature. As a result, heat losses are reduced, and low-temperature renewable energy sources are better incorporated [26]. Another key advantage of micro-thermal networks is they are electrified which provides the opportunity for energy optimization and synergistic operation. By coordinating the generation and utilization of electricity and thermal energy at a local level, the energy system can achieve a higher level of energy efficiency and reduce reliance on external energy sources. Moreover, each building has one heating and one cooling HP (or chiller), which helps harvest the residual/wasted heat of the cooling processes to offset the thermal demand of the building or surrounding buildings. [9].

5G-DESs can have two or one pipelines, unlike the conventional DESs with four pipelines. The two-pipeline network, usually called bidirectional low-temperature network (BLTN), includes a warm pipeline, operating in the range of 12-20°C, and a cold pipeline running within 8-12°C [7]. In the case of cooling demand in a building, water is guided from the cold pipeline to the heating HP, and the outlet warmed water is sent to the warm pipeline. Water flows opposite from the warm pipeline to the cold pipeline through the heating HP when heating is required. External low-temperature sources such as solar thermal panels, storage systems, or central HPs may be needed to balance the energy in the micro-thermal network. The one-pipeline variable-temperature micro-thermal networks are called unidirectional single pipe networks (USPNs). Energy harvesting and sharing in USPNs are similar to BLTNs, except that heating and cooling HPs of the buildings are connected to the same pipeline with variable temperature (10-60°C), and both warmed and cooled waters are discharged into the same pipeline [7].

Recent studies suggest that buildings will become decentralized thermal prosumers

by providing thermal energy from their DERs to DESs [27–29]. In this regard, 5G-DESs construct a foundation for a new type of thermal prosumers that buildings can contribute to balancing cooling and heating loads in the network by harvesting and sharing the residual energy without needing any DERs [6]. Another fundamental improvement is their higher exergy efficiency thanks to lower distribution losses and waste energy harvesting [30]. There is, however, still a lack of understanding of how to manage multiple variables to realize the full potential of 5G-DESs [31].

[32] has demonstrated the potential of USPNs to reduce GHG emissions. However, it has also shown that they can consume significantly more electricity than conventional business-as-usual (BAU) DESs because of the electrification of thermal demands [33]. [34] has studied the significance of the network temperature on the electricity demand of SESs equipped with BLTN and highlighted the necessity of studies devoted to network temperature optimization. [35] has illustrated the substantial impacts of the network temperature on energy harvesting and electricity consumption of the USPN. Furthermore, it has been depicted in [5] that excessive energy harvesting is likely in USPNs without proper temperature optimization and simultaneous heating and cooling demands. That means electricity is consumed in the cooling HP to provide the cooling demand and harvest the energy, and further electricity must be consumed to dump that harvested energy.

Optimizing 5G-DESs is a complex task because there are many competing factors involved. There have been only a few studies conducted so far in the literature on the optimization of 5G-DESs, the majority of which are based on energy balance analyses or predefined network temperatures [36, 37]. In this regard, [38] has proposed a linear model for the design and operation optimization of BLTNs equipped with DERs using

energy balance equations. The network temperature has not been modeled in [38], and predefined average coefficients of performance (COPs) have been assumed for HPs. Although [38] provided good insights into improving the smart energy system's performance, it highlighted the necessity of developing models considering mass flow and dynamic temperatures for future studies. In [39], an optimal operation and design methodology has been proposed for DERs connected to a BLTN. A linear optimization model has been described based on a predefined operating network temperature assumption for this aim. For future works, it was suggested that the optimal network temperature should be determined through optimization.

[40] has proposed an operation optimization for SESs with BLTN that considers network temperature as a variable and some nonlinearities in the physical system. The optimization problem was then relaxed by using a linear approximation for the COPs of the HPs and fixed profiles for mass flow rates in the branches of the BLTN. However, the linear relaxation used for the COPs is suitable only for low-temperature variations at the evaporator and will cause significant errors for large temperature fluctuations. Furthermore, using fixed profiles for the mass flow rates and not optimizing the mass flow rates and temperatures simultaneously based on the real-time demand can result in underestimating the capability and benefits of the system. Because if the mass flow rate of an HP in a branch is assumed to remain fixed, the temperature variances between the inlet and outlet of the HP will follow its injected/rejected thermal power. As a result, the operation optimization and the network temperature are severely constrained. Furthermore, the results of the [40] are limited to the condition that there is a balance between the rejected and injected energy in the network. However, it is envisioned that the total injected heat to the network can be higher/lower than

the demand, which implies that the network can be a thermal storage system. This can be realized thanks to the short pipeline length and low thermal mass of the micro-thermal network that allows for the mass flow rate and temperatures to be manipulated to benefit the system.

5G-DESs, especially USPNs, can be designed so that each building has an HP and a chiller paralleled with heat exchangers (HEXs). As a result, if the network temperature is higher than the supply heating temperature, direct heating (DRH) can be enabled through the HEX, or if the network temperature is lower, direct cooling (DRC) can be enabled by bypassing the chiller. However, although DRC is possible for the cold pipeline in BDTNs, they do not support DRH as the temperature for the hot pipeline is consistently maintained below 40°C.

In none of the studies mentioned above, DRH or DRC have been incorporated into the optimization models. [41] has proposed a mathematical model for temperature optimization of a BDTN considering DRC. The results demonstrated that if HEXs for DRC are available, the optimal network temperature allows the cold pipeline to cool the building directly. Consequently, BDTN has less excess harvested energy to dissipate during the summer when DRC is considered. In the mathematical model, the temperature is an optimization variable, but the temperature variances, gains, or losses throughout the pipeline are negligible. So, all the heating HPs have the same COP, as do all the cooling HPs.

For BLTNs, this assumption may be reasonable, but not for USPNs, since it can lead to an underestimation of total electricity demand. For instance, in cold climates with heating demand dominating cooling demand, USPN temperatures decrease after each building. This leads to lower COPs of subsequent heating HPs and higher

electricity demands. When cooling demand dominates heating demand in buildings, USPN temperature rises after each building. This results in lower COPs of the following cooling HPs and higher electricity demands. In addition, as we move further down the network or consider temperature losses to or gains from the surroundings, this approach's underestimation of electricity demand can increase. Furthermore, the effects of buildings' sizes, arrangements, and locations within the USPNs on the network temperature are overlooked. Furthermore, while the thermal storage capacity of the network has been included in the optimization model, the thermal and hydraulic constraints are not, resulting in an overestimation of its benefits [42].

In addition to the challenges and advantages associated with 5G-DESs, it is crucial to accurately model the performance of HPs within these systems, specifically considering the COP saturation. Surprisingly, previous studies have neglected the modeling of COP saturation in their models, which is a critical aspect for accurately assessing the energy efficiency and overall performance of the systems. Implementing COP saturation in HP models is highly nonlinear, posing challenges for system optimization and control. However, in this research, a novel mathematical model is developed that effectively linearizes the COP saturation, enabling more accurate predictions of HP performance and facilitating optimal system design and operation.

2.2 Summary

A summary of the studies on the operation of smart energy systems with 5G-DESs is presented in Table2.1. As observed, the studies that have implemented temperature optimization have only focused on BLTNs. The BLTNs and USPNs are fairly distinct, and the developed models and the gained insights from BLTNs operation cannot be

Table 2.1: Summary of studies on the operation of 5G-DESs in the literature

Ref.	USPN BLTN	Temperature Optimization	Flow Rate Optimization	DRC/DRH	COP Saturation	Pipeline Storage Capacity	Building's Location	Temperature/Heat Losses	Demand Management	Energy Arbitrage
[9]	*BLTN*	–	–	–	–	–	✓	✓	–	–
[29]	–	–	–	–	–	–	✓	✓	–	–
[30]	–	–	–	–	–	✓	✓	✓	–	–
[31]	–	✓	–	–	–	–	–	✓	–	–
[32]	*USPN*	–	–	–	–	✓	✓	✓	–	–
[35]	*USPN*	–	–	–	–	–	✓	–	–	–
[34]	*BLTN*	✓	–	–	–	–	✓	✓	✓	–
–										
[43]	*USPN*	–	–	–	–	✓	✓	✓	–	–
[38]	*BLTN*	–	–	–	–	–	–	*Heat*	–	–
[39]	*BLTN*	–	–	–	–	–	–	*Heat*	–	–
[40]	*BLTN*	✓	–	–	–	–	✓	✓	–	–
[36]	*BLTN*	–	–	*DRC*	–	✓	–	*Heat*	✓	–
[41]	*BLTN*	✓	–	–	–	✓	–	*Heat*	✓	–
This Study	*USPN*	✓	✓	✓	✓	✓	✓	✓	✓	✓

easily extended to the USPNs [34]. USPNs have higher temperature fluctuation and optimization capabilities, making them a great fit for cold or warm climate conditions [32]. Thus, further studies are necessary to identify and explore the potential opportunities of SESs with USPNs. setspace

Micro-thermal network modeling based on variable temperature and variable flow rate, while considering the physical system limits, can demonstrate the significant, yet realistic capabilities of 5G-DESs. Optimizing the network's temperatures and mass flow rates can improve energy harvesting and sharing and reduce total electricity consumption. This also means performing demand-side management by optimizing network variables rather than adjusting indoor temperatures and compromising occupant comfort.

Natural gas-fueled heat sources, such as CHPs and natural gas boilers (NGB), can

be integrated with the USPN through a high-temperature loop connected via a HEX [43]. By integrating these sources, the system can respond to real-time electricity and natural gas prices and arbitrage between the two. In this regard, the system can maximize its electricity consumption during off-peak hours to take advantage of zero or negative pricing and switch to natural gas during peak hours to minimize electricity imports. To our knowledge, this study is the first to investigate these aspects of smart energy systems with micro-thermal networks, specifically with USPNs.

However, it has also been anticipated that, in summer, there might be no need for all the thermal power recovered by CHP. Additionally, a significant amount of thermal energy will be injected into USPN from the chillers, exceeding the heating demand. These two forms of surplus energy can increase the network temperature, reduce the COPs of chillers, and exacerbate the situation. So, an energy storage solution can be utilized to alleviate seasonal imbalances in the systems. This can save the excess energy captured from cooling processes during the summer and surplus thermal power recovered from CHP for the cold months.

In this regard, it is suggested that long-term energy storage, such as a geothermal borehole field (GBF), and short-term thermal energy storage, such as a stratified hot water tank (SHWT), can be utilized simultaneously. SHWT aims to alleviate the daily mismatch between thermal energy generation and heat demand, whereas GBF deals with seasonal variability by storing excess thermal energy during the summer and releasing it during the winter. For this aim, it is necessary to develop a long-term optimization model for ICE-Harvest to fully capture short-term and seasonal dynamics since the simple representative day approach cannot reflect the interaction between the short-term and long-term periods. This, however, complicates the optimization

problem development and intensifies computational load.

There have been no studies that have developed USPN operation optimization in light of DRC and DRH, leaving a research gap in exploring the full potential of USPNs. In contrast to BDTNs, USPNs are expected to be capable of both DRC and DRH since there is no strict limit on the pipeline's temperature. As a result, USPNs are ideal for regions with cold winters and warm summers, such as Ontario, Canada [32, 35], and that is the reason ICE-Harvest is designed based upon USPNs. The DRC and DRH add more degrees of freedom in operation optimization, which affect not only energy harvesting and sharing but also total electricity consumption in the system. When heating demand dominates cooling demand, raising the temperature and DRH can reduce total electricity demand. In contrast, when cooling demand dominates the heating demand, decreasing the temperature and DRC can reduce harvesting energy and minimize excess harvest energy and electricity demand. This can be viewed as providing demand response solutions without adversely affecting occupant comfort, as the temperature variations occur in the network pipeline, not the building supply temperature. On the other hand, it is envisioned that the flexibility of UPSNs in temperature manipulation can be used to maximize the electricity demand during off-peak hours to take advantage of zero or negative pricing when surplus RE is generated. This represents them as a grid modernization solutions provider that can use free surplus RE that would otherwise be curtailed [44, 3, 43].

Chapter 3

Day-ahead Scheduling of a Building Microgrid

In this chapter, a day-ahead operation scheduling of a building microgrid (BMG) represented by electrical and thermal loads coupled with the energy generation center (EGC) is studied. The BMG can be viewed as a simplified version of the ICE-Harvest system. All the components, including heat exchangers (HEXs), water pumps, battery energy storage (BES), combined heat and power (CHP) unit, stratified hot water tank, backup boiler, and heat pump (HP), are modeled in detail. The electrical and thermal sections of the BMG are integrated through the coupled use of the CHP unit, HP, and water pumps. This integration provides the capability of manipulating thermal variables such as temperatures and mass flow rates in such a manner that the total electricity demand follows the desired profile and both electrical and thermal loads of customers are fully met. The objective is to showcase the competence of the developed operation strategy in levelizing loads through integrating thermal and electrical sections of a BMG by taking advantage of CHP, HP, and the hot water

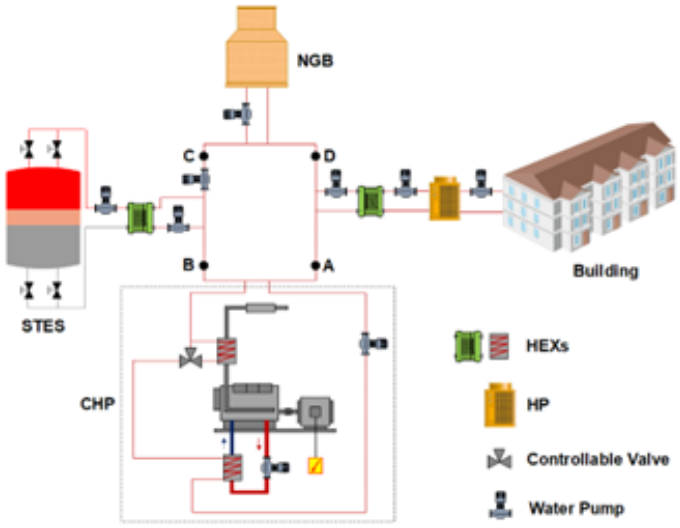

Figure 3.1: Schematic Representation of the Thermal Section of the BMG.

tank.

3.1 Mathematical Model

The BMG's structure encompasses two main sections; thermal and electrical. The configuration of the thermal section is constituted by a CHP unit, a backup natural gas boiler (NGB), a stratified hot water tank (SHWT), HP, HEX, water pumps, and a pipeline network (see Fig. 3.1). The electrical section of the BMG is composed of the CHP unit, BES, the point of common coupling (PCC), and the different electrical loads (see Fig. 3.2). The Electrical loads in the BMG can be split into two categories; controllable and uncontrollable. The first one encompasses electricity demanded by the HP and water pumps, and the latter one includes loads related to occupants, such as lighting, plug loads, etc. Regarding thermal load, through HP, a controllable portion of the load is satisfied by electricity and the rest by heat coming from CHP,

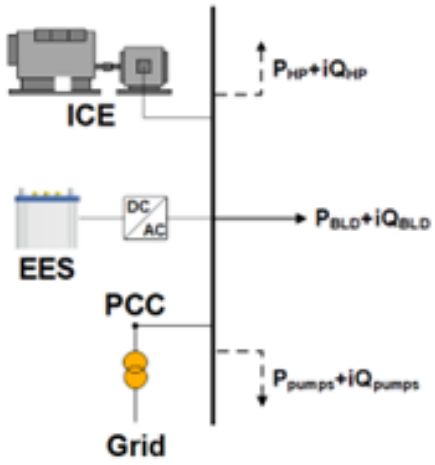

Figure 3.2: Schematic Representation of the Electrical Section of the BMG.

STES, or NGB. Therefore, it could be mentioned that the profiles of thermal and electrical loads are managed while the consumers' demands are fully met and their comfort is fully satisfied. The optimization problem representing the operation of the BMG is modeled as a mixed integer non-linear programming (MINLP) model. In this regard, some terms are linearized to simplify the optimization problem. Hereafter, a detailed description of this model is presented.

3.1.1 Electrical and Thermal Power Balance

The following equations correspond to the global power balance in the thermal and electrical sections.

$$H_t^{CHP} + H_t^{NGB} + H_t^{SHWT} \leq H_t^{HEX} \quad \forall t \in T \tag{3.1.1}$$

$$P_t^{CHP} + P_t^{PCC} + P_t^{BES} = P_t^{load} \quad \forall t \in T \tag{3.1.2}$$

$$P_t^{load} = P_t^{plugin} + P_t^{HP} + P_t^{WP} \quad \forall t \in T \tag{3.1.3}$$

3.1.2 Temperature and Mass Flow Rate Limits

The following equations summarize the temperatures and mass flow rates limitations of the components in the thermal section of the BMG :

$$\dot{m}_t^{loop} > \dot{m}_{s,t} \quad \forall t \in T \tag{3.1.4}$$

$$\dot{m}_{min}^{loop} \leq \dot{m}_t^{loop} \leq \dot{m}_{max}^{loop} \quad \forall t \in T \tag{3.1.5}$$

$$\dot{m}_{min} \leq \dot{m}_t^s \leq \dot{m}_{max} \quad \forall t \in T \tag{3.1.6}$$

$$To_{min}^s \leq To_{s,t} \leq To_{max}^s \quad \forall t \in T, s \in S \tag{3.1.7}$$

$$Ti_{min}^s \leq Ti_t \leq Ti_{max}^s \quad \forall t \in T, s \in S \tag{3.1.8}$$

where S represents the set of all components in the thermal network, including CHP, NGB, SHWT, HP, and HEXs. $\dot{m}_t^{loop}$ signifies the mass flow rate of the main loop, and $\dot{m}_{s,t}$ represents the mass flow rates of the components.

To consider the dynamics in the system, the variation of $\dot{m}_{t,s}$, $T_{t,s}$, $Ti_{t,s}$, and $To_{t,s}$ as well as P_t^{CHP}, P_t^{BES}, Q_t^{CHP}, Q_t^{NGB}, Q_t^{STES} indicated by Γ in 3.1.9 that must be within specific limits.

$$|\Gamma_t - \Gamma_{t-1}| \leq R_{max} \quad \forall t \in T \tag{3.1.9}$$

3.1.3 Mixing Fluids with Different Temperature

For incompressible fluids, when different branches run into the same node, the temperature of the mixed fluid is calculated using the energy conservation principle. Eq. 3.1.10 is applied to CHP, STES, NGB, and HEX.

$$(\dot{m}_t^{loop} - \dot{m}_{s,t}) \cdot Ti_{s,t} + \dot{m}_{s,t}^s \cdot To_{s,t} = \dot{m}_t^{loop} \cdot Ti_{s+1,t} \quad \forall t \in T, s \in S \tag{3.1.10}$$

3.1.4 CHP and NGB

Two heat recovery loops have been assumed in the CHP through jacket water and exhaust gas HEXs. Additionally, a controllable valve is in the way of the exhaust gas HEX to increase the level of freedom in the CHP control. Then, the output thermal power of CHP is calculated by:

$$H_{t,max}^{CHP} = P_t^{CHP} \left(\frac{(1 - \eta_{elec}^{CHP}) \cdot \eta_{rec}^{CHP}}{\eta_{heat}^{CHP}} \right) \quad \forall t \in T \tag{3.1.11}$$

$$H_t^{CHP} = H_t^{JW} + H_t^{EX} \quad \forall t \in T \tag{3.1.12}$$

$$H_t^{JW} = F_{JW} \cdot H_{t,max}^{CHP} \quad \forall t \in T \tag{3.1.13}$$

$$H_{t,max}^{EX} = H_{t,max}^{CHP} - H_t^{JW} \quad \forall t \in T \tag{3.1.14}$$

$$H_{t,min}^{EX} \leq H_t^{EX} \leq H_{t,max}^{EX} \quad \forall t \in T \tag{3.1.15}$$

A piece-wise linearization approximates the fuel consumption of CHP and NGB:

$$F_t = \sum_{v=1}^{n_v} (\alpha_v P_{v,t} + \beta_v B_{v,t}) \quad \forall t \in T \tag{3.1.16}$$

$$B_{v,t} \cdot P_{v,min} \leq P_{v,t} \leq B_{v,t} \cdot P_{v,max} \quad \forall t \in T \tag{3.1.17}$$

$$\sum_{v=1}^{n_v} B_{v,t} = U_t \quad \forall t \in T \tag{3.1.18}$$

The start-up and shut-down costs and minimum run/up times for both CHP and NGB are modeled as follows:

$$SU_t - SD_t \leq U_t - U_{t-1} \quad \forall t \in T \tag{3.1.19}$$

$$SU_t + SD_t \leq 1 \quad \forall t \in T \tag{3.1.20}$$

$$\sum_{t'=t}^{t+\delta^{on}-1} U_{t'} \geq \delta^{on} \cdot SU_t \quad \forall t \in T \tag{3.1.21}$$

$$\sum_{t'=t}^{t+\delta^{off}-1} (1 - U_{t'}) \geq \delta^{off} \cdot SD_t \quad \forall t \in T \tag{3.1.22}$$

3.1.5 Electrical and Thermal Storage Systems

Battery Energy Storage (BES):

To ensure a secure operation of the storage system, the following constraints are defined for the BES. Similar equations have been applied for the SHWT as well but for H_t^{SHWT}.

$$0 \leq P_t^{ch} \leq U_t^{ch} \cdot P^{ch,max} \quad \forall t \in T \tag{3.1.23}$$

$$0 \leq P_t^{dch} \leq U_t^{dch} \cdot P^{dch,max} \quad \forall t \in T \tag{3.1.24}$$

$$U_t^{ch} + U_t^{dch} \leq 1 \quad \forall t \in T \tag{3.1.25}$$

$$P_t^{BES} = P_t^{DCH} - P_t^{CH} \quad \forall t \in T \tag{3.1.26}$$

The following two equations are utilized to update the state of charge (SOC) of the BES:

$$SOC_t = SOC_{t-1} + \eta^{ch} \cdot P_t^{ch} - \eta^{dch} \cdot P_t^{dch} \quad \forall t \in T \tag{3.1.27}$$

$$SOC_{min} \leq SOC_t \leq SOC_{max} \quad \forall t \in T \tag{3.1.28}$$

Stratified Hot Water Tank (SHWT):

The equations corresponding to the SHWT tank are:

$$H_{\text{av}}^{\text{TES}} = V_t^h \cdot \rho \cdot cp \cdot (T^h - T^l) \tag{3.1.29}$$

$$H_{\text{av}}^{\text{TES}} = H_{\text{av}_{t-1}}^{\text{TES}} - q_t^{\text{STES}} - \Delta H_t^{\text{loss}} \quad \forall t \in T \tag{3.1.30}$$

$$\Delta H_t^{\text{loss}} = (V_t^{\text{mx}} - V_{t-1}^{\text{mx}}) \cdot \rho \cdot cp \cdot (T^h - T^l) \cdot \Delta\tau \tag{3.1.31}$$

$$V_t^{\text{mx}} - V_{t-1}^{\text{mx}} = \begin{cases} 0 & \text{if } V_t^h = 0 \\ \lambda^{\text{exp}} \cdot \Delta\tau & \text{if } 0 \leq V_t^h \leq V^t \\ 0 & \text{if } V_t^h = V^t \end{cases} \tag{3.1.32}$$

$$0 \leq H_{\text{av}t}^{\text{SHWT}} \leq H_{\text{av}_{\text{max}}}^{\text{SHWT}} \quad \forall t \in T \tag{3.1.33}$$

3.1.6 Heat Exchanger

Typically, based on the direction of the inlet and outlet fluids relative to each other, two types of HEXs are used in the BMG: parallel flow and counter flow. Equation (34) expresses the relation between the mass flow and temperatures of each side, and

(35) relates the inlet temperatures of the sides to each other.

$$H_{t,h}^{HEX} = \dot{m}_{t,h}^{HEX} \cdot cp \cdot (T_{t,h}^{HEX} - T_{t,h}^{HEX}) \tag{3.1.34}$$

$$H_{t}^{HEX} = \varepsilon \cdot \min((\dot{m}_{t,h}^{HEX,1}, \dot{m}_{t,h}^{HEX,2})) \cdot cp \cdot (T_{t}^{HEX,1} - T_{t}^{HEX,2}) \quad \forall t \in T \tag{3.1.35}$$

The HEX connecting the SHWT to the loop works as a counter-flow HEX in discharging and parallel flow in charging mode. The following equations ensure the heat transfer between HEX and STES. For the other HEXs, the same equations are applied.

Counter-flow HEX

$$T^{h} \geq T_{t,h}^{HEX} + \Delta \quad \forall t \in T \tag{3.1.36}$$

$$T^{h} \geq T_{t,h}^{HEX} + \Delta \quad \forall t \in T \tag{3.1.37}$$

Parallel flow HEX

$$T^{h} \leq T_{t,h}^{HEX} + \Delta \quad \forall t \in T \tag{3.1.38}$$

3.1.7 Heat Pump

The following are the equations and constraints that express the behavior of the HP.

$$H_t^{\text{bld}} = P_t^{\text{HP}} + (\dot{m}_t^{\text{HP}}) \cdot cp \cdot (T_t^{\text{bld}} - T_t^{\text{bld}}) \quad \forall t \in T \tag{3.1.39}$$

$$P_t^{\text{HP}} = H_t^{\text{bld}} \times \eta^{\text{HP}} \left(\frac{T_s^{\text{bld}} - T_t^{\text{bld}}}{T_s^{\text{bld}}} \right) \quad \forall t \in T \tag{3.1.40}$$

$$(\dot{m}_t^{\text{HEX}}) > (\dot{m}_t^{\text{HP}}) \quad \forall t \in T, s \in S \tag{3.1.41}$$

$$T_s^{\text{bld}} \geq T_t^{\text{bld}} + \Delta \quad \forall t \in T \tag{3.1.42}$$

3.1.8 Water Pumps

The electricity demand of a water pump is linearly dependent on the pressure the pump compensates. For the main loop, ΔP_t^{loop} can be determined using 3.1.43 while for the other components, it is taken from their data sheets. Then, the pump electricity demand can be calculated by 3.1.44:

$$\Delta P_t^{\text{loop}} = \frac{\mu \cdot f^{\text{loop}} \cdot ((\dot{m}_t^{\text{loop}})^2)}{((d^{\text{loop}})^5 \cdot (\rho^{\text{loop}})^2)} \quad \forall t \in T \tag{3.1.43}$$

$$P_{t,p}^{\text{pump}} = \frac{(\dot{m}_{t,p}^{\text{pump}}) \cdot \Delta P_{t,p}^{\text{pump}}}{\eta_p^{\text{pump}} \cdot \rho_p} \quad \forall t \in T \tag{3.1.44}$$

3.1.9 Objective Function

The objective of the optimization is to minimize the total costs incurred by the operation of BMG during the day, which includes the costs associated with CHP,

NGB, grid, and carbon tax.

$$\sum_{t=1}^{T} C_t^{CHP} + C_t^{NGB} + C_t^{grid} + C_t^{ctx} \tag{3.1.45}$$

Cost Equations

The cost equations for each component are as follows:

$$C_t^{CHP} = F_t^{CHP} \cdot Pr^{fuel} + P_t^{CHP} \cdot OM_t^{CHP} \tag{3.1.46}$$

$$C_t^{NGB} = F_t^{NGB} \cdot Pr^{fuel} + Q_t^{NGB} \cdot OM_t^{NGB} \tag{3.1.47}$$

$$C_t^{grid} = P_t^{grid,imp} \cdot HEP_t^{imp} - P_t^{grid,imp} \cdot HEP_t^{Exp} \tag{3.1.48}$$

$$C_t^{ctax} = (F_t^{CHP} + F_t^{NGB}) \cdot Pr^{tax} \tag{3.1.49}$$

where Pr^{fuel} represents the natural gas price ($/kWh), HEP_t^{imp} and HEP_t^{exp} signify the hourly electricity price (HEP) for import and export, respectively, and C_t^{ctax} and Pr^{tax} denotes carbon tax rate.

3.2 Simulation Studies and Discussions

3.2.1 Case Study

The day-ahead optimal scheduling of the BMG has been conducted for a representative day in winter. The load prediction is not the focus of this study, and real data from a case study located in Burlington, Ontario, Canada, has been used as the predicted load. The time resolution for the simulation is 10 minutes. The time-of-use electricity price of Ontario, Canada [8] has been used for simulation; however, the

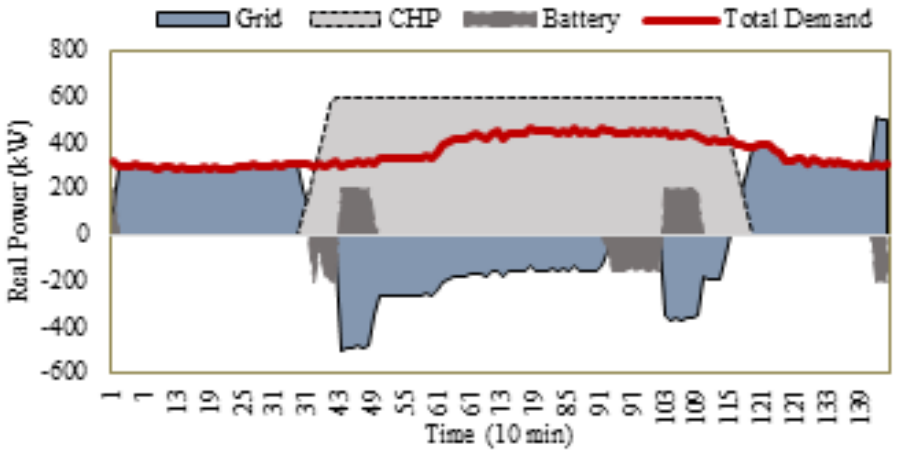

Figure 3.3: Optimal Operation of the BMG-Electrical Section

sell-to-grid factor of 0.9 has been considered to realize the exporting to the grid. The MINLP formulation developed in this study is implemented in GAMS using BARON.

3.2.2 Simulation Results

The operation of the electrical section of the BMG is illustrated in Fig. 3. In this figure, the controllable and uncontrollable loads of the BMG are accumulated, shown as the total demand. As can be observed, the CHP unit operates during peak and medium-peak hours. Its output gradually increases based on the defined ramp-rate limits. The BMG is importing electricity from the grid during off-peak hours while it contributes to meeting the peak demand of the distribution network. The BES is charged in 3 periods; the first happens during off-peak hours right before the peak time starts. Then it is discharged. The second one happens in medium-peak hours again right before the next peak time starts. The last one occurs to observe the defined constraint that the SOC of the BES at the beginning and end of the day must be the same. Intuitively, the BES can be charged and discharged during the

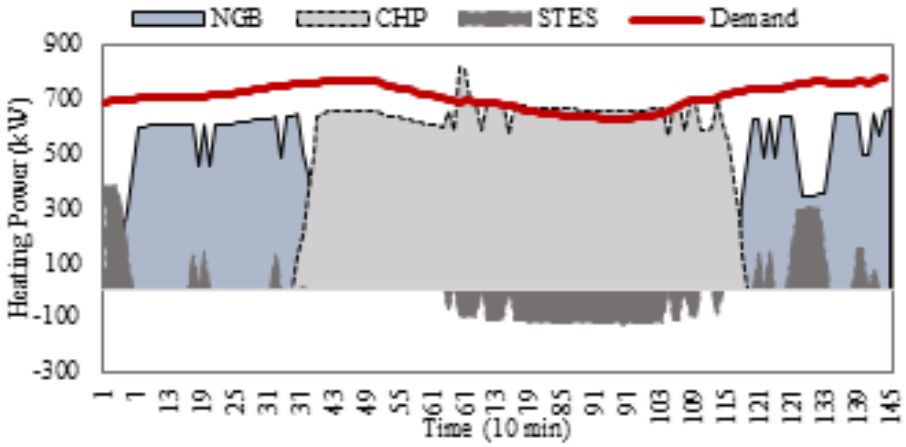

Figure 3.4: Optimal Operation of the BMG-Thermal Section.

periods in which the following equation is valid. Also, the other reason the charging and discharging of the BES are economically feasible is the overproduction of the on-site generation unit.

$$\eta^{\mathrm{ch}} \cdot \eta^{\mathrm{dch}} \cdot \mathrm{HEP}_t^{\mathrm{exp}} \geq \mathrm{HEP}_t^{\mathrm{imp}} \tag{3.2.1}$$

The thermal energy demanded by the occupants and provided by the different units are shown in Fig. 4. Given that the heat demand is higher than the total energy coming from the thermal, it is observed that the electricity consumed by HP provides a portion of the load. It is observed that NGB is used only during the early and later hours of the day when CHP is turned off. Due to the necessity of establishing precise control strategies for these types of systems, the variation of variables such as mass flow rate and temperature must be determined. The variation of mass flow rates in each unit and the main loop are shown in Fig. 5. Moreover, Fig. 6 illustrates the variation of temperature in four critical points of the thermal section.

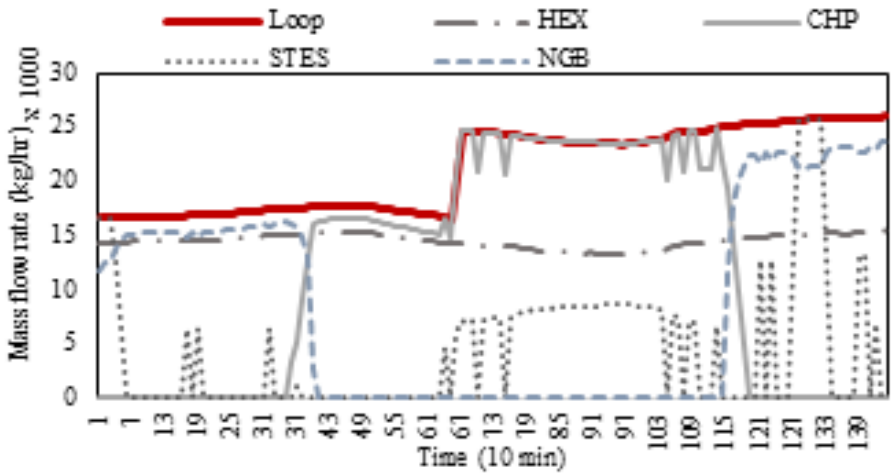

Figure 3.5: Variation of Mass Flow Rates in the System

In many studies in integrated systems, just energy-based management has been implemented. However, the simulation results show that approach not accurate enough. It can also be seen that HEX plays a key role in the charging and discharging of SHWT. Moreover, a sudden temperature increase in point A in period 67 implies less heat injection to the BMG. In other words, to meet the load, the HP compensates for the required heat while the excess heat in the loop is stored in STES to be used later. So, it can be concluded that HP plays a significant role in demand-side management in BMG.

3.3 Summary

In this work, an optimization model was presented to determine the optimal scheduling plan for the operation of a BMG. The proposed model integrated thermal and electrical sections of the system by coupling the operation of the CHP unit and the HP. This allowed the manipulation of variables such as temperatures and mass flow

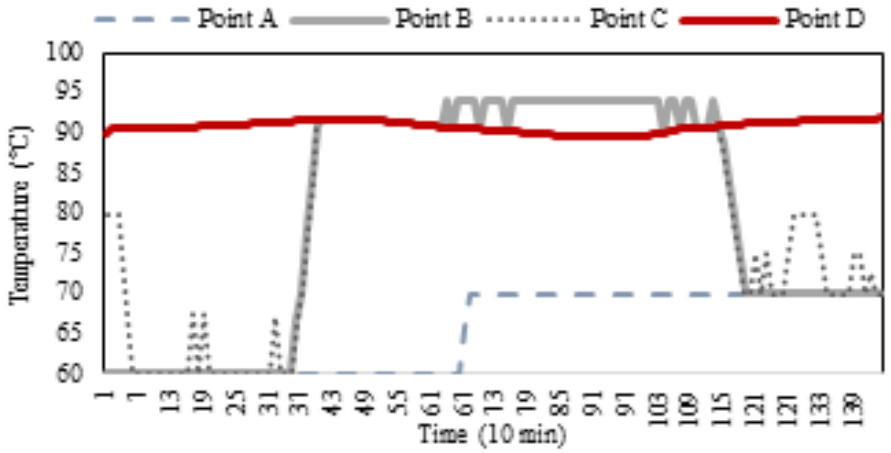

Figure 3.6: Temperature in Different Sections of the Main Loop.

rates so that the total electricity demand followed a desired profile. Results also showed the necessity of coordinating the operations of the different energy sources and storage systems in the BMG to fully meet both electrical and thermal loads.

Chapter 4

Day-ahead Optimal Dispatch of ICE-Harvest System

The main objective of this day-ahead operation optimization is to illustrate the capability of the ICE-Harvest system in harvesting waste energy to offset the community's thermal demands, performing demand management without affecting occupants' comfort, and realizing energy arbitrage. The day-ahead optimal dispatch of the ICE-Harvest system is proposed, and a detailed quasi-dynamic optimization model that incorporates thermal and hydraulic constraints is developed to achieve this goal. To solve the resulting mixed-integer nonlinear programming (MINLP) problem, a novel decomposition algorithm is proposed. The decomposition algorithm breaks down the MINLP problem into a linear sub-problem that determines the binary variables and a nonlinear sub-problem that determines the optimal dispatch of the system. In the proposed hierarchical decomposition framework for the optimal dispatch of ICE-Harvest, the linear and nonlinear subproblems are accommodated, respectively, in the second and third layers. Upon evaluating five distinct dispatch strategies, it

is enlightened that not considering thermal dynamics and heat transfer constraints will result in underestimating electricity and natural gas consumption. In contrast, if thermal pipeline capacity is not considered and mass flow and temperature are not manipulated, the system's capability will be underestimated.

4.1 Mathematical Model

ICE-Harvest comprises a variable-temperature micro-thermal network (see Fig. 6.1) and a micro-electrical network (see Fig. 4.2). A detailed mathematical representation proposed to describe the system is provided below.

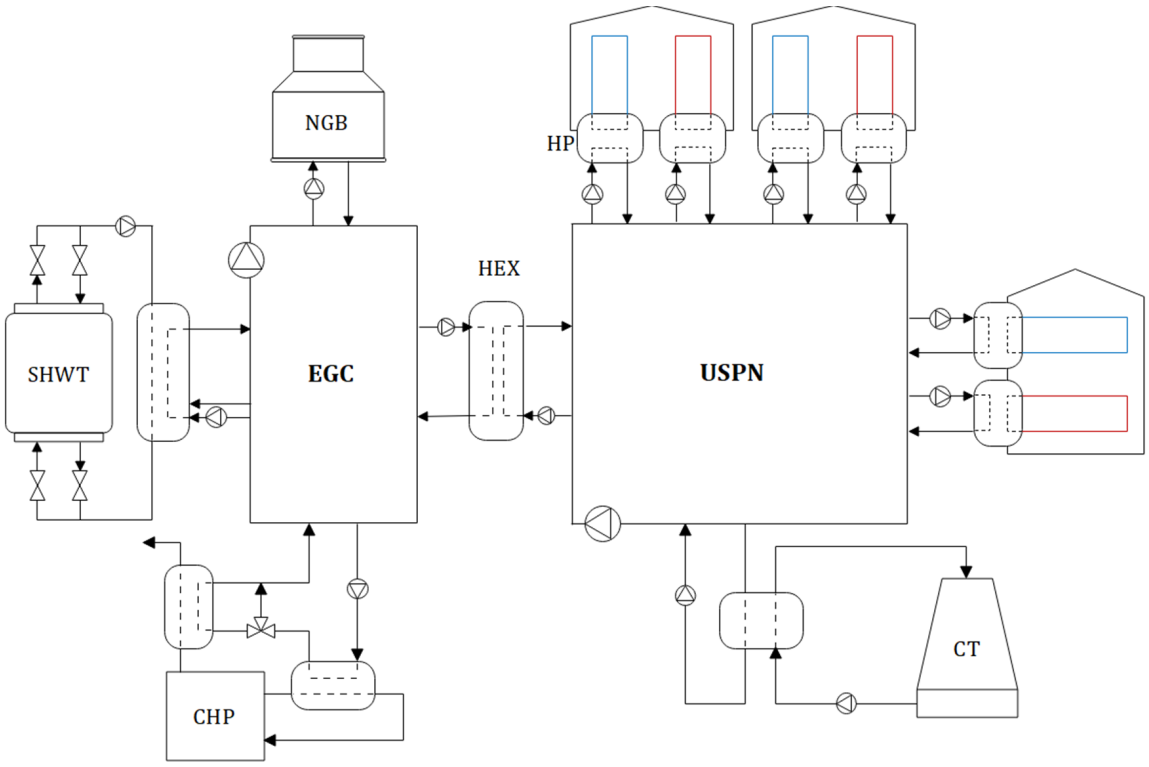

Figure 4.1: Schematic Representation of the Micro-Thermal Network of ICE-Harvest.

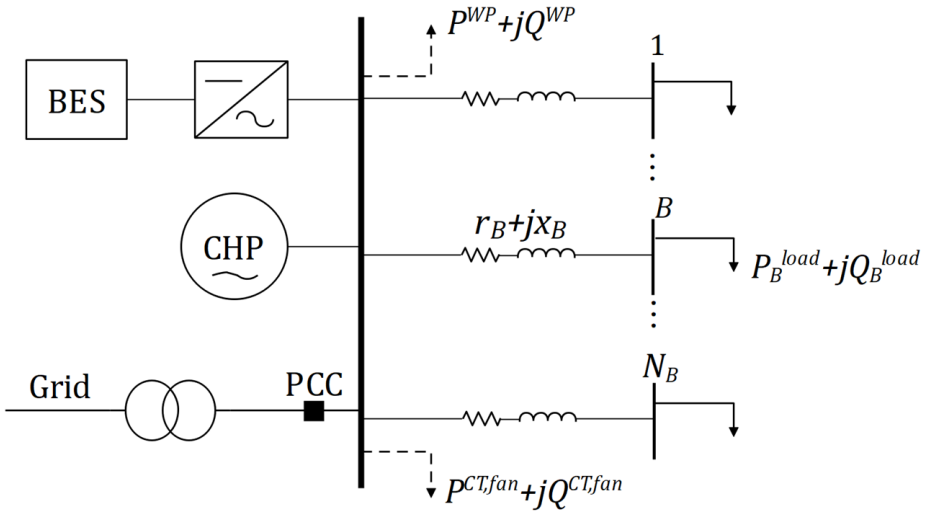

Figure 4.2: Schematic Representation of the Micro-Electrical Network of ICE-Harvest.

4.1.1 Micro-Thermal Network

The micro-thermal network comprises an energy generation center (EGC) and unidirectional single-pipe network (USPN), as shown in Fig.6.1. In EGC, thermal DERs, including a CHP, a stratified hot water tank (SHWT), and a natural gas boiler (NGB), are connected in series to a heat exchanger (HEX) via a high-temperature pipeline. In the unidirectional single-pipe network (USPN), a group of aggregated buildings and their heat pumps (HPs) and a cooling tower (CT) are connected in series to the HEX via the pipeline. Note that, as this chapter showcases the system's performance for a day, geothermal borehole storage is not considered.

CHP

As shown in Fig. 4.3, a controllable water valve (V1) controls water flow to the steam-to-water HEXs (jacket water and exhaust gas) that recover heat from the combustion process. The electricity and heat production, fuel consumption, and heat transfer

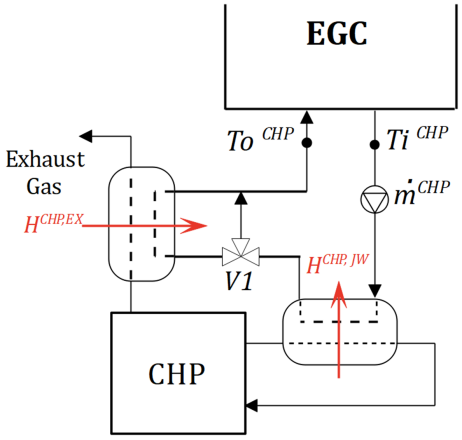

Figure 4.3: Schematic Representation of CHP.

constraints of the CHP are expressed as:

$$\eta_t^{CHP,elec} = \eta_0^{CHP,elec} \cdot \left[c + b.Pl_t^{CHP} + a.(Pl_t^{CHP})^2\right] \tag{4.1.1}$$

$$P_t^{CHP} = F_t^{CHP} \cdot \eta_t^{CHP,elec} \tag{4.1.2}$$

$$P_t^{CHP} = Pl_t^{CHP}.P_{max}^{CHP} \tag{4.1.3}$$

$$U_t^{CHP} \cdot Pl_{min}^{CHP} \leq Pl_t^{CHP} \leq U_t^{CHP} \cdot Pl_{max}^{CHP} \tag{4.1.4}$$

$$H_t^{CHP,Tot} = (F_t^{CHP} - P_t^{CHP}) \cdot \eta_0^{CHP,rec} \tag{4.1.5}$$

$$H_t^{CHP} = H_t^{CHP,JW} + H_t^{CHP,EX} \tag{4.1.6}$$

$$H_t^{CHP,JW} = k_{JW} \cdot H_t^{CHP,Tot} \tag{4.1.7}$$

$$0 \leq H_t^{CHP,EX} \leq H_t^{CHP,Tot} - H_t^{CHP,JW} \tag{4.1.8}$$

$$|P_t^{CHP} - P_{t-1}^{CHP}| \leq RR^{CHP} \cdot P_{max}^{CHP} \tag{4.1.9}$$

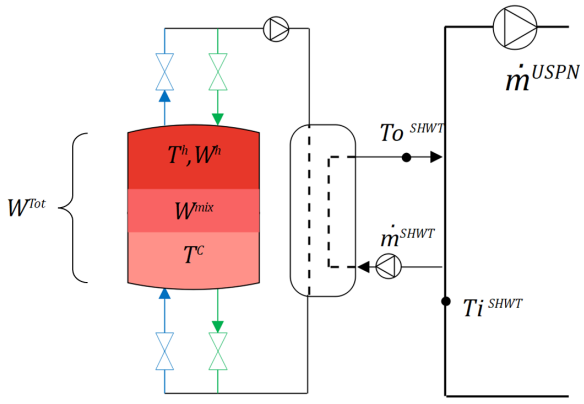

Figure 4.4: Schematic Representation of SHWT.

$$H_t^{CHP} = \dot{m}_t^{CHP} \cdot cp^w \cdot (To_t^{CHP} - Ti_t^{CHP}) \tag{4.1.10}$$

$$To_t^{CHP} - Ti_t^{CHP} \leq \Delta T^{max,CHP} \tag{4.1.11}$$

$$SU_t^{CHP} - SD_t^{CHP} \leq U_t^{CHP} - U_{t-1}^{CHP} \tag{4.1.12}$$

$$SU_t^{CHP} + SD_t^{CHP} \leq 1 \tag{4.1.13}$$

SHWT

The temperature in the SHWT is divided into three layers; high temperature (T^h) on top, mixing in the middle, and cold (T^c) on the bottom, as shown in Fig. 4.4. The heat transfer between the layers causes the middle layer expands, and the temperature linearly decreases from T^h to T^c. Assuming the middle layer expansion rate of λ^{exp}, the model of SHWT is summarized below.

$$SOC_t^{SHWT} = SOC_{t-1}^{SHWT} - (H_t^{SHWT} + H_t^{loss}) \cdot \Delta\tau \tag{4.1.14}$$

$$SOC_t^{SHWT} = W_t^h \cdot \rho^w \cdot cp^w \cdot (T^h - T^c) \tag{4.1.15}$$

$$H_t^{loss} = (W_t^{mix} - W_{t-1}^{mix}) \cdot \rho^w \cdot cp^w \cdot (T^h - T^c) \tag{4.1.16}$$

$$W_t^{mix} - W_{t-1}^{mix} = \begin{cases} 0 & if\ W_t^h = 0 \\ \lambda^{exp} \cdot \Delta\tau & if\ 0 \leq W_t^h \leq W^{Tot} \\ 0 & if\ W_t^h = W^{Tot} \end{cases} \tag{4.1.17}$$

$$0 \leq W_t^h \leq W^{Tot} \tag{4.1.18}$$

$$H_t^{SHWT} = H_t^{SHWT,dch} - H_t^{SHWT,ch} \tag{4.1.19}$$

$$H_t^{SHWT} = \dot{m}_t^{SHWT} \cdot cp^w \cdot (To_t^{SHWT} - Ti_t^{SHWT}) \tag{4.1.20}$$

$$|To_t^{SHWT} - Ti_t^{SHWT}| \leq \Delta T^{max,SHWT} \tag{4.1.21}$$

where, $H_t^{SHWT,ch}$ and $H_t^{SHWT,dch}$ are mutually exclusive.

$$U_t^{SHWT,ch} \cdot H_{min}^{SHWT,ch} \leq H_t^{SHWT,ch} \leq U_t^{SHWT,ch} \cdot H_{max}^{SHWT,ch} \tag{4.1.22}$$

$$U_t^{SHWT,dch} \cdot H_{min}^{SHWT,dch} \leq H_t^{SHWT,dch} \leq U_t^{SHWT,dch} \cdot H_{max}^{SHWT,dch} \tag{4.1.23}$$

$$U_t^{SHWT,ch} + U_t^{SHWT,dch} \leq 1 \tag{4.1.24}$$

NGB

Here are the equations used to represent the transferred heat, inlet and outlet temperatures, fluid mass flow rate, fuel consumption, and operation limits of the NGB

[45]:

$$F_t^{NGB} = \frac{H_t^{NGB}}{\eta_0^{NGB}} \tag{4.1.25}$$

$$U_t^{NGB} \cdot H_{min}^{NGB} \leq H_t^{NGB} \leq U_t^{NGB} \cdot H_{max}^{NGB} \tag{4.1.26}$$

$$|H_t^{NGB} - H_{t-1}^{NGB}| \leq RR^{NGB} \cdot H_{max}^{NGB} \tag{4.1.27}$$

$$H_t^{NGB} = \dot{m}_t^{NGB} \cdot cp^w \cdot (To_t^{NGB} - Ti_t^{NGB}) \tag{4.1.28}$$

$$To_t^{NGB} - Ti_t^{NGB} \leq \Delta T^{max,NGB} \tag{4.1.29}$$

$$SU_t^{NGB} - SD_t^{NGB} \leq U_t^{NGB} - U_{t-1}^{NGB} \tag{4.1.30}$$

$$SU_t^{NGB} + SD_t^{NGB} \leq 1 \tag{4.1.31}$$

HEXs

A counter flow HEX connects the EGC to the USPN (see Fig. 4.5), and a two-direction water-to-water HEX connects the SHWT to the loop. During discharging, it works in the counter flow state and for charging in the parallel flow mode. To ensure a heat transfer between fluids, Eqs. (4.1.32) and (4.1.33) for a counter flow and Eq. (4.1.34) for a parallel flow should be satisfied [46].

$$Ti_t^{HEX,h} \geq To_t^{HEX,c} + \Delta T_{min}^{HEX} \tag{4.1.32}$$

$$To_t^{HEX,h} \geq Ti_t^{HEX,c} + \Delta T_{min}^{HEX} \tag{4.1.33}$$

$$To_t^{HEX,h} \geq To_t^{HEX,c} + \Delta T_{min}^{HEX} \tag{4.1.34}$$

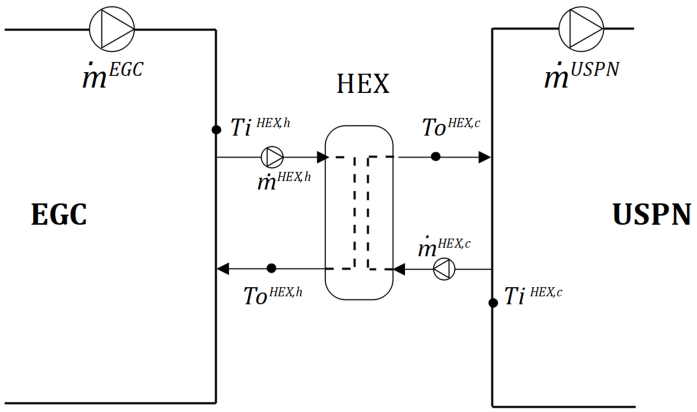

Figure 4.5: Schematic Representation of HEX.

The following equation expresses the heat transfer limits across a HEX:

$$H_t^{HEX} = \epsilon \cdot min(\dot{m}_t^{HEX,h}, \dot{m}_t^{HEX,c}) \cdot cp^w \cdot (Ti_t^{HEX,h} - Ti_t^{HEX,c}) \tag{4.1.35}$$

$$H_t^{HEX} = \dot{m}_t^{HEX} \cdot cp^w \cdot (Ti_t^{HEX} - To_t^{HEX}) \tag{4.1.36}$$

$$|To_t^{HEX} - Ti_t^{HEX}| \leq \Delta T_{max}^{HEX} \tag{4.1.37}$$

The HEX that connects EGC and USPN is the point at which two time-steps in a row are connected.

$$H_t^{HEX} = \dot{m}_t^{EGC} \cdot cp^w \cdot (Ti_t^{CHP} - Ti_{t-1}^{HEX,h}) \tag{4.1.38}$$

$$H_t^{HEX} = \dot{m}_t^{USPN} \cdot cp^w \cdot (Ti_t^{USPN} - Ti_{t-1}^{HEX,c}) \tag{4.1.39}$$

where Eq.4.1.38 and eq.4.1.39 correspond to the EGC and USPN sides, respectively. The total energy balance in the EGC can be stated as follows:

$$H_t^{HEX} = H_t^{CHP} + H_t^{NGB} + H_t^{SHWT} \tag{4.1.40}$$

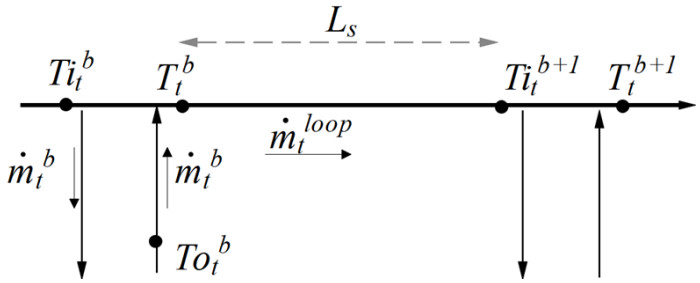

Figure 4.6: Schematic Representation of Two Consecutive Branches (one segment).

Pipeline

Modeling the pipeline of the USPN requires two sets of constraints: thermal and hydraulic. The first one represents temperature drops and thermal mass throughout the pipeline. The second one relates to the continuity of mass flow rate at branches, fluid pressures, and mass flow rate variations. Fig.4.6 shows segment s, which is constituted by two consecutive branches, b and $b+1$ in a pipeline. In this figure, $\dot{m}p_t^{loop}$ can signify both of the $\dot{m}_t^{EGC}$ and $\dot{m}_t^{USPN}$. $\dot{m}_t^b$, Ti_t^i, and To_t^i indicate mass flow rate and inlet and outlet temperatures of any branch in the micro-thermal network, respectively. Due to the short length of the EGC pipeline, thermal losses are neglected, but hydraulic constraints are used for both pipelines in EGC and USPN.

The temperature losses in segment s in the USPN can be estimated by [47]:

$$T_t^b - Ti_t^{b+1} = \frac{(1+\beta)\cdot L^s}{cp^w \cdot \dot{m}_t^{USPN}} \cdot \frac{(T_t^b - T_t^{amb})\cdot 2\cdot \pi \cdot \lambda^b}{ln(d_{ex}/d_{in}) + 2\cdot\pi\cdot\lambda^b \cdot R^e} \tag{4.1.41}$$

In addition, the thermal losses of each segment and the total losses of the pipeline

with N^s segments can be calculated as:

$$H_t^{loss,s} = \dot{m}_t^{USPN} \cdot cp^w \cdot (T_t^b - Ti_t^{b+1}) \tag{4.1.42}$$

$$H_t^{loss} = \sum_{s=1}^{N^s} H_t^{loss,s} \tag{4.1.43}$$

The pipeline in the USPN is the medium through which energy is exchanged between the HEX, HPs, and CT. However, the total injected energy is not necessarily equal to the total rejected energy at each time step. This feature visualizes the pipeline as a thermal storage system and is stated as:

$$SOC_t^{USPN} = SOC_{t-1}^{USPN} + H_t^{USPN} \cdot \Delta\tau \tag{4.1.44}$$

where, SOC_t^{USPN} signifies the storage level of the pipeline and can also be expressed as:

$$SOC_t^{USPN} = M^{USPN} \cdot cp^w \cdot (Tav_{t+1}^{USPN} - Tav_t^{USPN}) \tag{4.1.45}$$

$$SOC_{min}^{USPN} \leq SOC_t^{USPN} \leq SOC_{max}^{USPN} \tag{4.1.46}$$

$$SOC_{min}^{USPN} = M^{USPN} \cdot cp^w \cdot T_{min}^{USPN} \tag{4.1.47}$$

$$SOC_{max}^{USPN} = M^{USPN} \cdot cp^w \cdot T_{max}^{USPN} \tag{4.1.48}$$

Here, Tav_t^{USPN} is the average temperature in the pipeline, and H_t^{USPN} refers to the total heat of the pipeline, including both injections and rejection. The following

equation is the thermal energy balance in the USPN:

$$H_t^{HEX} = H_t^{USPN} + \sum_{B=1}^{N_B}(H_{t,B}^{inj} - C_{t,B}^{Hrv}) + H_t^{loss} + H_t^{CT} \tag{4.1.49}$$

where $H_{t,B}^{inj}$ and $C_{t,B}^{Hrv}$ represent the injected heat from the USPN to the heating HPs and harvested energy from cooling processes, respectively. Then, by extracting each term using and canceling out the same variables at both sides of the equation, we will have:

$$H_t^{USPN} = \dot{m}_t^{USPN} \cdot cp^w \cdot (Ti_t^{HEX} - Ti_{t-1}^{HEX}) \tag{4.1.50}$$

This equation indicates that the energy mismatch results in temperature changes in the USPN. For instance, if H_t^{USPN} is positive (the total heat injected into the USPN is higher than the thermal consumers), the temperature at the outlet of the pipeline at the current time-step (Ti_t^{HEX}) is higher than that at the previous time (Ti_{t-1}^{HEX}). This equation also demonstrates that a larger mass flow in the USPN results in a smaller temperature variation, and vice versa.

The hydraulic constraints must be satisfied for both of the pipelines in EGC and USPN. The mass flow rate continuity and fluid temperature at a mixing branch (see Fig.4.6) can be expressed by:

$$(\dot{m}_t^{loop} - \dot{m}_t^b) \cdot Ti_t^b + \dot{m}_t^b \cdot To_t^b = \dot{m}_t^{loop} \cdot T_t^b \tag{4.1.51}$$

$$k^{BP} \cdot \dot{m}_t^b \leq \dot{m}_t^{loop} \tag{4.1.52}$$

Finally, all the mass flow rates are constrained to prevent pipe vibration.

$$\dot{m}_{min} \leq \dot{m}_t \leq \dot{m}_{max} \tag{4.1.53}$$

$$|\dot{m}_t - \dot{m}_{t-1}| \leq RR^{WP}.\dot{m}_{max} \tag{4.1.54}$$

The pressure losses resulting from friction along the pipeline can be estimated by:

$$\Delta PS_t^{loop} = \mu \cdot \left(\dot{m}_t^{loop}\right)^2 \tag{4.1.55}$$

Note that, Eq. (4.1.55) is used to estimate the pressure losses of the pipeline in EGC and USPN, while for other components such as CHP, SHWT, NGB, HPs, HEX, and CT, pressure losses are adapted from their data-sheets. Electricity consumption of WPs is dependent on the pressure losses and the desired pipeline mass flow rate, as given below:

$$P_t^{WP} = (\dot{m}_t \cdot \Delta PS_t)/(\eta_0^{WP} \cdot \rho^w \cdot 3600) \tag{4.1.56}$$

Buildings and HPs

The power balance equations describing the heating and cooling HPs are as follows:

$$H_{t,B}^{load} = P_{t,B}^{HP,h} + H_{t,B}^{inj}\ ,\ C_{t,B}^{Hrv} = P_{t,B}^{HP,c} + C_{t,B}^{load} \tag{4.1.57}$$

where $H_{t,B}^{load}$ and $C_{t,B}^{Hrv}$ represent the heating demand of the building and the energy rejected to the UPSN by the cooling HP, respectively.

The heating demand is provided by the injected energy from the UPSN to the heating HP complemented by the electrical demand of the HP. On the other hand,

the total energy rejected by the HPs, referred to as the harvested energy, is the summation of the cooling demand of the building and the electricity consumed by the cooling HP. In this regard, the coefficient of performance (COP) for the heating and cooling HPs is defined as follows:

$$COP^{h}_{t,B} = \frac{H^{load}_{t,B}}{P^{HP,c}_{t,B}} \; , \; COP^{c}_{t,B} = \frac{C^{load}_{t,B}}{P^{HP,c}_{t,B}} \tag{4.1.58}$$

$$COP^{h}_{t,B} = min\left\{ \eta^{HP,h}_{0} \cdot \frac{Ts^{h} + 273.15}{Ts^{h} - Tav^{HP,h}_{t,B}} \; , \; COP_{max} \right\} \tag{4.1.59}$$

$$COP^{h}_{t,B} = min\left\{ \eta^{HP,h}_{0} \cdot \frac{Ts^{c}}{Tav^{HP,c}_{t,B} - Ts^{h}} \; , \; COP_{max} \right\} \tag{4.1.60}$$

$$COP^{h}_{t,B} \geq COP_{min} \; , \; COP^{c}_{t,B} \geq COP_{min} \tag{4.1.61}$$

$$Tav^{HP,h}_{t,B} = \frac{Ti^{HP,h}_{t,B} + To^{HP,h}_{t,B}}{2} \; , \; Tav^{HP,c}_{t,B} = \frac{Ti^{HP,c}_{t,B} + To^{HP,c}_{t,B}}{2} \tag{4.1.62}$$

As seen, the electricity an HP consumes depends on the temperature of the inlet and outlet fluids. Then, the heat balance in the HP can be stated by:

$$H^{inj}_{t,B} = \dot{m}^{HP,h}_{t,B} \cdot cp^{w} \cdot (Ti^{HP,h}_{t,B} - To^{HP,h}_{t,B}) \tag{4.1.63}$$

$$C^{Hrv}_{t,B} = \dot{m}^{HP,c}_{t,B} \cdot cp^{w} \cdot (To^{HP,c}_{t,B} - Ti^{HP,c}_{t,B}) \tag{4.1.64}$$

Some buildings may utilize their built-in refrigeration units. In that case, the cooling HP supplies cold water for their refrigeration units and recuperates waste heat. Therefore, the cooling demand of the HP can be calculated as follows:

$$C^{load}_{t,B} = C^{load,ref}_{t,B} \cdot \left(1 + \frac{1}{COP^{ref}_{t,B}} \right) \tag{4.1.65}$$

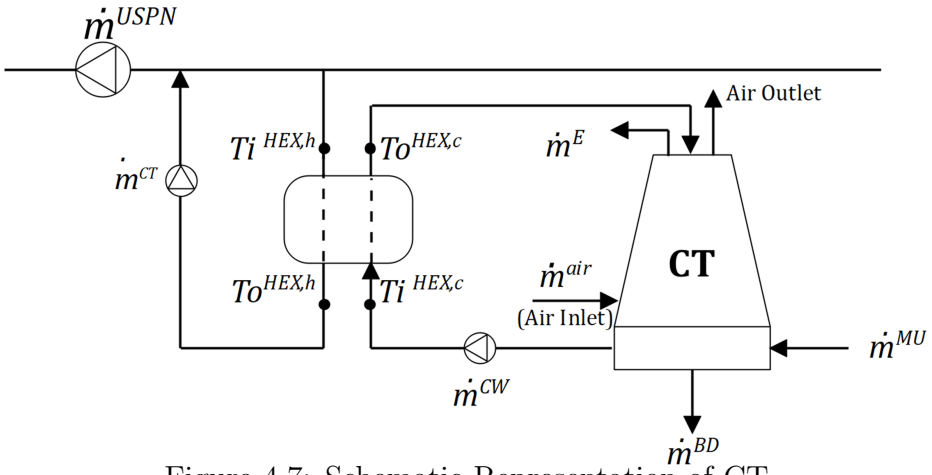

Figure 4.7: Schematic Representation of CT.

where $C_{t,B}^{load,ref}$ denote the actual cooling demand provided by the built-in refrigeration system, and $C_{t,B}^{load}$ is the total cooling demand seen by the HP.

CT

A counter-flow wet CT with mechanical air draft is used as the heat sink in the ICE-Harvest (see Fig. 4.7). The heat rejected by the CT can be estimated by the circulating water mass flow rate, $\dot{m}_t^{CW}$, and the range temperature, ΔT_{Rng}^{CT}, as given below:

$$H_t^{CT} = \dot{m}_t^{CW} \cdot cp^w \cdot \Delta T_{Rng}^{CT} \tag{4.1.66}$$

$$\Delta T_{Rng}^{CT} = (To_t^{CT,c} - Ti_t^{CT,c}) \tag{4.1.67}$$

$$H_t^{CT} = \dot{m}_t^{CT} \cdot cp^w \cdot (Ti_t^{CT,h} - To_t^{CT,h}) \tag{4.1.68}$$

Here, ΔT_{Rng}^{CT} is considered a fixed design parameter [48].

The performance of a CT is constrained by the wet-bulb temperature of the environment and its capacity, which is usually represented by the maximum circulating

water [49, 48].

$$To_t^{CT,h} \geq (T_t^{WB} + \Delta T_{min}^{CT}) \cdot U_t^{CT} \tag{4.1.69}$$

$$\dot{m}_t^{CW} \leq \dot{m}_{max}^{CW} \tag{4.1.70}$$

where the binary variable U_t^{CT} denotes the operating states of the CT.

Make-up water is required to compensate for losses during the heat transfer, especially evaporation, drift, and blow-down. The water mass balance in the CT can be estimated by [50–52]:

$$\dot{m}_t^{MU} = \dot{m}_t^{E} + \dot{m}_t^{BD} + \dot{m}_t^{DR} \tag{4.1.71}$$

$$\dot{m}_t^{E} = 0.03 \cdot \dot{m}_t^{CW} \tag{4.1.72}$$

$$\dot{m}_t^{BD} = \frac{\dot{m}_t^{E} - (N^{cycles} - 1) \cdot \dot{m}_t^{DR}}{N^{cycles} - 1} \tag{4.1.73}$$

$$\dot{m}_t^{DR} = 0.002 \cdot \dot{m}_t^{CW} \tag{4.1.74}$$

where $\dot{m}_t^{MU}$ is the make-up water mass flow rate; $\dot{m}_t^{E}$ is the evaporation mass flow rate; $\dot{m}_t^{BD}$ is the blow-down mass flow rate; and $\dot{m}_t^{DR}$ is the drift loss mass flow rate. To determine the power consumption of the fan, it is also necessary to calculate the mass flow rate of air in the tower using:

$$\dot{m}_t^{air} = cf \cdot \dot{m}_t^{CW} \tag{4.1.75}$$

$$P_t^{CT,fan} = \frac{\dot{m}_t^{air} \cdot Cfan}{\rho^{air}} \tag{4.1.76}$$

4.1.2 Micro-Electrical Network

The micro-electrical network comprises electrical loads, battery energy storage (BES), CHP, and a micro-distribution network.

Loads

Two general categories of electrical loads can be defined for ICE-Harvest: controllable and uncontrollable. The first one includes plugin loads and air conditioning of the buildings, and the latter one consists of HPs, WPs, and CT. The controllable loads and CHP tie the micro-thermal and micro-electrical networks and facilitate the energy arbitrage and demand management in the system. The real and reactive demands of a building can be expressed by:

$$P_{t,B}^{load} = P_{t,B}^{plugin} + P_{t,B}^{HP,h} + P_{t,B}^{HP,c} + P_{t,B}^{WP,h} + P_{t,B}^{WP,c} \tag{4.1.77}$$

$$\begin{aligned} Q_{t,B}^{load} = Q_{t,B}^{plugin} + tan(\phi^{HP}) \cdot (P_{t,B}^{HP,h} + P_{t,B}^{HP,c}) + \\ (P_{t,B}^{WP,h} + P_{t,B}^{WP,c}) \cdot tan(\phi^{WP}) \end{aligned} \tag{4.1.78}$$

BES

The state of charge (SOC) of BES is updated by:

$$SOC_t^{BES} = SOC_{t-1}^{BES} - (\eta_0^{BES,ch} \cdot P_t^{BES,ch} - \eta_0^{BES,dch} \cdot P_t^{BES,dch}) \cdot \Delta\tau \tag{4.1.79}$$

$$SOC_{min}^{BES} \leq SOC_t^{BES} \leq SOC_{max}^{BES} \tag{4.1.80}$$

$$P_t^{BES} = P_t^{BES,dch} - P_t^{BES,ch} \tag{4.1.81}$$

$$U_t^{BES,ch} \cdot P_{min}^{BES} \leq P_t^{BES,ch} \leq U_t^{BES,ch} \cdot P_{max}^{BES} \tag{4.1.82}$$

$$U_t^{BES,dch} \cdot P_{min}^{BES} \leq P_t^{BES,dch} \leq U_t^{BES,dch} \cdot P_{max}^{BES} \tag{4.1.83}$$

$$U_t^{BES,ch} + U_t^{BES,dch} \leq 1 \tag{4.1.84}$$

where $P_t^{BES,dch}$ and $P_t^{BES,ch}$ are mutually exclusive, and the initial and last SOC^{BES} must be the same.

Power Flow Equations

A convex optimal power flow model is adapted from [53]. ICE-Harvest can be either behind the meter or in front of the meter. In either case, the power at the point of common coupling (PCC) can be expressed by:

$$P_t^{PCC} = P_t^{exp} + P_t^{imp} \tag{4.1.85}$$

$$U_t^{exp} \cdot P_{min}^{PCC} \leq P_t^{exp} \leq U_t^{exp} \cdot P_{max}^{PCC} \tag{4.1.86}$$

$$U_t^{imp} \cdot P_{min}^{PCC} \leq P_t^{imp} \leq U_t^{imp} \cdot P_{max}^{PCC} \tag{4.1.87}$$

$$U_t^{exp} + U_t^{imp} \leq 1 \tag{4.1.88}$$

where, in the case of behind the meter, P_t^{exp} is zero. The reactive power of CHP, BES, and grid are constrained by:

$$\left(P_t^{CHP}\right)^2 + \left(Q_t^{CHP}\right)^2 \leq \left(S_{max}^{CHP}\right)^2 \tag{4.1.89}$$

$$\left(P_t^{BES}\right)^2 + \left(Q_t^{BES}\right)^2 \leq \left(S_{max}^{BES}\right)^2 \tag{4.1.90}$$

$$\left(P_t^{PCC}\right)^2 + \left(Q_t^{PCC}\right)^2 \leq \left(S_{max}^{PCC}\right)^2 \tag{4.1.91}$$

4.2 Optimization and Problem Decomposition

The optimization problem is to determine the optimal dispatch of all devices and energy resources over a 24-hour horizon. The objective function comprises operation and maintenance costs and is subject to the constraints presented in the previous section.

$$CS^{Tot} = \sum_{t=1}^{48}(CS_t^{fuel} + CS_t^{PCC} + CS_t^{O\&M} + CS_t^{w} + CS_t^{SU}) \tag{4.2.1}$$

$$CS_t^{fuel} = (F_t^{NGB} + F_t^{CHP}) \cdot Pr^{fuel} \cdot \Delta\tau \tag{4.2.2}$$

$$CS_t^{PCC} = (P_t^{imp} \cdot HEP_t^{imp} - P_t^{exp} \cdot HEP_t^{exp}) \cdot \Delta\tau \tag{4.2.3}$$

$$CS_t^{O\&M} = \sum_{g=1}^{3}(P_t^{g} \cdot Pr^{g,O\&M}) \tag{4.2.4}$$

$$CS_t^{SU} = \sum_{g=1}^{3}(SU_t^{g} \cdot Pr^{g,SU} + SD_t^{g} \cdot Pr^{g,SD}) \tag{4.2.5}$$

$$CS_t^{w} = \dot{m}_t^{MU} Pr^{w} \cdot \Delta\tau \tag{4.2.6}$$

4.2.1 Problem Decomposition

To solve the large-scale non-convex MINLP problem, it is proposed to decompose it into two sequential layers of MILP and NLP, which are solved successively, as illustrated in Fig. 4.8. The main idea behind the proposed decomposition is that the binary variables that determine the on/off operating states of the DERs do not vary with slight variations in the electrical and thermal demands of the system. The first sub-problem, named Electrical and Thermal Unit Commitment (ETUC), is a linear relaxation of the original problem and aims to determine the binary variables

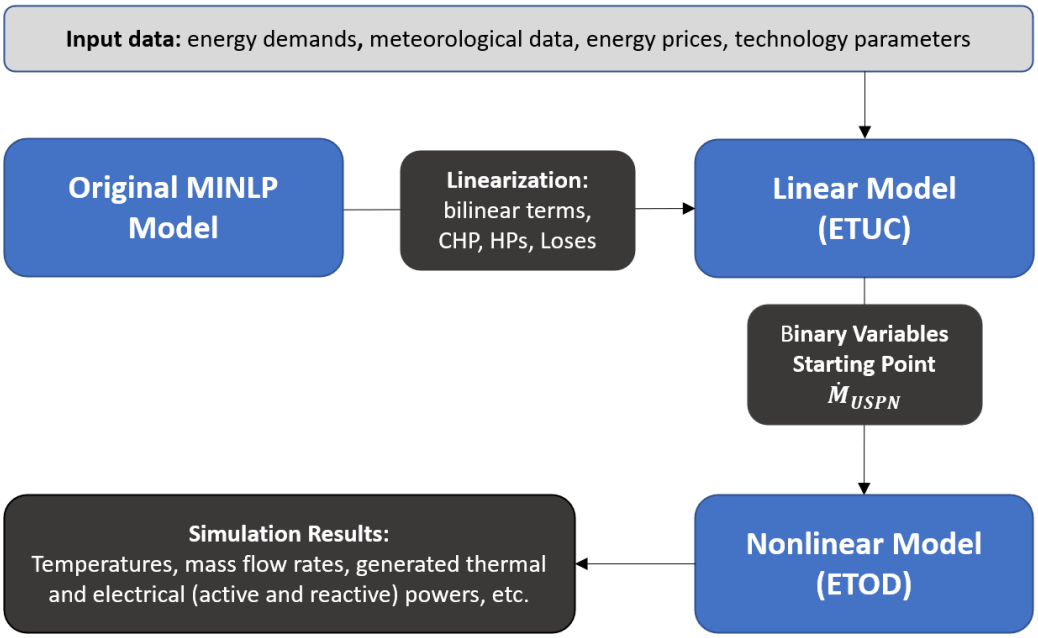

Figure 4.8: Proposed Framework for the Decomposition of the Optimization Problem.

as well as a starting point for the second sub-problem. The second sub-problem uses the binary variables as fixed parameters and the starting point from the ETUC and determines the optimal values for the rest of the variables. This sub-problem is called Electrical and Thermal Optimal Dispatch (ETOD) and includes all model details and non-linearities. These two sub-problems are accommodated in the second and third layers of the hierarchical decomposition framework introduced in Chapter 1.

Linearization of heat transfer equation

Some constraints of the optimization problem need to be linearized or reformulated in advance. The amount of heat injected in or rejected from a component is expressed as $Q_t = \dot{m}_t \cdot cp^w \cdot \Delta T_t$. Due to the presence of a nonconvex bilinear term which is a product of two continuous variables ($\dot{m}_t \cdot \Delta T_t$), this equation cannot be used in the

ETUC. Hence, it is proposed to discretize $\dot{m}_t$ as illustrated below:

$$\dot{m}_t = \sum_{k=1}^{4} (U^z_{k,t} \cdot Z_k) \tag{4.2.7}$$

where, $U^z_{k,t}$ is a binary variable that selects the kth Z_k in $Z = \{10, 20, 40, 80\}$ at time t. The defined elements in Z and Eq. 4.2.7 allows us to generate values for $\dot{m}_t$ within the desired range of 10-150 kg/hr with 10 kg/hr resolution. Then, defining $A_{k,t} = U^z_{k,t} \cdot \Delta T_t$ and substituting it in Q_t yields:

$$Q_t = cp^w \cdot \sum_{k=1}^{4} (A_{k,t} \cdot Z_k) \tag{4.2.8}$$

$A_{k,t}$ is a bilinear term composed of a continuous variable ΔT_t and a binary variable $U^z_{k,t}$. However, unlike the original bilinear term, it has a linearized representation as expressed below:

$$0 \leq A_{k,t} \leq \Delta T_{max} \tag{4.2.9}$$

$$U^z_{k,t} \cdot \Delta T_{min} \leq A_{k,t} \leq U^z_{k,t} \cdot \Delta T_{max} \tag{4.2.10}$$

$$\Delta T_t - (1 - U^z_{i,t}) \cdot \Delta T_{max} \leq A_{i,t} \leq \Delta T_t - (1 - U^z_{i,t}) \cdot \Delta T_{min} \tag{4.2.11}$$

This linearization is applied to any equations containing the product of the mass flow rate and temperature, such as Eq. (4.1.51).

Linearization of CHP Model

In the CHP model, Eqs. (4.1.1)-(4.1.2) are non-linear and non-convex. To obtain a linear model for the CHP while the model's accuracy is not sacrificed, Eqs. (4.1.1)-(4.1.3) are compactly rewritten as follows:

$$F_t^{CHP} = \frac{P_{max}^{CHP}}{\eta_o^{CHP,elec}} \cdot \frac{Pl_t^{CHP}}{\left[c + b \cdot Pl_t^{CHP} + a \cdot (Pl_t^{CHP})^2\right]} \tag{4.2.12}$$

Then, the above equation can be linearized and F_t^{CHP} can be expressed as:

$$F_t^{CHP} = \frac{P_{max}^{CHP}}{\eta_o^{CHP,elec}} \cdot (\alpha \cdot Pl_t^{CHP} + \beta \cdot U_t^{CHP}) \tag{4.2.13}$$

Reformulation of HP's Model

Although the model of HP is nonlinear due to variables in the denominators, it is proposed to reformulate the Eqs. (6.1.30)-(6.1.33) by a set of linear equations with new variables, named $POC_{t,B}^h$ and $POC_{t,B}^c$, which are respectively the inverses of $COP_{t,B}^h$ and $COP_{t,B}^c$, as illustrated below:

$$P_{t,B}^{HP,h} = H_{t,B}^{load} \cdot POC_{t,B}^h \ , \ P_{t,B}^{HP,c} = C_{t,B}^{load} \cdot POC_{t,B}^c \tag{4.2.14}$$

$$POC_{t,B}^h \geq \frac{Ts^h - Tav_{t,B}^{HP,h}}{\eta_0^h \cdot Ts^h + 273.15} \tag{4.2.15}$$

$$POC_{t,B}^c \geq \frac{Tav_{t,B}^{HP,c} - Ts^c}{\eta_0^c \cdot Ts^c + 273.15} \tag{4.2.16}$$

$$POC_{min} \leq POC_{t,B}^h \leq POC_{max} \tag{4.2.17}$$

$$POC_{min} \leq POC_{t,B}^c \leq POC_{max} \tag{4.2.18}$$

This new set of linear inequality constraints is used in both ETUC and ETOD layers.

Linearization of Energy Losses

In Eq. (4.1.41), which is implemented in the ETED, $\dot{m}_t^{USPN}$ appears in the denominator, making the equation extremely nonlinear [54]. To avoid that, the first order Taylor expansion of the $\frac{1}{\dot{m}_t^{USPN}}$ around $\dot{m}_t^{USPN} = \dot{M}_t^{USPN}$ is used:

$$\frac{1}{\dot{m}_t^{USPN}} \approx (2 - \frac{\dot{m}_t^{USPN}}{\dot{M}_t^{USPN}}) \cdot \frac{1}{\dot{M}_t^{USPN}} \tag{4.2.19}$$

where $\dot{M}_t^{USPN}$ is the mass flow rate determined in the ETUC layer and is fed into the ETOD as a parameter and represents an estimation for the $\dot{m}_t^{USPN}$. In the next subsection, it is explained how $\dot{M}_t^{USPN}$ is computed. The temperature losses between the two consecutive nodes in the USPN are approximated by:

(4.2.20)

Note that, for calculating the $H_t^{loss,s}$ from Eq.(4.1.42), the $\dot{m}_t^{USPN}$ in the numerator and denominator will cancel out. By using this linearization, the only form of nonlinearity left in the ETOD layer will be bilinearity, which allows a wider range of nonlinear optimization solvers to be used.

ETUC

To keep the linearity of the thermal section model in ETUC, the EGC is implemented as a single-node thermal power balance model ignoring the temperatures and mass flow rates constraints. That is, the Eqs. (4.2.13),(4.1.3)-(4.1.9), (4.1.12)-(4.1.13),

(4.1.14)-(4.1.19), (4.1.22)-(4.1.24), (4.1.25)-(4.1.27), (4.1.30)-(6.1.28), (4.1.40) are used to represent a simplified but sufficiently accurate model for the EGC.

A similar approach would not suit the USPN as HP temperatures and mass flow rate directly affect the system's thermal and electrical performance. Therefore, to maintain linearity in ETUC while at the same time ensuring a high level of accuracy, the linearized heat transfer model (Eqs. (4.2.8)-(4.2.11)) is used. The remaining constraints on temperature and mass flow rate in USPN (Eqs. (4.1.51)-4.1.54)) are observed whilst the mass flow rate is linearized by using Eqs. (4.2.7)-(4.2.11). HPs are described by the proposed relaxed mathematical model (Eqs. (6.2.7)-(6.2.11)), while another non-linearity still remains in HPs, which is associated with Eqs. (4.1.63)-(4.1.64). This nonlinearity is handled by a rule of thumb, suggesting that the temperature difference between the inlet and outlet of an HP ($Ti_{t,B}^{HP,h} - To_{t,B}^{HP,h}$) and ($To_{t,B}^{HP,c} - Ti_{t,B}^{HP,c}$) can be considered constant with a value of 6-10$^{\circ}C$ degree. The developed mathematical model for CT is entirely linear.

In ETUC, a single-node power balance model with controllable and uncontrollable loads is developed without considering power losses and reactive powers. For this aim, Eqs. (4.1.77), (4.1.79)-(4.1.88) are included in the optimization problem to represent the electrical section. The resultant optimization model is an MILP, which is significantly faster to solve than the original MINLP.

ETOD

Taking the binary variables and the starting point from the ETUC, the ETOD determines the optimal dispatch for the ICE-Harvest. The Eqs. (4.1.1)-(4.1.11), (4.1.14)-(4.1.23), (4.1.25)-(4.1.29), (4.1.32)-(4.1.40), (4.1.42)-(6.1.30), (6.1.35)-(4.1.83),(4.1.85)-(4.1.87), (4.1.89)-(4.1.91), and (6.2.7)-(4.2.20) are used to build the NLP model of the ETOD.

ETUC solutions could lead to ETOD infeasibility due to insufficient/extra reactive/real power generation. To correct this, the binary variables for the charging and discharging of the BES are not sent to the ETOD, as the charging and discharging efficiencies force the optimal $P_t^{BES,dch}$ or $P_t^{BES,ch}$ in Eqs.(4.1.79) to be mutually exclusive. In addition to solving the infeasibility issue, this increases the flexibility of the ETOD in dispatching the BES.

4.3 Simulation Studies and Discussions

4.3.1 Test System Description

The proposed day-ahead optimal dispatch strategy is verified using data from a real case study in Ontario, Canada. This case study encompasses three public complex buildings, including a library, a seniors' center, and a YMCA, and is situated behind the meter. The capacities of DERs and other parameters are calculated based on the approach described in [44]. The cumulative heating, cooling, and plug-in electrical demands of the buildings, along with the real-time hourly electricity price (HEP), are given in Fig. 4.9. It is evident that the total heating demand of the system outweighs

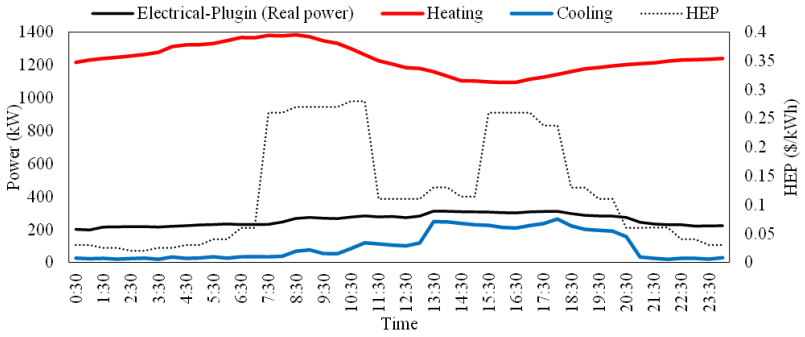

Figure 4.9: Plugin Electrical Demand, Heating Demand, Cooling Demand, and HEP.

the total cooling demand, indicating that the case study location is primarily characterized by heating needs. Moreover, in the HEP curve, the distinct price associated with peak hours, mid-peak hours, and off-peak hours can be seen. The length of the USPN is 700 m, and the initial states of charge of BES and SHWT are optimization variables. Taking into account the length of the USPN and the minimum velocity of water in the pipeline, 30 minutes is chosen as the time step, so that the time delay between buildings can be neglected. The ETUC and ETOD are solved using CPLEX and BARON [55], with relative convergence gaps of 0.05% and 0.5%, respectively. The whole algorithm converges in less than an hour; however, when solving the original MINLP without decomposition, neither BARON nor Gurobi 9.0 found a feasible solution within hours.

4.3.2 Electrical and Thermal Power Balance

Fig. 4.10(a) and (b) illustrate the performance of the electrical and thermal DERs, respectively. As shown in Fig. 4.10(a), during peak and mid-peak hours, the CHP and the BES meet the electrical load, while the grid has the minimum contribution.

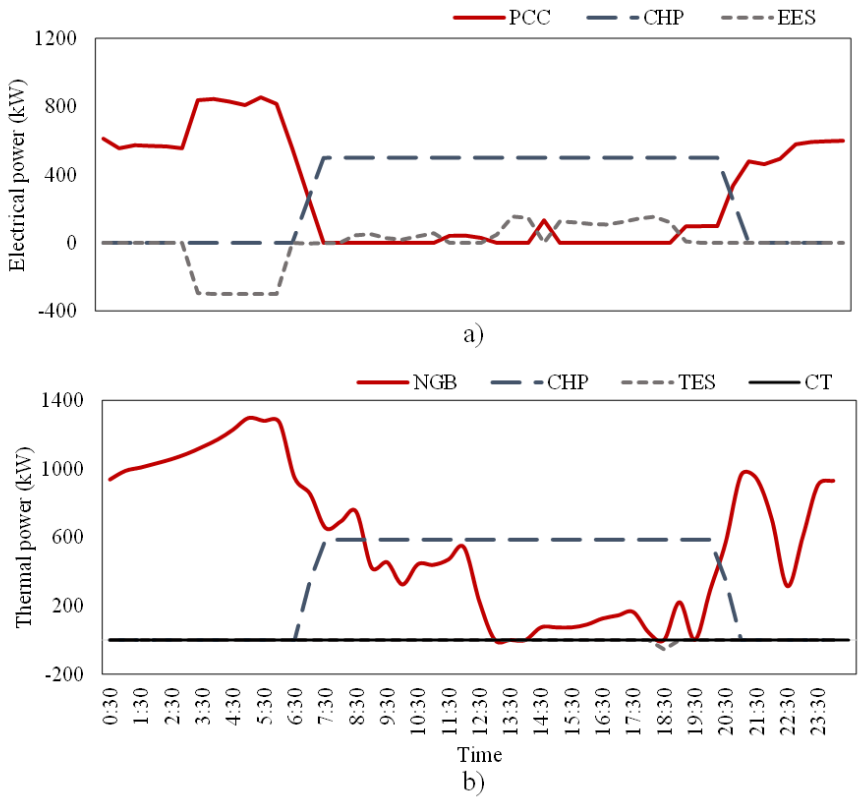

Figure 4.10: Overall Performance of (a) Electrical and (b) Thermal DERs in EGC.

CHP is turned on at 7:00, 30 minutes before the start of peak hours, to overcome ramp rate limits, and then operates at maximum capacity. During off-peak times, ICE-Harvest imports power from the grid to satisfy the electrical demand and charge the BES.

Fig.4.10(b) presents the heating power of the CHP and NGB and the charging and discharging power of the SHWT. It is observed that the NGB is utilized during both peak and off-peak hours. SHWT does not contribute to providing the heating power during the simulation day; however, it is charged to compensate for the losses so that the initial and last SOC^{SHWT} are the same. Also, SHWT is charged when NGB is not operating, which means it is charged by the extra recovered heat from

CHP.

Fig. 4.11 better enlightens the thermal power flow in ICE-Harvest. There are three types of thermal power providers in ICE-Harvest; DERs (Fig.4.10(b)), electricity power in heating HPs, and harvested energy from the cooling processes. In addition, three types of thermal consumers pull energy from the USPN; heating HPs, CT, and thermal losses.

It is illustrated that the electricity power of heating HPs decreases when energy harvesting increases, and vice versa. This implies that when the cooling demand increases in the system, a portion of the electricity consumption in the heating HPs is turned into electricity consumption in the cooling HPs so that the total electricity demand (and operation cost) is minimum. Therefore, the reduced electricity demand in heating HPs is offset by the cooling HPs to harvest the energy that would otherwise be wasted.

Furthermore, the total harvested energy under the proposed optimal dispatch strategy is utilized, and no heat is dumped via the CT. Later in this study, it is shown that other dispatch strategies can lead to harvesting energy from cooling processes and then dumping it via the CT.

As depicted in Fig.4.11, the total heat injected into the USPN by thermal providers can be higher/lower than the thermal consumers. Thanks to the thermal mass, the pipeline functions as a thermal storage unit and compensates for the mismatch between the thermal providers and consumers. It is also observed that the thermal losses in the USPN are negligible. The electricity consumption switching phenomenon is evident in Fig. 4.12, which displays the breakdown of electrical loads. For this to happen, when the total cooling demand increases, the average temperature of the

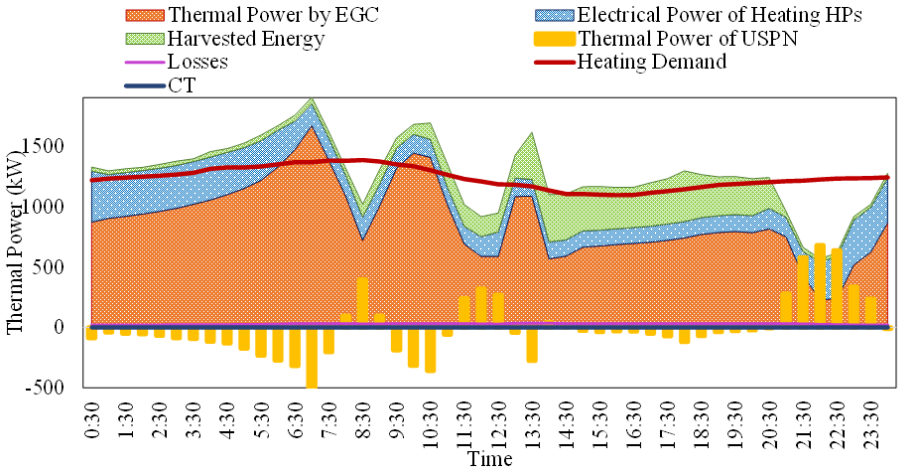

Figure 4.11: Thermal power flow in ICE-Harvest.

USPN must rise so that the COPs of the heating HPs increase and the COPs of cooling HPs decrease (see Fig. 4.12). The details of the temperature variations in the USPN will be explained later. Fig. 4.12 showcases the demand management capability of the ICE-Harvest under the proposed optimal dispatch strategy. As observed, the total electricity demand profile is fairly smooth, and the difference between the electricity demand during peak, mid-peak, and off-peak hours is relatively small. It is also observed that the WPs' electricity demand and micro-electrical network losses are relatively small but still need to be accounted for in the optimization model.

4.3.3 Energy Harvesting and Sharing

Fig. 4.13 illustrates the flow of the harvested energy from the cooling processes of various buildings in the USPN and how this energy is used.

It is observed that when the harvested energy from the cooling process of a building exceeds its heating demand, as in the Library, the residual energy is shared with adjacent buildings. However, when the heating demand of a building exceeds the

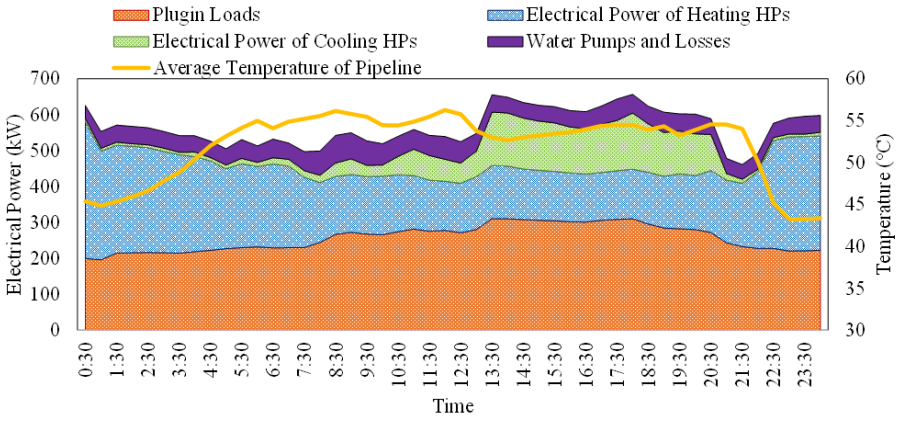

Figure 4.12: Breakdown of electrical loads in ICE-Harvest.

harvested energy, the building does not share the energy.

4.3.4 Energy Arbitrage

To illustrate energy arbitrage, imported electricity and natural gas of ICE-Harvest and the conventional BAU scenario are analyzed and compared. In the BAU, the grid is the only source of electricity to provide the plugin loads and the electricity demand for the cooling system, there is no HP, and NGB is the only natural gas-fired energy source that provides the heating demands of the buildings.

Fig.4.14(a) and (b) illustrate ICE-Harvest switching between electricity and natural gas consumption in response to real-time energy carriers' prices. As observed, ICE-Harvest imports more electricity and burns less natural gas than BAU during off-peak hours. During peak times, however, it reduces importing electricity from the grid to zero, and burns more natural gas, the more affordable energy carrier. The dynamical energy carrier switching in response to the HEP and natural gas price can be regarded as energy arbitrage and is another form of demand-side management

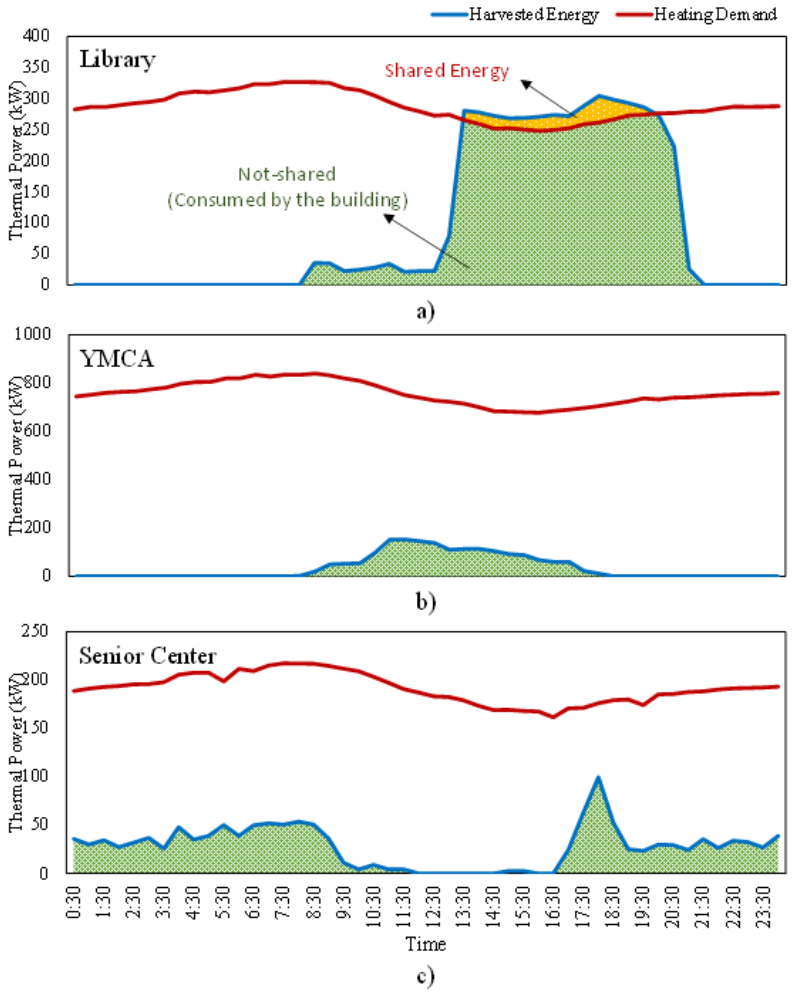

Figure 4.13: Flow of the harvested energy from the buildings in ICE-Harvest.

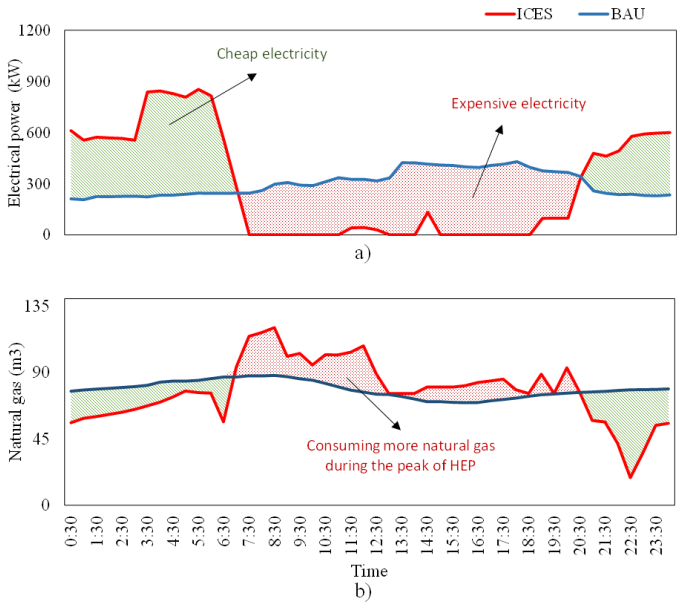

Figure 4.14: (a) Comparison of Imported power and (b) On-Site Natural Gas Consumption of ICE-Harvest vs BAU.

measure realized within the ICE-Harvest.

4.3.5 Comparison of Different Dispatch Strategies

To further investigate the impact of the accuracy level of the optimization model, four other dispatch strategies are developed and compared in Table 4.1. This comparison also helps further explore the capacity for demand management, energy arbitrage, and energy harvesting within the ICE-Harvest. Assuming that the proposed optimal dispatch strategy is called ETOD1, the second strategy is called ETOD2, where the USPN mass flow rates remain constant throughout the day, while they are optimization variables. ETOD2 is still non-convex, but with fewer variables and easier to solve. However, it is essential to determine to what extent the system's performance will be sacrificed.

Table 4.1: Comparison of Different Dispatch Strategies

Dispatch Strategies	Temperature Optimization	Flow Rate Optimization	Flow Rate Manipulation	Pipeline Storage Capacity	Building's Location	Temperature Losses	Optimization Type
ETOD1	✓	✓	✓	✓	✓	✓	MINLP
ETOD2	✓	✓	–	✓	✓	✓	MINLP
ETOD3	✓	✓	✓	–	✓	✓	MINLP
ETOD4	✓	✓	–	–	✓	✓	MINLP
ETOD5	✓	–	–	✓	–	–	MILP

In ETOD1, the pipeline in USPN is visualized as a thermal battery. The third strategy (ETOD3) is developed to evaluate this model's capability. ETOD3 is similar to ETOD1, except pipeline storage capacity is not considered. Therefore, the total energy injected into the pipeline must equal the total energy pulled at each time step. This implies that the average temperature of the USPN remains constant while its value is not predefined. Solving ETOD3 appeared harder to converge as the pipeline storage capacity relaxes the thermal power balance equation. In ETOD4, the mass flow rate manipulation capability and pipeline storage capacity are neglected.

ETOD5 is based on the latest study proposed by [41] for BLTNs but altered for use in USPNs. In ETOD5, the network temperature is an optimization variable, but temperature losses, gains, or drops along the network are neglected. Therefore, the temperature remains constant throughout the entire network, although it can vary over time. Moreover, the mass flow rates have not been represented in the model, while the pipeline storage capacity is included. In addition, a single-node power balance approach represents the EGC and micro-electrical network. These assumptions make the optimization problem linear.

Fig.4.15 illustrates temperatures at eight key points in the USPN, including at the inlet of the HPs, CT, and HEX, determined by the dispatch strategies. It is noticeable in Fig.4.15 (a)-(d) that the inlet temperature of the heating HP in a building (H1,

H2, and H3) is always higher than or equal to the cooling HP of that building (C1, C2, and C3). Because, in the case of cooling demand, the cooling HP will inject heat into the USPN, which results in a higher network temperature at the inlet of the following heating HP. On the other hand, the inlet temperature of a cooling HP is always lower than that of the heating HP of the previous building. Because a heating HP, as a thermal consumer, pulls heat from the network, the network's temperature after that will drop. It is also observed in Fig.4.15 (a)-(d) that there is a gap between the inlet temperatures of the HPs of the first two buildings (C1, H1, C2, H2) and the inlet temperatures of the third building, CT, and HEX (C3, H3, CT, HEX). The heating demand of the second building is more than double that of the first building and triple that of the third building, resulting in a temperature drop in the network after H2, that the subsequent cooling HP cannot compensate for (see Fig. 4.13).

Fig.4.15(a) shows that during the early and late hours of the day when HEP is low, the temperatures are lower than during peak and mid-peak times. This results in lower heating COPs and higher cooling COPs during off-peak times, and lower cooling COPs and higher heating COPs during peak and mid-peak times, based on Eq.(6.1.31). The Eqs.(6.1.32)-(6.1.33) show that a lower COP corresponds to higher electricity consumption and the other way around. Therefore, during the off-peak hours, ICE-Harvest under ETOD1 tends to increase the electricity consumption in the heating HPs and reduce it in the cooling HPs. Instead, it reduces electricity consumption during peak and mid-peak hours in heating HPs but increases it in cooling HPs. The rationale behind this is that the case study belongs to a cold climate where the heating demands of the buildings dominate the cooling demands, resulting in a much higher electricity demand for heating than cooling. Thus, increasing or

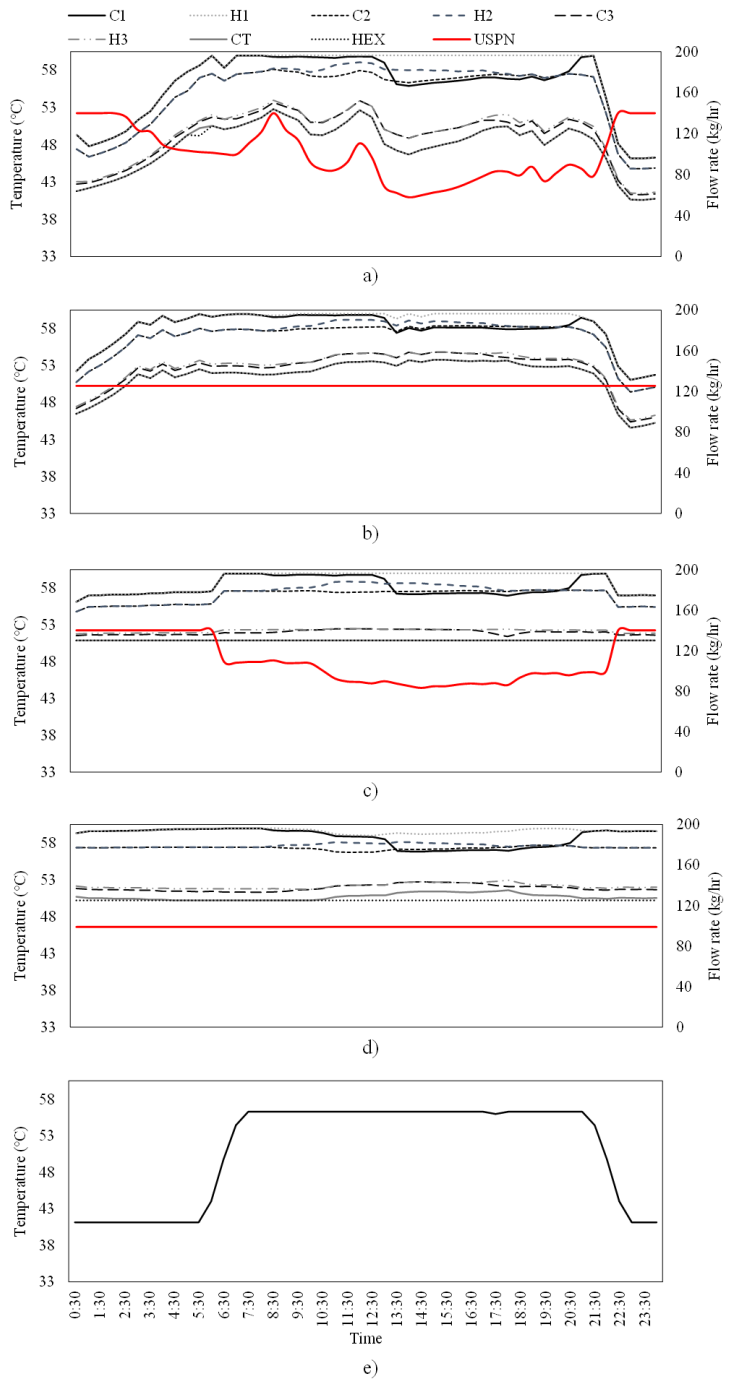

Figure 4.15: Temperatures and Mass Flow Rate in USPN Under (a) ETOD1, (b) ETOD2, (c) ETOD3, (d) ETOD4, e) ETOD5

decreasing the electricity demand in heating HPs represents increasing or decreasing the system's total electricity demand. Aside from this, most of the cooling demands occur during peak and mid-peak hours. Therefore, during peak and mid-peak hours, the contribution of electricity in heating HPs to serve the heating demand decreases, and this energy is directed to the cooling HPs. It allows for the harvested energy from the cooling processes to substitute for the electricity used by the heating HPs, thereby reducing the total electricity usage. The same behavior is also seen in other dispatch strategies.

Fig. 4.15(b) elucidates that the constant mass flow rate of USPN under ETOD2 is relatively high to minimize the temperature losses along the network. Furthermore, a high mass flow rate results in a lower temperature drop after heating HPs along the USPN. This prevents the COPs of heating HPs from falling as we move further down the network. Additionally, minor temperature variations are observed across HPs and, consequently, along USPN. Under ETOD3, as shown in Fig. 4.15(c), the profiles of mass flow rate and temperatures are slightly different from ETOD1's. Since the network's storage capacity is not considered, the total amount of energy injected into and drawn from the USPN must be equal at the time. Thus, the average temperature of the network remains constant during the day. Since ETOD3 has a lower degree of freedom in manipulating the temperature of the network than ETOD1, a smaller range of temperature variation is observed. In addition, ETOD3 maintains the average temperature of the network relatively higher for the same reason as ETOD2.

The operation of ICE-Harvest under ETOD4 is illustrated in Fig. 4.15(d). The

mass flow rate of the USPN is constant, and USPN has a constant average temperature throughout the network. Moreover, ETOD4 has the slightest temperature variation between all dispatch strategies and provides a relatively constant temperature along the USPN. Also, the average temperature of the network is higher than that of ETOD1, ETOD2, ETOD3, and ETOD5. The reason for that is, ETOD4 has less flexibility to change the temperatures at different nodes and, consequently, a tighter temperature variation range. So, the average temperature is optimized to reduce the electricity demand during peak hours when it has the greatest impact on operation costs.

Unlike the other dispatch strategies, ETOD5 does not consider temperature variations by heat injection/rejection or losses/gains throughout the USPN. Therefore, there is only one temperature for the USPN, as seen in Fig. 4.15(e). It is observed that, similar to ETOD1, the temperature is lower during the early and late hours of the day than during peak and mid-peak times. Moreover, the range of the network temperature variation is similar to ETOD1. That is, the network temperature ranges from 38°C to almost 58°C. This indicates that ETOD5 determined the optimal network temperature using the relaxed model similar to the average temperatures at different network nodes calculated by ETOD1.

Note that the temperature and mass flow rate variations do not affect comfort in ICE-Harvest, since they relate to the network side of HPs, not the building side. In other words, the buildings' energy demands are fully satisfied.

Fig. 4.16 and Fig. 4.17 can complement the investigation of the performance of ICE-Harvest under the developed dispatch strategies. Fig. 4.16 illustrates the profile of the electricity demand and, thereby, the demand management capability

of the system, while Fig.4.17 depicts the dumped energy via CT under the dispatch strategies.

As depicted in Fig.4.16(a) ICE-Harvest under ETOD1 exhibits more flexibility than ETOD2 in taking advantage of cheap electricity during off-peak hours. However, the electricity demand profile under each strategy is pretty similar during peak and mid-peak hours, and ETOD1 outperforms ETOD2 only for a few hours. Fig.4.16(b) illustrates that the electricity demand profile under ETOD3 is similar to ETOD2, but the gap between the ETOD1's and ETOD3' is wider than that between the ETOD1's and ETOD2's. In other words, ETOD3 has slightly fewer demand management capabilities than ETOD2.

The difference between the electricity demand profile of ETOD1 and ETOD4 is even more significant than the previous two (see Fig.4.16(c)). It is observed that ICE-Harvest under ETOD4 has not only lower flexibility to take advantage of low HEP but also lower flexibility to minimize the electricity demand during the peak and mid-peak hours, both of which lead to higher operating costs.

In Fig.4.17, it is demonstrated that under ETOD1, ETOD2, and ETOD5 dispatch strategies, ICE-Harvest can utilize all of the harvested energy wasted in conventional BAU. However, under ETOD4, a small portion of the energy is wasted via the CT.

As observed in Figs.4.16(d), the electricity demand of ETOD5 is consistently below ETOD1's; the green gap is not explained by ETOD5's superior capability to reduce electricity demand. The model used in ETOD5 is not accurate enough to estimate the actual electricity demand of the system since it does not consider the electricity consumption by WPs and temperature variations and losses along the network. In a dominant heating location similar to ICE-Harvest, the network's temperature

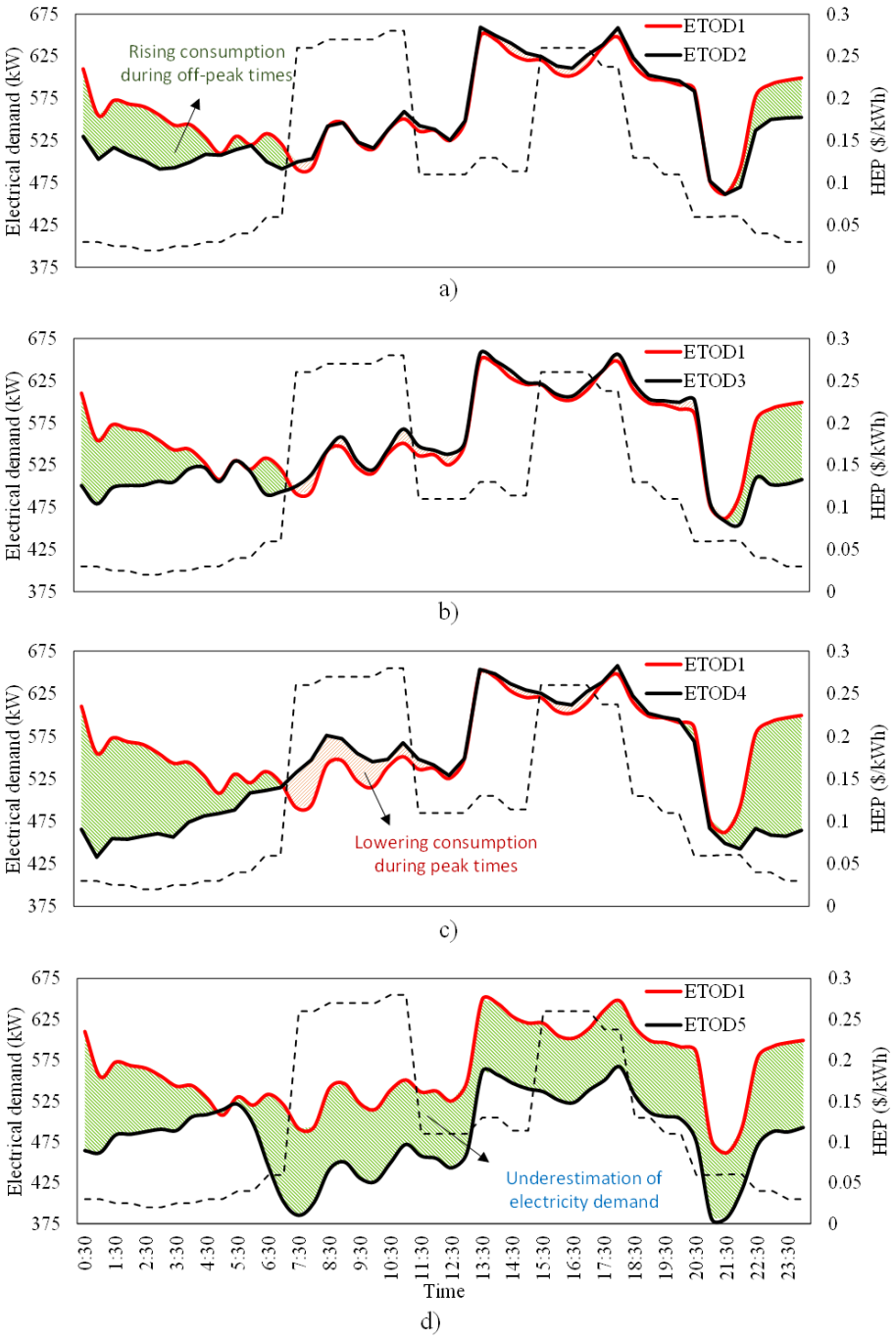

Figure 4.16: Electricity Demand of ICE-Harvest Under Different Optimal Dispatch Strategies.

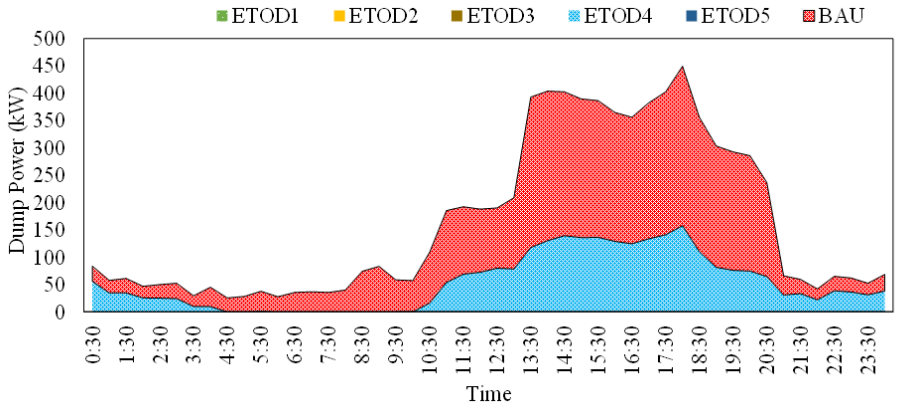

Figure 4.17: Dumped Power in the CT in BAU vs. ICE-Harvest Under Different Dispatch Strategies.

decreases after each building, resulting in lower COPs of the subsequent heating HPs, and, consequently, higher electricity demand than what ETOD5 is estimated. This temperature drop phenomenon is not represented in the optimization model of ETOD5.

4.3.6 Quantification of the simulation results

Table4.2 quantifies the comparison between BAU and ICE-Harvest. The operation cost of ICE-Harvest under ETOD1 is CA$ 829 per day lower than BAU. The operation cost of ICE-Harvest under ETOD1 is also lower than that under ETOD2, ETOD3, and ETOD4. However, the operation cost under ETOD5 is CA$1545 per day, CA$110 below the ETOD1's, which is due to the optimization model not taking all the details into account.

The conventional BAU system dumps 2.65 MWh of energy into the atmosphere by the CTs of the buildings. It is demonstrated in this study that ICE-Harvest has the capability to harvest and utilize that energy; however, the utilization of the harvested

Table 4.2: Results of the Operating Strategies vs. BAU

	ETOD1	ETOD2	ETOD3	ETOD4	ETOD5	BAU
Operation cost(CA$)	1655	1670	1674	1757	1545	2484
Dumped Energy in CT (MWh)	0	0	0	1.29	0	2.65
Imported Electricity in Peak Times (MWh)	0	0	0	0	0	2.34
Imported Electricity in Mid-peak Times (MWh)	0.25	0.28	0.31	0.39	0	2.95
Imported Electricity in Off-peak Times (MWh)	6.69	6.33	6.27	5.86	6.07	1.82
On-site Natural Gas Consumption (m^3)	3568	3627	3624	3807	3392	3581

energy depends on the employed dispatch strategy. Under ETOD1, ETOD2, ETOD3, and ETOD5, 100% of the harvested energy is utilized, while under ETOD4, 52% of that energy is used, and 48%, i.e., 1.29 MWh is dumped to the atmosphere via the CT.

ICE-Harvest maximizes off-peak power usage and minimizes peak power use, regardless of dispatch strategy. So, it does not import electricity from the grid during peak hours, while BAU imports 2.34 (MWh). However, during mid-peak hours, ICE-Harvest imports only 3.73%, 4.4%, 4.9%, and 6.6 % of the total imported electricity from the grid under ETOD1, ETOD2, ETOD3, and ETOD4, respectively. However, ETOD5 estimates the electricity import of the system during mid-peak hours to be zero.

In Ontario, Canada, gas power plants are the marginal power plants during the peak hours to follow demand fluctuations. Therefore, any variations in electricity demand during those hours will directly impact natural gas consumption and, consequently, GHG emissions. However, the total natural gas consumption in Table 4.2 reflects only the on-site consumption and does not account for the natural gas consumed in power plants to provide the electricity demand. So, ICE-Harvest that does not import power during peak hours and burns natural gas in the CHP with 60-70% efficiency will not cause natural gas to be burned in the peak natural gas

power plants with efficiency as low as 40%. Consuming less electricity during the peak from gas power plants and capturing heat from the cooling processes implies that the ICE-Harvest can reduce global GHG emissions. Also, ICE-Harvest can reduce the penetration rate of marginal power plants during peak hours and reduce the curtailment of renewable power plants during off-peak hours, both beneficial to the Ontario power grid.

4.4 Summary

This chapter proposes a detailed optimization model for the optimal dispatch of an ICE-Harvest equipped with a USPN. An accurate quasi-dynamic mathematical model for optimal dispatch of ICE-Harvest is developed, considering all the thermal and electrical characteristics to provide a deeper insight into the model. The proposed dispatch strategy accounts for temperature and mass flow rate manipulation, heat transfer, hydraulic constraints, and the thermal mass of the pipeline. Further, the optimization model incorporates constraints associated with the micro-electrical network, such as power flow constraints, part-load limitations, and ramping constraints of DERs.

The resultant optimization problem is an MINLP model that commercial solvers could not solve in the desired time. To solve the problem, a novel decomposition algorithm is proposed that breaks down the problem into two sequential layers, ETUC and ETOD. ETUC is a linear relaxation of the original problem and aims to determine the binary variables and a starting point for ETOD that uses the binary variables as fixed parameters and the starting point to determine the optimal values for the rest of the variables.

The proposed optimal dispatch (named ETOD1) showcases the flexibility of ICE-Harvest in performing waste energy harvesting and sharing, demand management, and switching between electricity and natural gas in response to the HEP. Four additional optimal dispatches (ETOD2, ETOD3, ETOD4, and ETOD5) are developed to explore further the necessity and effectiveness of the detailed modeling of the thermal and electrical characteristics in the optimization model.

In ETOD2, the mass flow rate in the USPN is not manipulated at each time step throughout the day and remains constant, but it is not predefined and determined throughout the optimization. In ETOD3, the pipeline storage capacity is not included in the model. ETOD4 does not consider the mass flow rate manipulation capability and pipeline storage capacity, while the optimal mass flow rate is computed through optimization. In ETOD5, it is assumed that the network temperature remains constant along the network while it is an optimization variable. So, the temperature losses, gains, or drops are neglected. In addition, the mass flow rates of the network are not represented in the model.

ICE-Harvest under ETOD1 is more energy-efficient and economical than under ETOD2, ETOD3, and ETOD4. Moreover, it exhibits more flexibility in altering the electricity demand in response to HEP. By not considering the thermal dynamics and heat transfer constraints, the ICE-Harvest' advantages and capabilities are overestimated under ETOD5. It is shown that the electricity demand of ICE-Harvest under ETOD5 is consistently below ETOD1's. Moreover, the natural gas consumption under ETOD5 is less than the rest of the dispatch strategies. Nevertheless, this is not due to the ETOD5's greater capability, but rather to the insufficient accuracy of the model. Under ETOD1, ETOD2, ETOD3, and ETOD5, the total harvested energy

from the cooling processes is used, while under ETOD4, 48% of that is dumped into the atmosphere via the centralized CT.

It is anticipated that the utilization of long-term geothermal storage and distributed CTs at buildings can help to minimize the dumped energy and maximize energy utilization, especially for cooling-dominated locations. So, it is recommended to expand this study further by incorporating those in the model.

Chapter 5

Multi-objective Operation-Aware Optimal Design of ICE-Harvest System

The objective of this chapter is to develop an optimization framework for the optimal design and operations of of the ICE-Harvest system. For this aim, a novel and detailed optimization framework for the optimal design and operation of the ICE-Harvest system is proposed and then linearized. A multi-objective approach is utilized considering the total annual cost (TAC) and GHG emissions as the objective functions. To assess the GHG emissions of energy systems, two approaches can be envisioned; average emission factor (AEF) and marginal emission factor (MEF). The AEF is calculated by dividing the total CO2 emissions of electricity generation by total electricity generation over a given period [56]. This implies that a change in demand will be spread equally across all generators, which does not match how electricity markets function as the marginal generator will compensate for the change

[56]. Therefore, AEF cannot properly reflect the effects of dispatchable demands on GHG emissions. The MEF concept, defined by the marginal generator, tracks the marginal change in the demand, and as such, it can reflect the actual change in GHG emissions caused by a change in the electricity demand. This allows a more accurate analysis of the benefits of manipulating the temperatures in reducing GHG emissions. Finally, a Pareto front curve using ϵ-constraint method is obtained, the compromise solution is chosen, and its operation is discussed.

5.1 Mathematical Formulation

5.1.1 Energy Generation Centre

To maintain the linearity of the thermal section, the energy generation center (EGC) is implemented as a single-node thermal power balance model ignoring the temperatures and mass flow rates constraints.

Combined Heat and Power Unit

The design and operation of the combined heat and power (CHP) unit can be modeled by a set of linear and nonlinear equations, given below [45]:

$$\eta_{d,t}^{CHP,elec} = \eta_0^{CHP,elec} \cdot \left[c + b \cdot Pl_{d,t}^{CHP} + a \cdot (Pl_{d,t}^{CHP})^2\right] \tag{5.1.1}$$

$$\eta_{d,t}^{CHP,elec} = \frac{P_{d,t}^{CHP}}{F_{d,t}^{CHP}} \tag{5.1.2}$$

$$Pl_{d,t}^{CHP} = \frac{P_{d,t}^{CHP}}{Cap^{CHP}} \tag{5.1.3}$$

$$Q_{d,t}^{CHP,max} = (F_{d,t}^{CHP} - P_{d,t}^{CHP}) \cdot \eta_0^{CHP,rec} \tag{5.1.4}$$

$$Q_{d,t}^{CHP,max} = Q_{d,t}^{JW} + Q_{d,t}^{EX,max} \tag{5.1.5}$$

$$Q_{d,t}^{JW} = k_{JW} \cdot Q_{d,t}^{CHP,max} \tag{5.1.6}$$

$$Q_{d,t}^{EX} \leq Q_{d,t}^{EX,max} \tag{5.1.7}$$

$$Q_{d,t}^{CHP} = Q_{d,t}^{JW} + Q_{d,t}^{EX} \tag{5.1.8}$$

$$|P_{d,t}^{CHP} - P_{d,t-1}^{CHP}| \leq \omega^{CHP} \cdot Cap^{CHP} \tag{5.1.9}$$

$$Cap^{CHP,min} \cdot U_{Cap}^{CHP} \leq Cap^{CHP} \leq Cap^{CHP,max} \cdot U_{Cap}^{CHP} \tag{5.1.10}$$

where U_{Cap} in this chapter signifies the existence of the asset.

Thermal and Electrical Energy Storage Systems

The detailed formulations for operating thermal and electrical storage systems units have already been introduced in chapter 4. The capacities of the stratified hot water tank (SHWT) and battery energy storage (BES) are defined as the volume of the tank (Cap^{TES}) and the maximum energy stored in the BES, respectively. The following equations are used to accommodate the capacities of the SHWT and BES in the

model.

$$SOC_{max}^{SHWT} = Cap^{SHWT} \cdot \rho^{w} \cdot cp^{w} \cdot (T^{h} - T^{c}) \tag{5.1.11}$$

$$SOC_{t}^{BES} \leq Cap^{BES} \cdot \tag{5.1.12}$$

$$Cap^{SHWT,min} \cdot U_{Cap}^{SHWT} \leq Cap^{SHWT} \leq Cap^{SHWT,max} \cdot U_{Cap}^{SHWT} \tag{5.1.13}$$

$$Cap^{BES,min} \cdot U_{Cap}^{BES} \leq Cap^{BES} \leq Cap^{BES,max} \cdot U_{Cap}^{BES} \tag{5.1.14}$$

Natural Gas Boiler

The operation of the NGB has already been explained in 4. The following equation relates the output heat power of the NGB and its capacity.

$$Q_{d,t}^{NGB} \leq Cap^{NGB} \tag{5.1.15}$$

$$|Q_{d,t}^{NGB} - Q_{d,t-1}^{NGB}| \leq \omega^{NGB} \cdot Cap^{NGB} \tag{5.1.16}$$

$$Cap^{NGB,min} \cdot U_{Cap}^{NGB} \leq Cap^{NGB} \leq Cap^{NGB,max} \cdot U_{Cap}^{NGB} \tag{5.1.17}$$

Heat Exchanger

The thermal power balance at the heat exchanger (HEX) connecting the EGC and unidirectional single-pipe network (USPN) is as follows:

$$Q_{d,t}^{HEX} = Q_{d,t}^{CHP} + Q_{d,t}^{NGB} + Q_{d,t}^{TES} \tag{5.1.18}$$

The following constraint describes the heat transfer across the HEX and relates two time-steps in a row.

$$H_{d,t}^{HEX} = \dot{m}_{d}^{USPN} \cdot cp^{w} \cdot (Ti_{d,t}^{USPN} - Ti_{d,t-1}^{HEX}) \tag{5.1.19}$$

Finally, the capacity of the HEX is defined by its area (A^{HEX}) as stated in the following equation:

$$H_{d,t}^{HEX} = U_{Cap}^{HEX} \cdot A^{HEX} \cdot \Delta T_{LM} \tag{5.1.20}$$

Cooling Tower

The operation of a cooling tower (CT) has been described in Chapter 4. The capacity of the CT is defined by the circulating water and can be expressed by the following set of equations.

$$\dot{m}_{d,t}^{CW} \leq Cap^{CT} \tag{5.1.21}$$

The on/off operation state of the CT ($U_{d,t}^{CT}$) is constrained by the existence of the unit, which is decided by UB^{CT}:

$$Cap^{CT,min} \cdot U_{Cap} \leq \dot{m}_{d,t}^{CW} \leq Cap^{CT,max} \cdot U_{d,t}^{CT} \tag{5.1.22}$$

$$U_{d,t}^{CT} \leq U_{Cap}^{CT} \tag{5.1.23}$$

5.1.2 Micro-Thermal Network

Unidirectional Single-Pipe Network

The detailed mathematical model used to describe the temperature drop and heat losses, pressure drop resulting from the friction, and water pumps' (WPs) electricity consumption are presented in Chapter 4. The only part that still needs to be added to the USPN's model is the maximum thermal energy that can be transferred by the pipeline, or in other words, its capacity:

$$\sum_{B=1}^{N_B}(Q_{d,t,B}^{load,H}) \leq Cap^{USPN} \tag{5.1.24}$$

Buildings and Heat Pumps

The mathematical model and the corresponding linearization proposed to describe the buildings and heat pumps (HPs) are introduced in Chapter 4. The remaining part corresponds to the capacity design of the HPs and chillers which is as follows:

$$Q_{d,t,B}^{load,H} \leq Cap_B^{HP,H}, Q_{d,t,B}^{load,C} \leq Cap_B^{HP,C} \tag{5.1.25}$$

Thermal Power Balance in USPN

The thermal energy balance in the USPN is described as follows:

$$Q_{d,t}^{HEX} = \sum_{B=1}^{N_B}(Q_{d,t,B}^{inj} - Q_{d,t,B}^{rej}) + \sum_{b=1}^{N_B} Q_{d,t}^{loss,b} + Q_{d,t}^{CT} \tag{22a}$$

$$Q_{d,t}^{HEX} = Q_{d,t}^{CHP} + Q_{d,t}^{SHWT} + Q_{d,t}^{NGB} \tag{22b}$$

5.1.3 Micro-Electrical Network

A single-node power balance model is developed to describe the micro-electrical network without considering losses and reactive powers. The electrical power balance can be written as

$$P_{d,t}^{CHP} + P_{d,t}^{BES} + P_{d,t}^{PCC} = \sum_{B=1}^{N_B}(P_{d,t}^{load,B}) + \sum_{i=1}^{N_{WP}}(P_{d,t,i}^{WP}) + P_{d,t}^{CT,fan} \tag{5.1.26}$$

$$P_{d,t,B}^{load} = P_{d,t,B}^{plug} + P_{d,t,,B}^{HP,H} + P_{d,t,B}^{HP,C} \tag{5.1.27}$$

where the system is assumed to be behind the meter and not allowed to export power to the grid. Two types of electrical loads can be assumed; controllable and uncontrollable loads. Uncontrollable loads are plugin loads, air conditioning, etc. and controllable loads are HPs and WPs

5.2 Optimization Problem

The optimization problem is represented by a mixed-integer non-linear programming (MINLP) model. To maintain a linear optimization problem, the nonlinear equations are linearized, so that the resultant optimization problem is a mixed integer linear programming (MILP) problem and is solved by CPLEX.

5.2.1 Linearization of the Model

CHP model

Non-linearity in the CHP model corresponds to Eqs. (5.1.1)-(5.1.3). To tackle this issue, these equations are merged, and the resultant equation is linearized, as follows:

$$F_{d,t}^{CHP} = \alpha \cdot P_{d,t}^{CHP} + \beta \cdot Cap^{CHP} \tag{5.2.1}$$

However, this equation does not work for the case that CHP is off, so it is modified by including the ON/OFF status of the CHP unit, as shown below:

$$F_{d,t}^{CHP} = \alpha \cdot P_{d,t}^{CHP} + \beta \cdot Cap^{CHP} \cdot U_{d,t}^{CHP} \tag{5.2.2}$$

Although there is still another non-linearity from the product of a binary variable ($U_{d,t}^{CHP}$) and a continuous variable (Cap^{CHP}), this non-linearity has an exact linear representation by considering $\Phi_{d,t}^{CHP}$=$Cap^{CHP} \cdot U_{d,t}^{CHP}$, as follows:

$$\Phi_{d,t}^{CHP} \leq Cap^{CHP} \tag{5.2.3}$$

$$LB^{CHP} \cdot U_{d,t}^{CHP} \leq \Phi_{d,t}^{CHP} \leq UB^{CHP} \cdot U_{d,t}^{CHP} \tag{5.2.4}$$

$$\Phi_{d,t}^{CHP} \leq Cap^{CHP} - (1 - U_{d,t}^{CHP}) \cdot LB^{CHP} \tag{5.2.5}$$

$$\Phi_{d,t}^{CHP} \geq Cap^{CHP} - (1 - U_{d,t}^{CHP}) \cdot UB^{CHP} \tag{5.2.6}$$

$$\Phi_{d,t}^{CHP} \leq Cap^{CHP} + (1 - U_{d,t}^{CHP}) \cdot UB^{CHP} \tag{5.2.7}$$

$$\Phi_{d,t}^{CHP} \cdot Pl_{min}^{CHP} \leq P_{d,t}^{CHP} \leq \Phi_{d,t}^{CHP} \tag{5.2.8}$$

Mass Flow rate in USPN

The mass flow rate in USPN ($\dot{m}_d^{USPN}$) is not an optimization variable, as it will not have a significant effect on the optimal sizes of the components, which are the preliminary goals of this optimization problem. Therefore, $\dot{m}_d^{USPN}$ is determined in the preprocessing stage using Eq. (5.1.18) under the worst-case scenario.

HPs Model

Nonlinearity exists in the HPs are linearized by the approach proposed in Chapter 4.

5.2.2 Objective functions

The objective functions of the optimization problem are TAC and GHG emissions. TAC includes capital expenditures of the selected units and operating costs such as operation and maintenance of equipment, imported electricity, and fuel consumption. GHG emissions are narrowed down into CO_2 levels.

TAC

The following equation describes the TAC of the system.

$$TAC = IC + \sum_{d=1}^{N_d} \sum_{t=1}^{N_t} (OMC_{d,t} + FLC_{d,t} + GC_{d,t} + WC_{d,t}) \tag{5.2.9}$$

where the following linear expressions are employed to estimate the investment (IC) and operation and maintenance (MC) costs of each component [2]:

$$IC = \sum_{q \in Q} IC^q \cdot CEPC^q \tag{5.2.10}$$

$$IC^q = kf \cdot (FC^q \cdot U^q_{cap} + VC^q \cdot Cap^q) \tag{5.2.11}$$

$$OMC = \sum_{q \in Q} OMC^q \tag{5.2.12}$$

$$OMC = OMF^q \cdot IC^q \tag{5.2.13}$$

The fuel costs ($FLC_{d,t}$), grid costs ($GC_{d,t}$), and water consumption costs ($WC_{d,t}$) are calculated by:

$$FLC_{d,t} = Pr^{fuel} \cdot (F_{d,t}^{CHP} + F_{d,t}^{NGB}) \tag{5.2.14}$$

$$GC_{d,t} = Pr_{d,t}^{elec} \cdot P_{d,t}^{PCC} \tag{5.2.15}$$

$$WC_{d,t} = Pr^{w} \cdot \dot{m}_{d,t}^{MU} \tag{5.2.16}$$

GHG Emissions Calculation

The sources of GHG emissions in the system are CHP, NGB, and grid. There are two approaches to evaluating the GHG emissions. In the first one, AEF is used as the grid's emission factor, which is determined by dividing the total CO_2 emissions of generators by total electricity generation, over a given period. Thereby, a change in demand will be spread equally across all generators. This approach does not take the effects of demand response and controllable loads on GHG emissions into account as, in reality, the change in demand will be compensated by the marginal generator, not all generators.

In the second approach, changes in the generation of the marginal generator are the main criteria to evaluate the emissions of a system with controllable loads. With this approach, base loads (noncontrollable loads) are handled by base-load generators, and marginal changes in demand are compensated by marginal generators. Therefore, to calculate the GHG emissions resulting from the noncontrollable loads, AEF is used, whereas MEF (emission factor of the marginal generator) is used for controllable loads. BES can act as a positive or negative controllable load; that is, during charging, it pulls power from the marginal generator, while during discharging, it reduces the

power of the marginal generator. So, the total GHG emissions by ICE-Harvest can be written as follows:

$$GHG = \sum_{d=1}^{N_d}\sum_{t=1}^{N_t}\{ef^{NGB}\cdot F_{d,t}^{NGB} + AEF_{d,t}\cdot P_{d,t,B}^{plug} + MEF_{d,t}\cdot(\sum_{B=1}^{N_B}(P_{d,t}^{load,B} - P_{d,t,B}^{plug}) + \sum_{i=1}^{N_{WP}}(P_{d,t,i}^{WP}) + P_{d,t}^{CT,fan} + P_{d,t}^{BES,ch} - P_{d,t}^{BES,dch})\} \quad (5.2.17)$$

where it is assumed that, when CHP unit is working, it plays the role of a marginal generator and determines the MEF.

5.2.3 Implementation of ϵ-constrain method

To solve the multi-objective optimization problem, ϵ- constraint method is employed, in which one of the objective functions is optimized, and the other one is turned into an extra constraint for the problem [57]. In this study, TAC is maintained as the objective function to be minimized while restricting GHG emissions within certain limits. This can be expressed as follows:

$$\begin{aligned} \min \quad & TAC \\ \text{s.t.} \quad & GHG \leq \epsilon \\ & Rest\ of\ the\ Constraints \end{aligned} \quad (5.2.18)$$

As these two objectives tend to be in conflict, the final solution of the optimization will be a set of points that lie on the Pareto front that presents the compromise between the two criteria. Then, a fuzzy logic-based method is utilized to determine the best compromise design solution for the ICE-Harvest.

Table 5.1: Simulation Parameters

	FC	VC	OMF	$CEPC$	Parameters
CHP	125	500	0.015	1.091	$\alpha = 2.48, \beta = 0.39, k_{JW} = 0.6$
NGB	23307	20	0.020	1.091	$\eta_0^{NGB} = 0.8, \omega^{NGB} = 0.5$
SHWT	125	156.3	0.015	1.091	$T^h = 80, T^c = 60$
BES	40.72	170.7	0.015	1.091	
HP	12195	327.1	0.008	1.055	$Ts^{B,C} = 10, Ts^{B,H} = 80$
HEX	-207	267.7	0.015	1.542	$U^{HEX} = 3.942, T^{LM} = 27$
CT	3402	0.104	0.015	1	$N_{cycles} = 6, EVF = 0.03$
Pipe	0.003	1130.5	0	1.166	$BPF = 0.8$

5.3 Simulation Studies and Discussions

For this study, real loads and meteorological data from a real case study in Ontario, Canada, are used. Regarding the electricity price, hourly Ontario electricity price (HOP) is employed. For the sake of simplicity, we consider a design day with an hourly resolution for each season (Winter, Spring, Summer, and Fall) to run the one-year simulation. The life span of the system is assumed to be 30 years, and the simulation data is given in Table 5.1. The optimization variables are capacities of the components, installation of the components, and operating variables such as on/off states of units, outputs of units, temperatures at different spots in USPN, COPs of HPs, fuel consumption, etc.

Results illustrate that relaxing the GHG emissions constraint displaces the TAC from the top left of the Pareto front to the bottom right (upper plot in Fig. 5.1). In the bottom of Fig. 5.1, the optimal configurations of the system obtained from the different points in the Pareto front are observed. Tightening the GHG emissions constraint leads to larger CHP and BES units and, consequently, a smaller NGB. It is important to notice that the NGB is installed once the GHG emissions overpasses

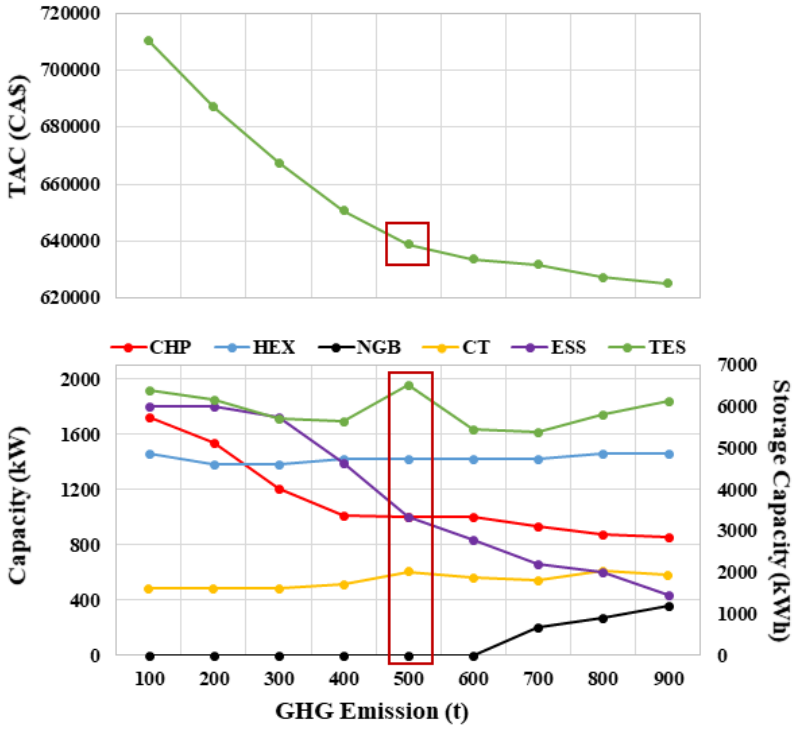

Figure 5.1: Pareto front (top) and the corresponding capacities of the components (bottom) relative to the GHG emission level.

600 tons. This is related to the fact that the CHP can generate both thermal and electrical energy at the expense of large investment costs. This would lead to more electricity being utilized in the HPs to mitigate the lack of another thermal energy source while avoiding large electricity imports from the grid. The HPs and CT capacities experience a slight decrease when TAC increases, but their variability is not so pronounced. The red rectangles in the Pareto front and system configuration plots distinguish the compromise design solution. In the compromise design solution, the TES achieves its maximum capacity, and the NGB is not required in the ICE-Harvest system. Note that, CHP is not the only source of heat in the system; there is also harvesting heat via cooling HPs, which provides a great deal of heat in the system.

The optimal operation of the system for the compromise configuration in different design days is illustrated in Fig. 5.2. In the winter, CHP represents the main thermal energy source, and storage systems have minor contributions. However, in other seasons, BES and TES have a critical role in correcting any kind of unbalances between supplies and demands. In the spring, TES is charged during the day and discharged during the night. CHP is partially utilized to charge the TES and meet the electricity demand when the electricity price is proportionally high. As expected, only during the summer, when the heating requirements are lower than the cooling, the CT participates in the system's operation by dumping the extra heat and decreasing the temperature of the USPN.

Several factors can affect the temperatures of different spots in the USPN, such as the type of previous HP (cooling or heating) and the size of its load, electricity price, etc. In Fig. 5.2, the average temperature at different spots in the USPN is shown in red dots for each season. It is observed that the average temperature in

winter is relatively high during the day. This is because the heating load of the system during the winter is so much higher than the cooling load, so the heating HPs are the dominant electrical load in the system. Therefore, by increasing the temperature of the USPN, the electricity demand for the heating HPs decreases while the electricity demand for cooling increases. This leads to lower electricity consumption in the winter, in which the peak demand of the Ontario grid occurs. However, during spring, the average temperature is even higher than that in the winter. The heating and cooling loads are almost at the same level, and electricity price is lower due to the curtailment of renewable sources in the power grid. Thus, the optimal solution is to consume more electricity in the cooling HPs from the grid than burning natural gas in CHP to provide the heating load. It is also noticed that when cooling demand is high, the average of temperatures in the USPN decreases, so the COPs of cooling HPs increase, and the electricity consumption and heat rejection from the HPs to USPN decrease. This also leads to lower energy waste in the CT. Note that, the higher the temperatures in the USPN, the higher the electricity demand for cooling HPs, and the greater the heat rejection from the USPN.

The capability of the ICE-Harvest system to manipulate the temperatures in the USPN to alter the electricity demand is demonstrated. Aside from this, the ICE-Harvest system has the capacity to diminish the energy that would have been curtailed in Ontario's power grid during the spring, by switching from natural gas consumption to electricity consumption. It is worth mentioning that demand response occurs in the ICE-Harvest system without affecting the comfort level of the occupants, as temperature manipulation takes place in the USPN and not in the buildings. In addition, 1072.409 MWh of energy has been harvested from the cooling HPs that

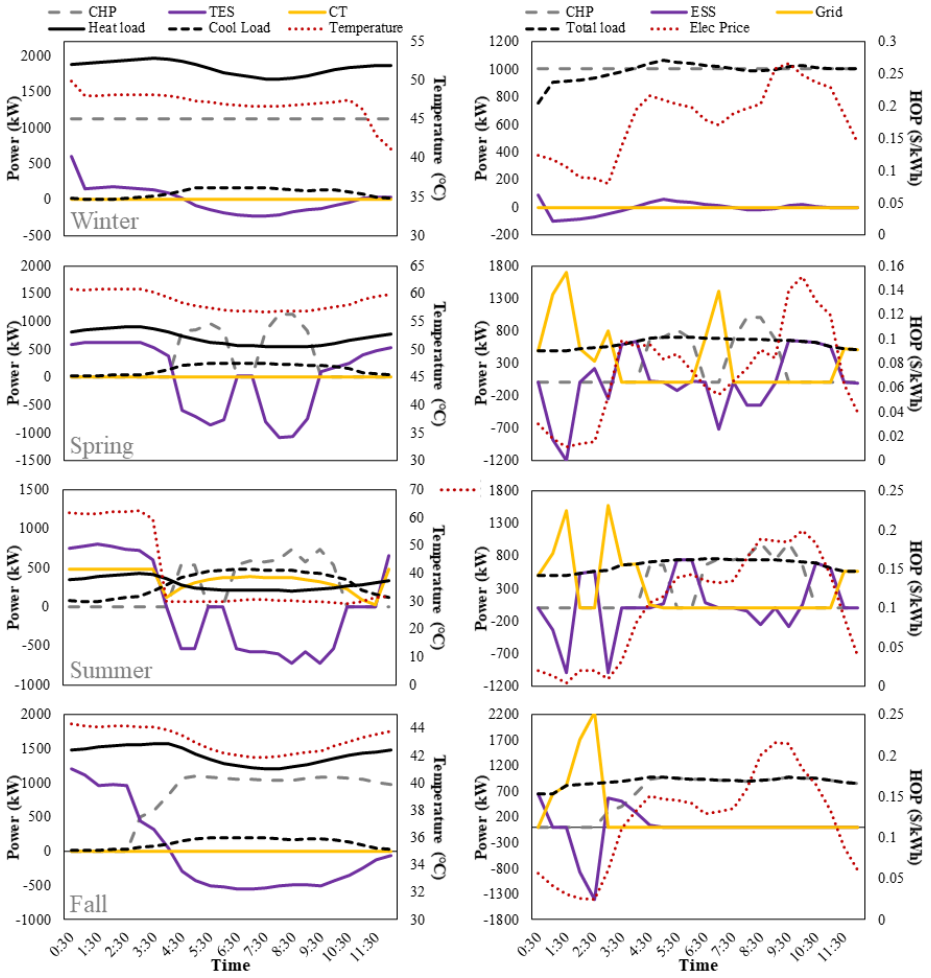

Figure 5.2: ICE-Harvest system's operation in each design day.

would normally be wasted in the CTs of the buildings.

5.4 Summary

This chapter tends to provide an accurate optimization model for the optimal design and operation of the ICE-Harvest system. The resultant nonlinear optimization model is linearized, and a multi-criteria approach is utilized considering TAC and GHG emissions. The MEF approach is applied to calculate GHG emissions and showcase

how dispatchable loads can reduce them. Finally, a Pareto front is obtained, and the compromise solution is determined. An increase in TAC to reduce GHG emissions is directly associated with a higher capital investment in CHP capacity. In addition, the compromise optimal configuration depicts the predominant participation of the CHP, SHWT, and BES in the operation of the ICE-Harvest system. Then, the capability of the ICE-Harvest system to manipulate the temperatures in USPN to maximize energy utilization and demand management without affecting the comfort of the occupants is demonstrated. In addition, it is shown that 1072.409 MWh of energy is harvested for the case study that would normally be wasted in conventional district heating networks.

Chapter 6

Long-Term Operation Optimization of ICE-Harvest System

The objective of this chapter is to develop a long-term optimization framework for the ICE-Harvest system to exploit the system's full potential in minimizing cost and GHG emissions by coordinating all the assets, realizing demand response and energy arbitrage, and energy harvesting and sharing. In this chapter, the full configuration of the ICE-Harvest system is implemented, taking into account the geothermal borehole field (GBF), direct heating (DRH) and direct cooling (DRC), and COP saturation.

For optimization, the problem is formulated as a mixed-integer nonlinear program (MINLP) that accurately describes the physical behavior of the system. The MINLP problem is then linearized into a mixed-integer linear program (MILP) that encapsulates the most relevant aspects and features.

6.1 Mathematical Model

6.1.1 Micro-Thermal Network

The micro-thermal network comprises an energy generation center (EGC) and a uni-directional single-pipe network (USPN), as shown in Fig.6.1. In the EGC, distributed energy resources (DERs) such as CHP, NGB, stratified hot water tank (SHWT), and GBF are installed in series to an HEX via a high-temperature header. The GBF is also connected to a mid-temperature header, linked to the high-temperature header via an HP. The mathematical models used to describe the CHP, SHWT, NGB, CT, and

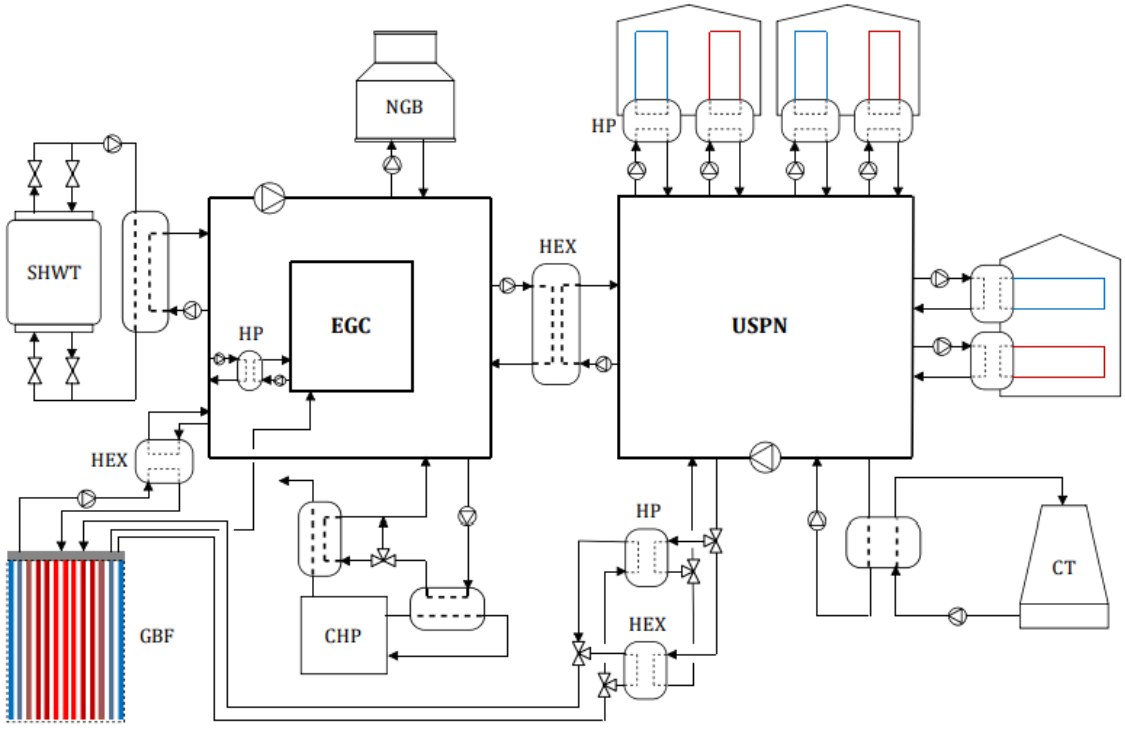

Figure 6.1: Schematic representation of the micro-thermal network of ICE-Harvest.

pipeline are fully explored and discussed in Chapter4. For the long-term operation optimization study of the ICE-Harvest system specifically, the exact mathematical

models proposed in Electrical and Thermal Unit Commitment (ETUC) explained in Chapter4 are utilized to maintain the linearity of the problem.

In the USPN, a group of buildings and their energy transfer stations (ETSs) are connected in series with a cooling tower (CT). In addition, there is a path that connects the USPN to the GBF via an ETS to store the excessively harvested energy in the GBF.

6.1.2 Energy Transfer Station

In the ICE-Harvest system, the ETS comprises an HP and an HEX that can be utilized for both heating and cooling purposes (see Fig. 6.2). This combined setup enables more efficient energy transfer based on the temperature of the USPN.

When the USPN temperature is sufficiently high for heating (or cold for cooling), heat transfer occurs directly through the HEX, eliminating the need for electricity consumption. However, if the USPN temperature is not suitable for direct heating (or cooling), the HP is employed to adjust the temperature by consuming electricity. The USPN temperature directly influences the electricity usage of the HP. As the USPN temperature approaches the desired temperature at the receiving end, the electricity consumption of the HP decreases, and vice versa. Therefore, it can be stated that the ETS plays a crucial role in managing electricity demand in the ICE-Harvest system.

The mathematical formulation devised to represent the parallel operation of the HEX and HP in ETS, considering HP's COP saturation, exhibits nonlinearity and nonconvexity. However, to simplify the equations, various techniques are employed

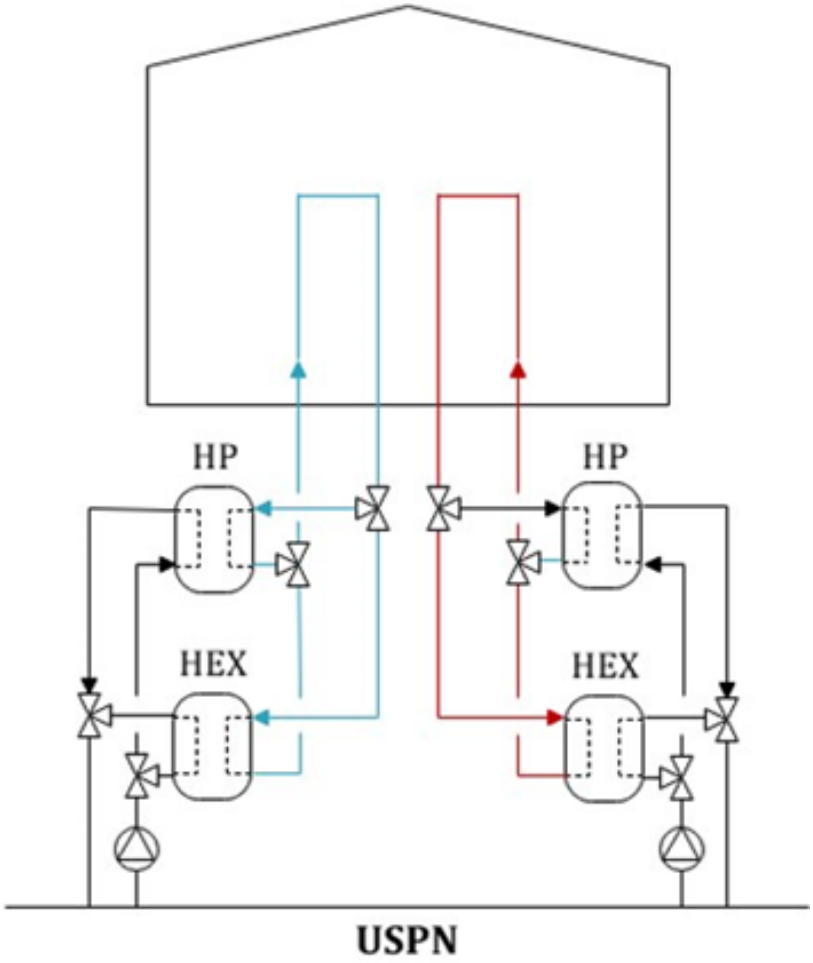

Figure 6.2: Schematic representation of the ETSs in a building

to linearize them, which are elaborated as follows.

$$T_t^{USPN} \geq T_t^{sc} \cdot (1 - U_t^c - U_t^h) + (T_t^{sc} - \Delta T^c) \cdot U_t^c + (T^{sh} + \Delta T^h) \cdot U_t^h \tag{6.1.1}$$

$$T_t^{USPN} \leq T^{sh} \cdot (1 - U_t^h) + T_{max} \cdot U_t^h \tag{6.1.2}$$

$$T_t^{USPN} - T^{sh} - \Delta T^h \leq (1 - U_t^h) \cdot M \tag{6.1.3}$$

$$T_t^{USPN} - T_t^{sc} + \Delta T^c \leq (1 - U_t^c) \cdot M \tag{6.1.4}$$

Heating

In the given context, the binary variables U_t^c and U_t^h are responsible for the realization of DRC and DRH, respectively. The constraints presented above establish a connection between these binary variables and the temperature of the USPN.

In Chapter 4, which presents the linearization of a single HP, the explanation primarily revolves around utilizing the inverse of COP, denoted as POC, instead of COP in the equations, while the implementation of HP's COP saturation and DRC and DRH are not covered in that particular chapter. The subsequent set of equations is intended to establish a relationship between the COP (or POC) of the HP and DRH.

$$POC_t^h = \frac{T^{sh} + T_t^{USPN}}{(T^{sh} + 273.15) \cdot \eta_h} \tag{6.1.5}$$

$$POC_t^{act} = \max\{POC_t^h, POC^{min}\} \tag{6.1.6}$$

where POC_t^h is the inverse of COP of the HP that is theoretically computed. In order to add the COP saturation, POC_t^{act} is defined as the actual POC.

If DRH occurs, U_t^h is 1, then HP is bypassed by the HEX. Hence, the COP of HP and, consequently, its electricity consumption cannot take any values. Therefore, the following equations are developed to take care of that.

$$POCU_t^h = POC_t^{h,act} \cdot (1 - U_t^h) \tag{6.1.7}$$

$$P_t^{HP,h} = H_t^{load} \cdot POCU_t^h \tag{6.1.8}$$

$$H_t^{load} = P_t^{HP,h} + H_t^h \tag{6.1.9}$$

Cooling

In the case of a cooling HP, if the temperature is sufficiently low, it becomes possible to directly meet the cooling demand by utilizing the HEX, bypassing the heat pump. DRC allows for more efficient cooling operations by leveraging the lower network temperature for direct cooling supply. If the network temperature is higher and the cooling demand cannot be met directly through the HEX, the cooling HP comes into play to lower the temperature. The following set of equations, similar to those used for the heating HP, represents this cooling operation.

$$POC_t^c = \frac{T_t^{USPN} - Ts_t}{(Ts_t + 273.15) \cdot \eta_c} \tag{6.1.10}$$

$$POC_t^{c,act} = \max\{POC_t^c, POC^{min}\} \tag{6.1.11}$$

$$POCU_t^c = POC_t^c \cdot (1 - U_t^c) \tag{6.1.12}$$

$$P_t^{HP,c} = C_t^{load} \cdot POCU_t^c \tag{6.1.13}$$

$$H_t^c = C_t^{load} + P_t^{HP,c} \tag{6.1.14}$$

Here, the equations possess non-linear terms that need to be linearized. These required linearizations are developed in the subsection 3.1.2. The same approach as the one presented in this section is utilized to represents the parallel operation of the HEX and HP that connect the GBF and USPN.

6.1.3 Geothermal Borehole Field

The GBF represents an underground structure comprising an array of boreholes designed to store significant amounts of thermal energy. In the ICE-Harvest system, this unit receives thermal energy from two distinct pathways (see Fig.6.3). The first pathway involves a direct transfer from the CHP via a HEX that connects to the hot header located within the EGC. The second pathway is in USPN, through the combined use of a heat pump (HP) and a parallel HEX. This energy would be wasted in the cooling tower (CT) in Chapter 4. When it comes to discharging, the GBF re-

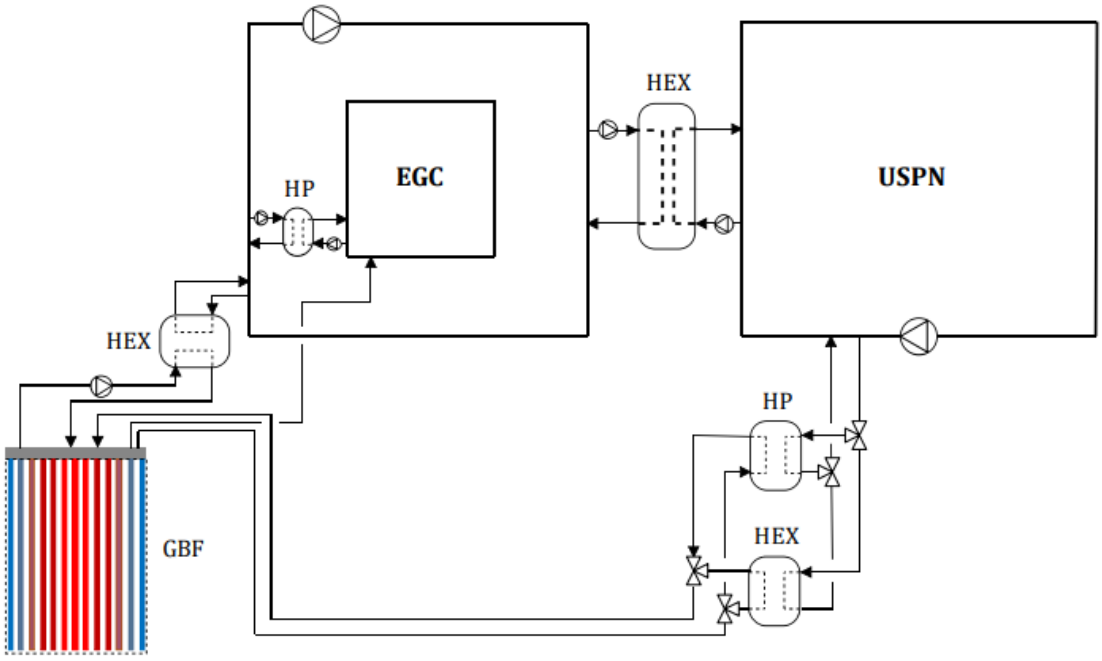

Figure 6.3: Schematic representation of the GBF.

leases the thermal heat to the mid-temperature header within the EGC. Subsequently, an HP facilitates the enhancement and transmission of the thermal heat to the high-temperature header. Further elaboration on the mathematical modeling of the GBF's

charging and discharging processes can be found in the subsequent sections.

It is assumed that the GBF, as the long-term thermal storage, remains constant in its charging and discharging state throughout the day, while its power level may vary hourly. On the other hand, the SWHT, which functions as the short-term thermal storage in the system, is responsible for handling minor fluctuations between the thermal supply and demand, and its charging or discharging state can change every hour.

EGC Side

$$H_{d,t}^{Dch,GBF} = Hs_{d,t}^{Dch,GBF} + P_{d,t}^{HP,EGC} \tag{6.1.15}$$

$$H_{d,t}^{Dch,GBF} = P_{d,t}^{HP,EGC} \cdot COP_{d,t}^{HP,EGC} \tag{6.1.16}$$

$$\begin{aligned} SOC_{d,t}^{GBF} = SOC_{d,t-1}^{GBF} \cdot \eta_{loss}^{GBF} + (H_{d,t}^{Chr,GBF} \cdot \eta^{Chr,GBF}) - \\ Hs_{d,t}^{Dch,GBF} / \eta^{Dch,GBF}) \cdot \Delta\tau \end{aligned} \tag{6.1.17}$$

$$SOC_{d,t}^{GBF} \leq SOC_{max}^{GBF} \tag{6.1.18}$$

$$H_{d,t}^{EMC,GBF} = H_{d,t}^{Dch,GBF} - H_{d,t}^{Chr,GBF} \tag{6.1.19}$$

$$H_{d,t}^{Chr,GBF} \leq U_{d}^{Chr,GBF} \times H_{Max}^{Chr,GBF} \tag{6.1.20}$$

$$Hs_{d,t}^{Dch,GBF} \leq U_{d}^{Dch,GBF} \times H_{Max}^{Dch,GBF} \tag{6.1.21}$$

USPN Side

In the Energy Transfer Station section, a comprehensive description of the HEX and HP operation, along with their mathematical representation, is provided. The same approach can be used to represent the HP and HEX connecting GBF and USPN, as follows:

$$H_{d,t}^{HR2ST} + H_{d,t}^{CT} \leq H_{d,t}^{LP,CL} \tag{6.1.22}$$

where this constraint is to ensure that the total recovered heat from the cooling process is higher than the summation of the energy rejected by the CT and sent to the GBF.

$$POC_{d,t} = \frac{T_t^f + T_{d,t}^{USPN}}{(T_{d,t}^f + 273.15) \cdot \eta} \tag{6.1.23}$$

$$POC_{d,t}^{act} = \max\{POC^{min}, POC_{d,t}\} \tag{6.1.24}$$

$$U'_{d,t} \cdot P_{min}^{HP,USPN} \leq P_{d,}^{hp} \leq U'_{d,} \cdot P_{max}^{HP,USPN} \tag{6.1.25}$$

$$U_{d,t} \cdot H_{min}^{HR2ST} \leq H_t^{HR2ST} \leq U_t \cdot H_{max}^{HR2ST} \tag{6.1.26}$$

$$U'_{d,t} \leq U_{d,t}\ ,\ U_{d,t} + U_d^{Dch,GBF} \leq 1\ ,\ U'_t + U_d^{Dch,GBF} \leq 1 \tag{6.1.27}$$

$HR2ST$ signifies heat recovery to storage, which means the recovered energy stored in the GBF. $U'_{d,t}$ indicates whether the charging of the GBF from USPN is occurring by HEX or HP, where a value of 1 indicates that the HP is responsible for charging, and a value of 0 indicates that the HEX is responsible, and $U_{d,t}$ signifies if charging CBG from the USPN is being realized at all. $U'_{d,t}$ and $U_{d,t}^{GBF}$ are mutually exclusive with $U_d^{Dch,GBF}$ meaning that if GBF is discharging, then GBF cannot be charged from the USPN at that time step.

However, it is important to note that the same mathematical model cannot be applied to represent the HEX and HP of the GBF. This is due to the fact that in buildings, the heating (and cooling) loads are predetermined, allowing the 6.1.8 and 6.1.13 to be linear. In GBF, the corresponding parameter in the model is the amount of total heat sent to the GBF, denoted as $H_{d,t}^{Chr}$, which is variable, introducing an additional nonlinearity. The objective is to mathematically model the parallel operation of the HEX and HP that connect the GBF and the USPN. The proposed approach involves the development of a linear regression model to approximate the relationship between $H_{d,t}^{Chr}$ and its influencing factors, which are the actual COP of the HP and the recovered energy stored from the cooling processes that are sent to the GBF.

The regression model is formulated using the following equation,

$$H_{d,t}^{Chr} = U_t' \cdot (k_1 + k_2 \cdot H_{d,t}^{HR2ST} + k_3 \cdot POC_{d,t}^{act}) \tag{6.1.28}$$

Here, k_1, k_2, and k_3 are the regression coefficients associated with the respective variables. The influencing factors considered in the regression model include $H_{d,t}^{HR2ST}$ and $POC_{d,t}^{act}$.

By applying the nonlinear mathematical model to fit the data into the regression model, the value of $H_{d,t}^{Chr}$ based on the known values of $H_{d,t}^{HR2ST}$ and $POC_{d,t}^{act}$. This linear regression approach provides a simplified representation of the relationship between the variables, enabling more efficient modeling and analysis of the parallel operation of the HEX, HP, and GBF within the USPN context.

Fig. 6.4 depicts the training data that has been fitted to the model, along with the corresponding estimated values. Notably, it can be observed that there is a strong

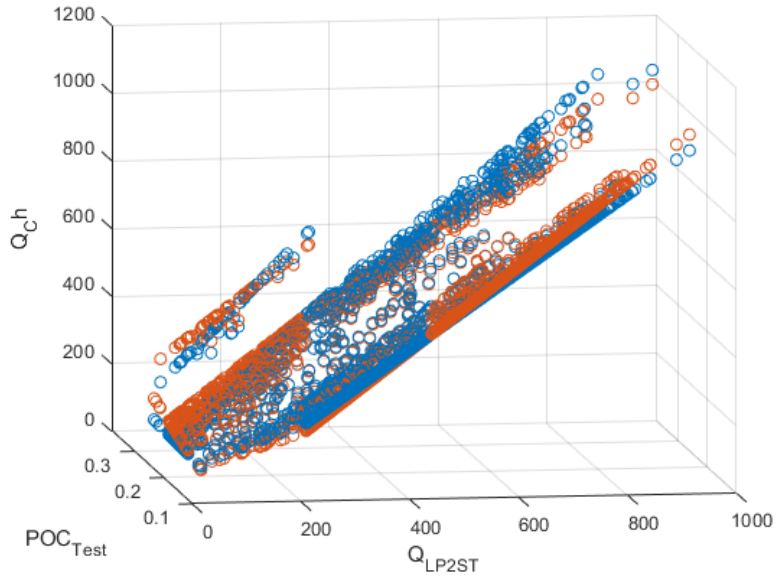

Figure 6.4: 3D plot for the fitted regression of GBF's COP

agreement between the fitted data and the estimated values, indicating a favorable alignment between the two.

The following set of equations is used to ensure

$$(1 - U'_t) \cdot H_t^{HR2ST} + (U_t - U'_t) \cdot (T_t^f + \Delta T) \leq T_t^{USPN} \tag{3h}$$

$$T_t^{USPN} \leq (2 - U_t - U'_t) \cdot T^{max} + U'_t \cdot T_t^f \tag{3i}$$

The high-temperature header in the EGC is connected to the pipeline in the USPN by a HEX. This allows the thermal energy generated by the different DERs to be transferred to the pipeline in the USPN. The following thermal energy balance expresses this:

$$H_t^{HEX} = H_t^{CHP} + H_t^{NGB} + H_t^{SHWT} + H_t^{GBF} \tag{6.1.29}$$

Pipeline

The thermal and hydraulic constraints associated with the USPN are discussed in 4. a simplified version of the proposed model fo pipeline in 4 is used in this chapter. The pipeline in the USPN is the medium through which thermal energy is exchanged between HEXs and HPs located in the buildings, the CT and the GBF. However, the total injected thermal energy is not necessarily equal to the total rejected energy at each time step. This feature turns this pipeline into a defacto thermal storage system, which can be mathematically stated as:

$$SOC_{d,t}^{USPN} = SOC_{d,t-1}^{USPN} + H_{d,t}^{USPN} \cdot \Delta\tau \tag{6.1.30}$$

where $SOC_{d,t}^{USPN}$ signifies the storage level of the pipeline, and it can also be expressed as:

$$SOC_{d,t}^{USPN} = M^{USPN} \cdot cp^{w} \cdot (T_{d,t+1}^{USPN} - T_{t}^{USPN}) \tag{6.1.31}$$

$$SOC_{min}^{USPN} \leq SOC_{d,t}^{USPN} \leq SOC_{max}^{USPN} \tag{6.1.32}$$

$$SOC_{min}^{USPN} = M^{USPN} \cdot cp^{w} \cdot T_{min}^{USPN} \tag{6.1.33}$$

$$SOC_{max}^{USPN} = M^{USPN} \cdot cp^{w} \cdot T_{max}^{USPN} \tag{6.1.34}$$

Here $T_{d,t}^{USPN}$ is the average temperature in the pipeline, and $H_{d,t}^{USPN}$ refers to the total heat of the pipeline, including both injections and rejection. To better understand that, the following is the thermal energy balance in the USPN:

$$H_{d,t}^{HEX} = H_{dmt}^{USPN} + \sum_{B=1}^{N_B} (H_{d,t,B}^{inj} - C_{d,t,B}^{Hrv}) + H_{t}^{loss} + H_{d,t}^{CT} + H_{d,t}^{HR2ST} \tag{6.1.35}$$

where $H^{inj}_{d,t,B}$ and $C^{Hrv}_{d,t,B}$ represent the injected heat from the USPN to the heating HPs and harvested energy from cooling processes, respectively.

6.1.4 Micro-Electrical Network

The micro-electrical network consists of electrical loads, a BES, a CHP system, and a micro-distribution network. In the long-term optimization, the mathematical model employed to describe the micro-electrical network is identical to the model utilized in the ETUC discussed in Chapter 4.

6.2 Optimization

The optimization problem is to determine the optimal dispatch of all devices and energy resources over a one-year horizon. The objective function is comprised of operation and maintenance costs and subject to the constraints presented in the previous section and those that are cited from Chapter 4.

$$CS^{Tot} = \sum_{d=1}^{365}(\sum_{t=1}^{24}(CS^{fuel}_{d,t} + CS^{PCC}_{t} + CS^{O\&M}_{t} + CS^{w}_{d,t} + CS^{SU}_{t})) \tag{6.2.1}$$

$$CS^{fuel}_{d,t} = (F^{NGB}_{t} + F^{CHP}_{t}) \cdot Pr^{fuel} \cdot \Delta\tau \tag{6.2.2}$$

$$CS^{PCC}_{t} = (P^{imp}_{d,t} \cdot HEP^{imp}_{t} - P^{exp}_{d,t} \cdot HEP^{exp}_{t}) \cdot \Delta\tau \tag{6.2.3}$$

$$CS^{O\&M}_{d,t} = \sum_{g=1}^{3}(P^{g}_{t} \cdot Pr^{g,O\&M}) \tag{6.2.4}$$

$$CS^{SU}_{d,t} = \sum_{g=1}^{3}(SU^{g}_{d,t} \cdot Pr^{g,SU} + SD^{g}_{t} \cdot Pr^{g,SD}) \tag{6.2.5}$$

$$CS^{w}_{d,t} = \dot{m}^{MU}_{d,t} Pr^{w} \cdot \Delta\tau \tag{6.2.6}$$

6.2.1 Linearization

To simplify and handle the non-linear terms within the proposed non-convex MINLP model, various linear approximations have been devised. Specifically, the linearizations for the CHP and HP, excluding COP saturation, were previously discussed in Chapter 4. Furthermore, the linearization method for the GBF USPN-side HP was presented earlier in its corresponding subsection. The following is the linearization approach developed for any HP and HEX employed in the system, whether it is the ETS of the buildings or the GBF. The equations provided below are specific to a heating ETS, but the same equations can be applied to other HPs parallel with HEXs.

HEXs/HPs Model

Some of the equations in the model that described the parallel operation of HEXs and HPs have to be also linearized. For instance, COPs are reformulated by implementing a new set of linear equations with new variables, named $POC^{h}_{t,B}$ and $POC^{c}_{t,B}$. These new variable are the inverse expressions of $COP^{h}_{t,B}$ and $COP^{c}_{t,B}$, respectively:

$$P^{HP,h}_{t,B} = H^{load}_{t,B} \cdot POC^{h}_{t,B} \ , \ P^{HP,c}_{t,B} = C^{load}_{t,B} \cdot POC^{c}_{t,B} \tag{6.2.7}$$

$$POC^{h}_{t,B} \geq \frac{Ts^{h} - T^{USPN}_{t}}{\eta^{h}_{0} \cdot Ts^{h} + 273.15} \tag{6.2.8}$$

$$POC^{c}_{t,B} \geq \frac{T^{USPN}_{t} - Ts^{c}}{\eta^{c}_{0} \cdot Ts^{c} + 273.15} \tag{6.2.9}$$

$$POC_{min} \leq POC^{h}_{t,B} \leq POC_{max} \tag{6.2.10}$$

$$POC_{min} \leq POC^{c}_{t,B} \leq POC_{max} \tag{6.2.11}$$

Here, the linearization of Eq. 6.1.6 requires the definition of the binary variable y and the following equaitons:

$$POC_t - POC_{act}^{min} \leq M \cdot y_t \tag{6.2.12}$$

$$POC_{act}^{min} - POC_t \leq (1 - y_t) \cdot M \tag{6.2.13}$$

Then, another set of eqs. is defined:

$$POC_t^{act} \geq POC_t \tag{6.2.14}$$

$$POC_t^{act} \geq POC_{act}^{min} \tag{6.2.15}$$

$$POC_t^{act} \leq POC_t + M \cdot (1 - y_t) \tag{6.2.16}$$

$$POC_t^{act} \leq POC_{act}^{min} + M \cdot y_t \tag{6.2.17}$$

To represent the saturation of the HPs, the following eqs. are required:

$$POC_h^{max} = \frac{T^{sh} - T_t^{sc} + \Delta T^c}{(T^{sh} + 273.15) \cdot \eta_h} \tag{6.2.18}$$

$$POC_c^{max} = \frac{T^{max} - T_t^{sc}}{(T_t^{sc} + 273.15) \cdot \eta_c} \tag{6.2.19}$$

There is a relationship between y and U_t^c and U_t^h, which is highlighted in the following set of eqs.:

$$U_t^c + U_t^h \leq 1 \tag{6.2.20}$$

$$y_t + U_t^h \leq 1 \tag{6.2.21}$$

$$U_t^c \leq 1 \tag{6.2.22}$$

Now, Eq. 6.1.7 is linearized by using the following set of equations:

$$0 \leq POCU_t^h \leq POC_h^{max} \tag{6.2.23}$$

$$POC_{act}^{min} \cdot (1 - U_t^h) \leq POCU_t^h \leq POC_h^{max} \cdot (1 - U_t^h) \tag{6.2.24}$$

$$POC_t^{h,act} - (U_t^h \cdot POC_h^{max}) \leq POCU_t^h \leq POC_t^{h,act} - (U_t^h \cdot POC_{act}^{min}) \tag{6.2.25}$$

$$POCU_t^h \leq POC_t^{h,act} + (U_t^h \cdot POC_h^{max}) \tag{6.2.26}$$

6.3 Simulation Studies and Discussions

6.3.1 Test System Description

The effectiveness of the proposed long-term optimal dispatch strategy is validated by utilizing data from an actual case study conducted in Ontario, Canada. This particular study focuses on four public complex buildings—namely, a residential building, a library, a seniors' center, and a YMCA—all located behind the meter. Fig. 6.7 depicts the hourly energy demands of the system during the course of the year. As for the hourly electricity price, the most recent suggested Time-of-Use electricity tariff by Ontario Energy Board is used, according to which the weekly electricity price has profile shown in 6.6.

The capacities of DERs and other relevant parameters are determined using the methodology outlined in the publication by Cotton et al. [44]. The USPN has a length of 1000 m, and the initial states of charge for the GBF, BES, and SHWT are considered as optimization variables. The simulation time interval is set at 1 hour. In this system, it is assumed that the GBF remains consistently either in a charging or discharging state throughout the day, with its power level potentially varying hourly. Conversely, the BES and SHWT, serving as short-term thermal storage components, are responsible for managing minor fluctuations between supply and demand. Consequently, their charging or discharging state may change every hour.

6.3.2 Community-Wide Waste Heat Harvesting and Sharing

To gain insights into the effectiveness of the ICE-Harvest system in community-wide waste heat harvesting and sharing, the cumulative heating and cooling demand of

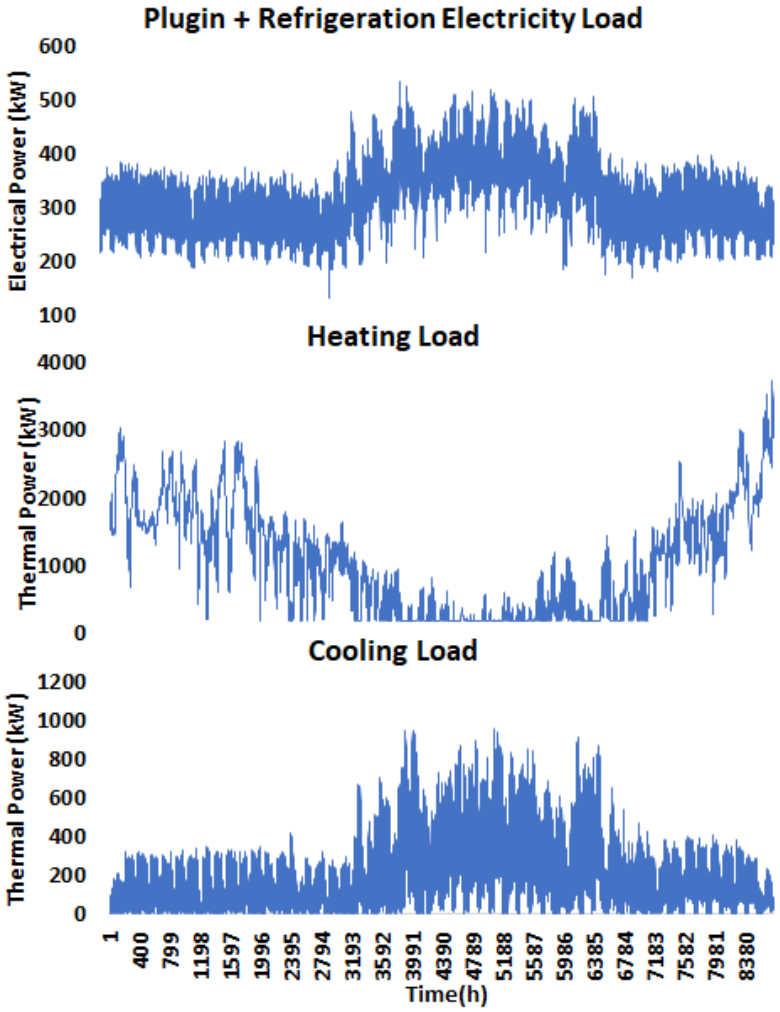

Figure 6.5: Instantaneous Energy Demands in ICE-Harvest System

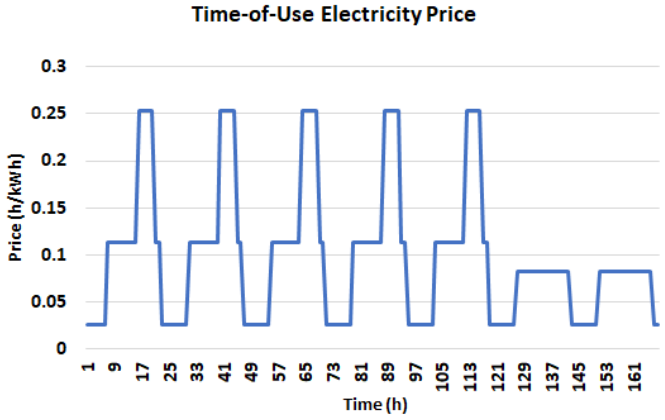

Figure 6.6: Time-of-Use Electricity Price

the community is presented in Fig. 6.7. It is evident that in this community, the total heating load surpasses the cooling load during the winter, whereas the cooling load exceeds the heating load during the summer. This observation helps to better understand the system's performance.

As thoroughly explained and showcased in Chapter 4, the ICE-Harvest system achieves waste heat recovery through the utilization of cooling ETSs. The total energy supplied by each cooling ETSs is the combination of the building's cooling/refrigeration load and the electricity consumed by the HP. The proportion of these two components is determined by the COP of the HPs, which, in turn, depends on the optimization variable of the network temperature. Fig. 6.8 displays the ratio between the electricity consumption of the cooling HPs and the cooling/refrigeration loads in the system for each month. It is illustrated that, during the summer and spring, the cooling loads/refrigeration significantly dominate the electrical consumption of the cooling HPs. This dominance of cooling loads over electrical consumption is still present during colder seasons, although the difference is not as significant.

It can be observed in the pie-chart that the proportion of electricity consumption

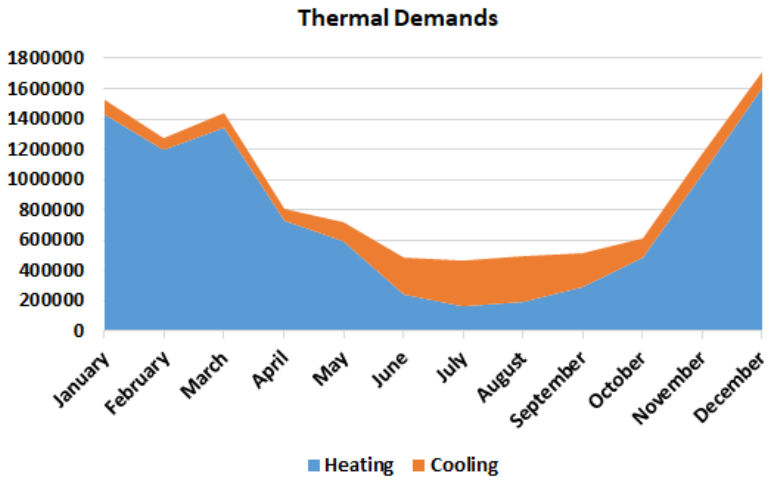

Figure 6.7: The Cumulative Heating and Cooling Demands.

for the cooling heat pumps is 21%, while the remaining 79% is attributed to the cooling loads. This indicates that the annual COP of all cooling ETFs together is 4.762, which is notably higher than the annual COP of individual cooling HPs alone, which would be below 3.

Regarding the utilization of the harvested energy, Fig. 6.9 demonstrates that in colder seasons, the majority of the harvested heat is instantly shared within the community to fulfill the heating demand. Conversely, during the summer months, when cooling demand rises and heating demand declines, a larger proportion of the harvested heat is stored in the GBF.

Furthermore, it is observed in the pie-chart of Fig. 6.9 that only 1% of the harvested energy is discarded by the CT. However, this energy dumping occurs exclusively during the months of July and August, as depicted in Fig. 6.8. During this period, the harvested energy primarily originates from the Heat Exchanger (HEX) and cooling loads, with the electrical consumption of the cooling HPs making a minimal contribution. Consequently, we can conclude that no energy is consumed by the

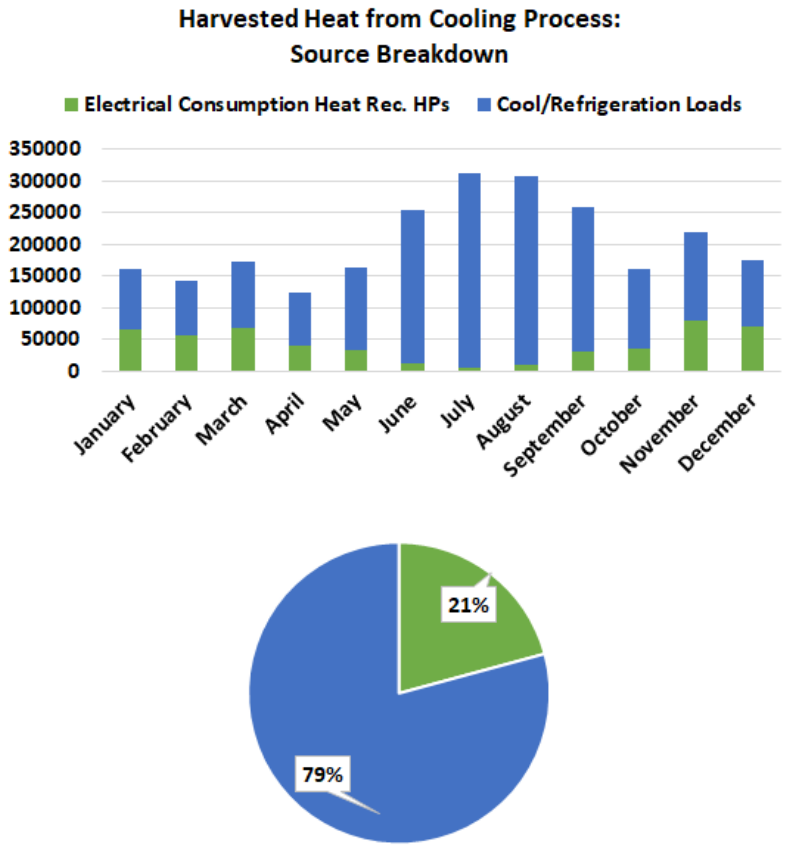

Figure 6.8: The Breakdown of Sources of Harvested Heat from Cooling Process

cooling HPs to harvest the energy that is subsequently dumped by the CT.

6.3.3 Overall Performance of System

The temperature of the network serves as one of the primary driving forces for the phenomena discussed in this chapter and those to be discussed later. Fig. 6.10 depicts the monthly average network temperature throughout the year. It can be inferred that the average network temperature is higher during the colder seasons compared to the warmer seasons. This can be attributed to the fact that a higher network

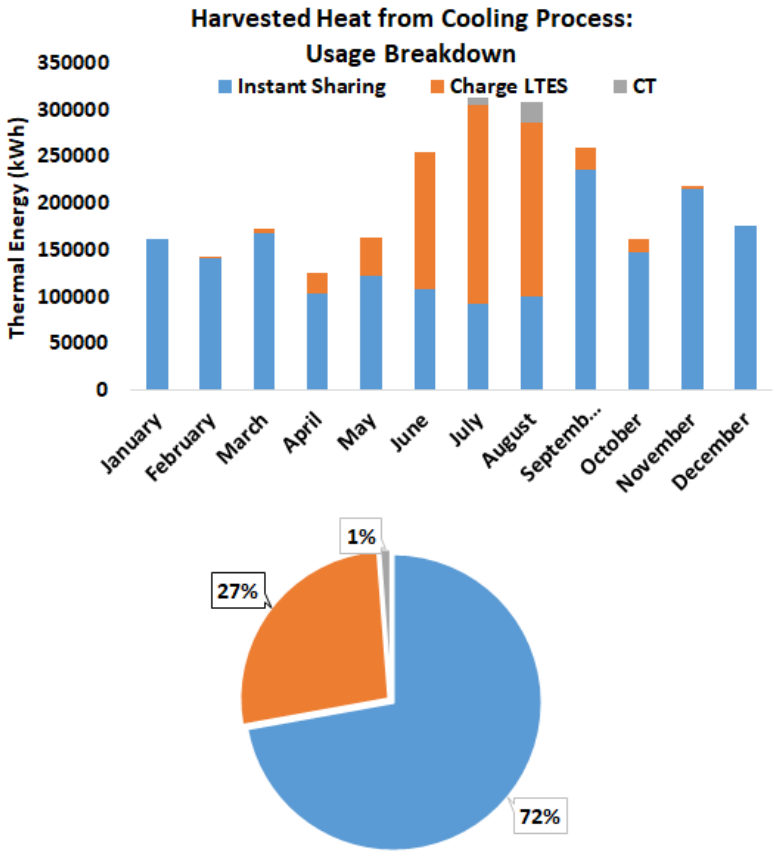

Figure 6.9: The Breakdown of Utilization of Harvested Heat from Cooling Process.

temperature results in a higher Coefficient of Performance (COP) for heating Heat Pumps (HPs), leading to lower electricity consumption. As shown in Fig. 6.7, during the winter and fall seasons, heating demands outweigh cooling demands, hence increasing the network temperature reduces the total electricity consumption of the system. Similar reasoning applies to the warmer seasons, where lower network temperatures lead to the decreased total electricity consumption of the system due to the dominance of cooling demands over heating demands. Furthermore, lowering the network temperature results in reduced energy injected into the network from cooling

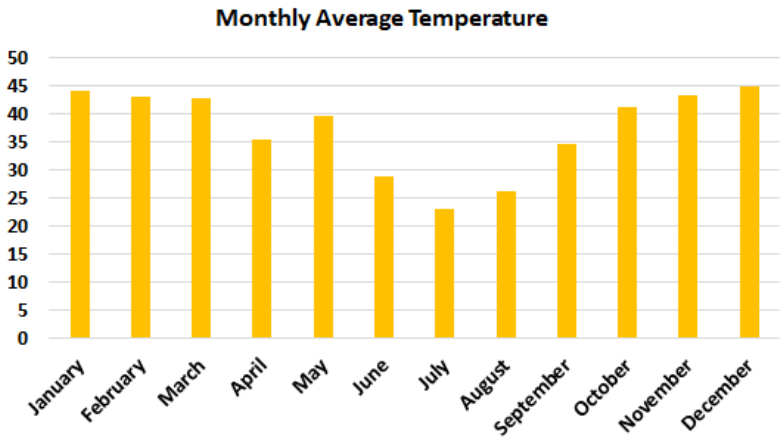

Figure 6.10: Monthly Network Temperature Over the Year

processes, which is advantageous during the warmer seasons when heating demands are minimal.

Fig. 6.11 presents the monthly total electrical power generated by the CHP unit. As anticipated, it is evident that, in line with the network temperature, the CHP system generates more energy during the colder seasons compared to the warmer seasons. This can be attributed to the higher heating demand during the colder seasons. Conversely, during the warmer seasons, the heating demand is considerably reduced, and as shown earlier, a significant portion of the harvested energy from cooling processes is directly stored in the GBF. It is important to note that this figure only represents the monthly operation of the CHP and does not account for hourly variations. In other words, there may be specific hours during the summer when there is no cooling demand and, subsequently, no harvested energy. During such times, the CHP system may provide the required heat power for the system. More details about the hourly operation of the system have been discussed in Chapter 4. To provide further clarity on the monthly operation of the CHP system, Fig. 6.12

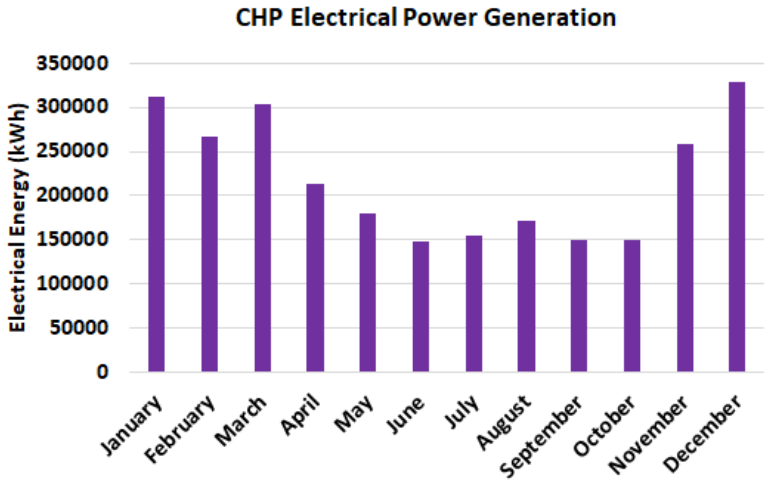

Figure 6.11: Monthly Electrical Power of CHP

showcases the surplus heating energy generated by the CHP stored in the GBF. It can be observed that during February and December, only a negligible amount of heating energy is sent to the GBF for storage. In January, the entire heating power of the CHP is either immediately utilized by the heating demand or stored in the SHWT for same-day usage. As mentioned earlier, during the summer season, a substantial quantity of the CHP's heating energy is stored in the GBF.

Regarding the analysis of electrical demand, Fig. 6.13 presents the breakdown of electricity consumption within the system. It can be observed that 47% of the total electricity consumption is attributed to plugin loads. Heating HPs account for approximately 29% of the total electricity consumption, which is more than three times higher than the 8% consumed by cooling HPs. In the third position, the HP in the EGC utilized for GBF discharging is, while the other HP of the GBF in the USPN contributes only 2% to the total electricity consumption. Fig. 6.14 showcases the distribution of electricity consumption by the cooling HPs according to Time-of-Use. The figure reveals that a minor portion of electricity consumption occurs

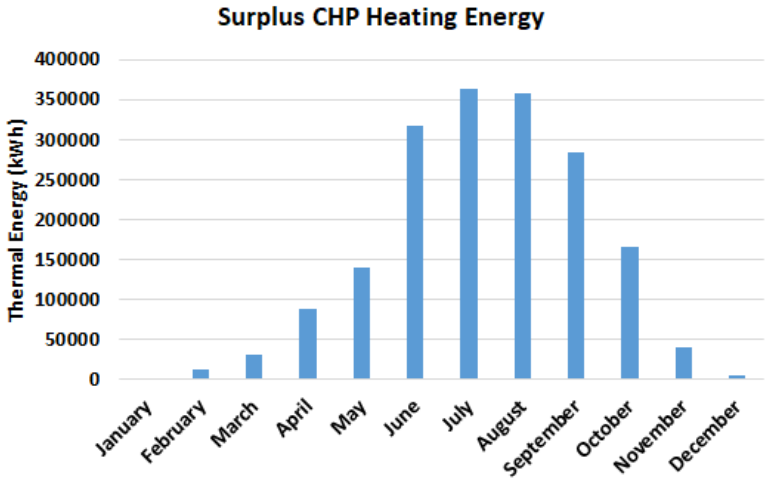

Figure 6.12: Monthly Surplus Heat Energy of CHP

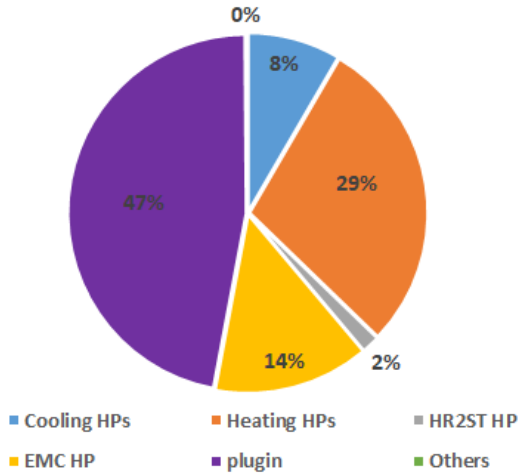

Figure 6.13: Distribution of Electricity Consumption in the ICE-Harvest System

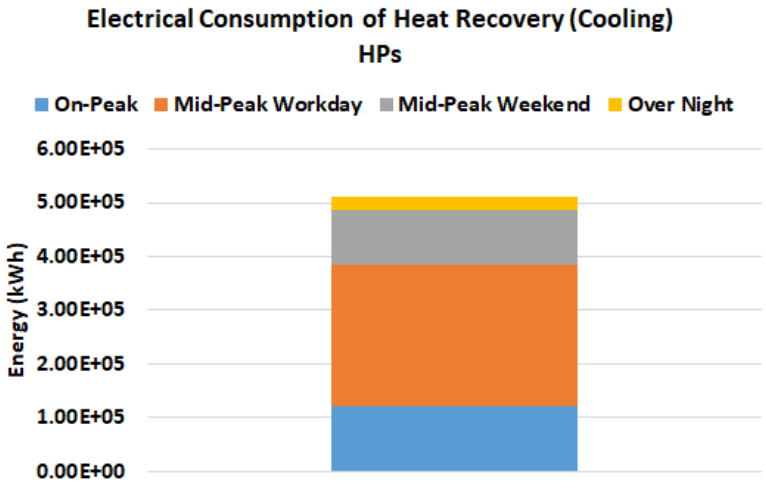

Figure 6.14: Electricity Consumption Analysis of Cooling HPs Based on Time-of-Use

during the overnight period when electricity prices are low, while the majority of consumption takes place during mid-peak hours.

6.3.4 Long-Term Operation of Geothermal Borehole Field

Fig. 6.9 presented the stored amount of harvested energy in the GBF. In Fig. 6.15, the total energy stored in the GBF from the USPN path is depicted, which generally can be broken down into the amount of harvested energy sent to the GBF and the electricity consumption of the GBF's HP on USPN side. As discussed in the previous subsection, it is observed that the GBF primarily receives energy from the USPN path during the summer and spring seasons, with a significant portion corresponding to the harvested energy. This indicates that the average annual COP of the ETS for the GBF is 7.692, surpassing that of the ground source HP.

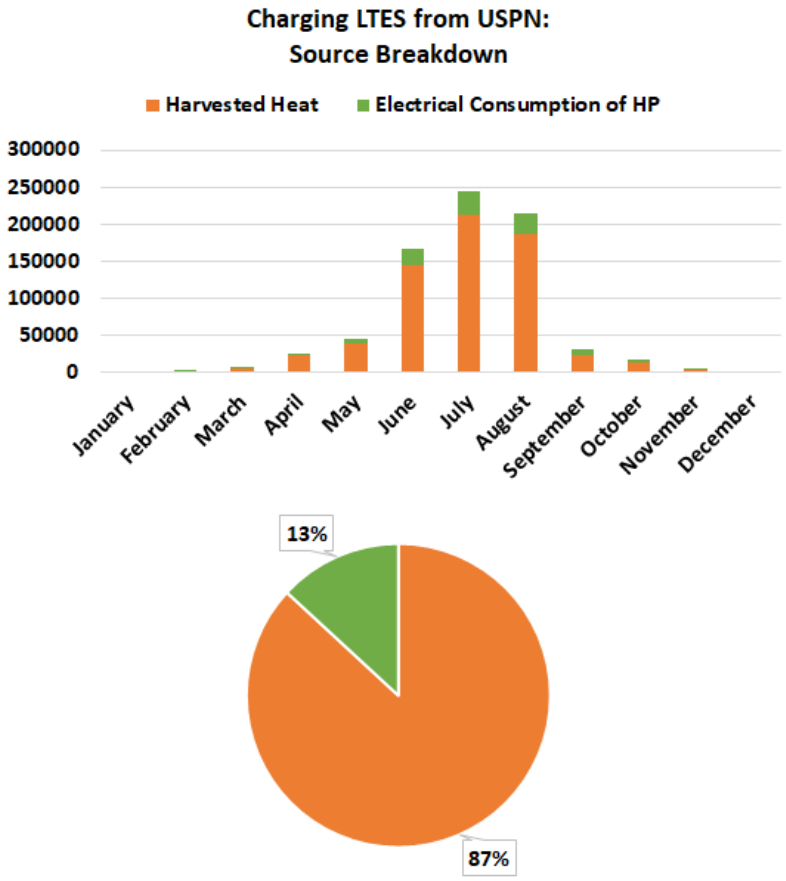

Figure 6.15: Breakdown of Energy Sources Contributing to GBF Charging

Fig. 6.16 illustrates the state-of-charge of the GBF, offering insights into its performance across different seasons. It can be observed that, in general, the GBF undergoes charging during the warmer seasons and discharging during the colder seasons. Upon closer examination of the figure, it becomes apparent that during the winter, the GBF is discharged to meet the heating demand until its usable state-of-charge (SOC) reaches zero in the early days of spring. During spring, there is no specific trend for the GBF's SOC as it experiences both charging and discharging periods. As summer arrives, the GBF begins to charge, gradually reaching its maximum SOC

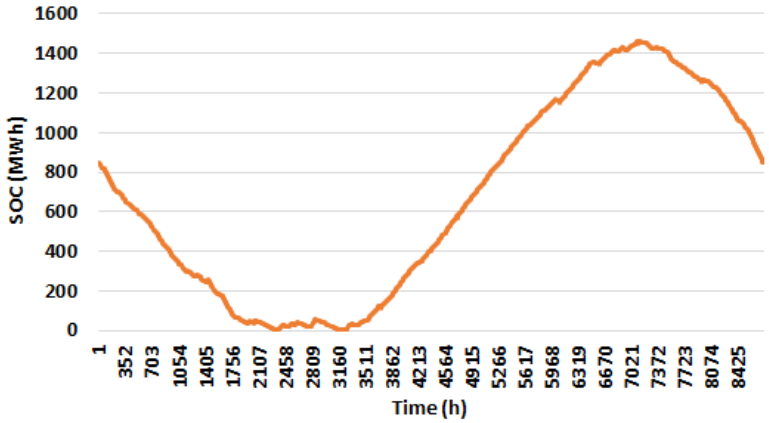

Figure 6.16: State-of Charge of the GBF

point, which serves as a turning point for its operation. Subsequently, the GBF starts discharging again to fulfill heating demands in the fall.

6.3.5 Offset Fossil Fuel-Burned Power Plants

To showcase the ability of the ICE-Harvest System in reducing reliance on fossil fuel power plants operating during peak hours in Ontario, examining the imported power by the system during different electricity price intervals can provide valuable insights. In this context, Fig. 6.17 compares the imported power of the ICE-Harvest system with the Business-as-Usual (BAU) scenario for on-peak hours, mid-peak hours on workdays, mid-peak hours on weekends, and overnight hours. The BAU scenario represents actual data. It can be observed that the ICE-Harvest system does not import electricity power except during off-peak hours when renewable energy resources contribute significantly to the Ontario power grid. Additionally, there is only a negligible amount of imported power during mid-peak hours on weekends.

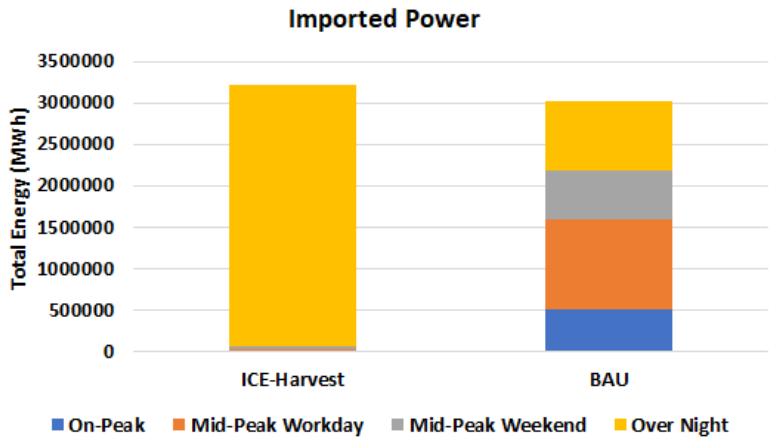

Figure 6.17: Distribution of Imported Power of ICE-Harvest System Vs. Business-as-Usual

This figure also highlights the ICE-Harvest system's capacity to implement demand response strategies without compromising occupant comfort. The system's operation aligns with the desired grid conditions by importing power exclusively during off-peak hours while ensuring that the energy demands of the community occupants are fully met without any impact on their comfort.

Furthermore, to gain a deeper understanding of the ICE-Harvest system's ability to offset fossil fuel power plants in the Ontario power grid, the operation of the CHP unit during on-peak hours, mid-peak hours on workdays, mid-peak hours on weekends, and overnight hours is depicted in Fig. 6.18. It can be observed that the CHP unit is not utilized during overnight hours when renewable energy resources and nuclear energy predominantly meet the electricity demand in Ontario.

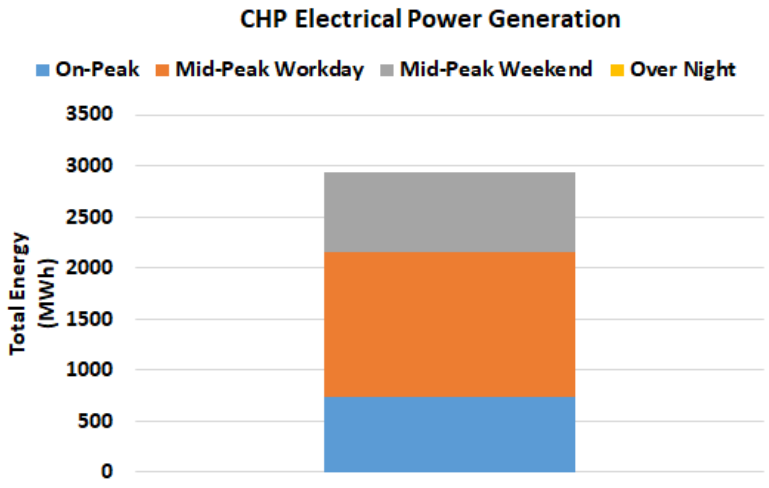

Figure 6.18: Distribution of Electricity Generation of CHP

6.3.6 Demand Response Without Affecting Occupant Comfort

The ICE-Harvest system's ability to implement demand response strategies while ensuring occupant comfort has been extensively discussed in Chapter 4. This capacity is further demonstrated in the long-term simulation of the system. As illustrated in Fig. 6.17, the system exclusively imports power during off-peak hours. Furthermore, Fig. 6.19 provides a specific example by comparing the imported electricity power of the ICE-Harvest system to the BAU scenario on the 24th of January. It is evident that, as previously explained, the ICE-Harvest system avoids importing electricity during peak hours, which differs from the BAU scenario. Instead, the CHP unit in the ICE-Harvest system effectively handles the electrical load during peak and mid-peak hours. The CHP unit operates at near-maximum capacity, starting at 7 am. Conversely, during off-peak hours, the ICE-Harvest system imports power from the grid to fulfill the electrical demand while the CHP unit remains inactive.

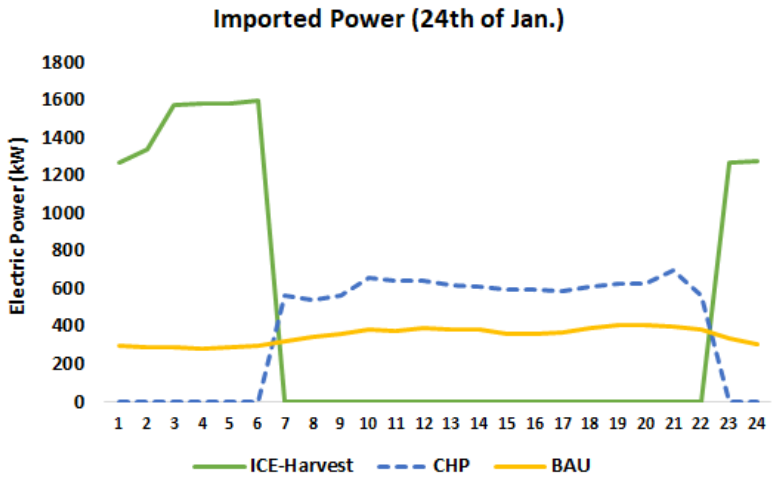

Figure 6.19: Imported Power and CHP Generation between ICE-Harvest and BAU

6.3.7 Simulation of Different Scenarios

Fig. 6.20 illustrates the range of network temperature variations across four distinct scenarios: No DRC and No DRH (NO DRCH), DRH only, DRC only, and both DRC and DRH (DRCH). It can be observed that, as expected, the presence of DRH in the system leads to higher network temperatures, resulting in a generally higher average temperature. Conversely, when DRC is feasible in the system, the network temperature tends to be lower. When both DRC and DRH are implemented in the system, the network temperature spans a broader range from $5°C$, which represents the cooling demand supply temperature for direct cooling, to $70°C$, which represents the required heating supply temperature for direct heating. On the other hand, this temperature profile difference between the scenarios results in different operation performances and costs. For example, Fig. 6.21 presents a representation of the CHP power generation at different electricity price ranges for each scenario. The overall performance of the CHP unit is similar for all scenarios, but it is also evident

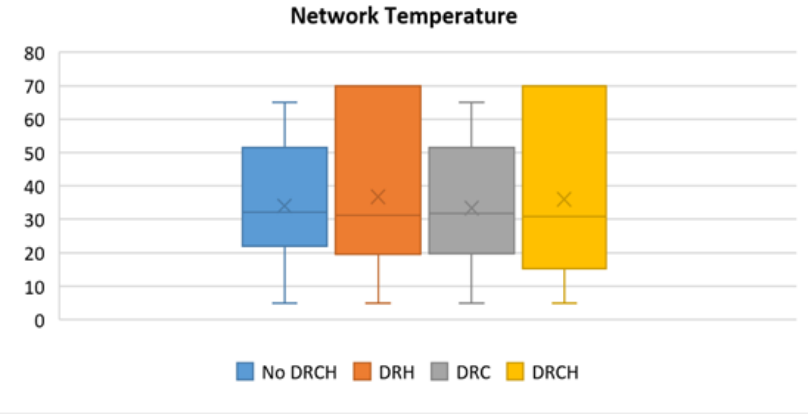

Figure 6.20: The Range of Network Temperature Variations Across the Scenarios

that the CHP unit does not run overnight when DRH is feasible (DRH and DRCH). The imported power from the grid under different scenarios is observed in Fig. 6.22 that the performance of all scenarios is similar. All of the scenarios do not import electricity during peak hours. However, when DRH is feasible (DRH and DRCH), the system imports less power during mid-peak hours.

6.4 Summary

This chapter presents the development of a comprehensive optimization framework for the long-term optimization of the ICE-Harvest system, specifically focusing on scheduling the geothermal borehole field (GBF) for optimal performance. The complete configuration of the ICE-Harvest system is considered, incorporating direct heating (DRH), direct cooling (DRC), and COP saturation. To address the optimization problem, a mixed-integer nonlinear program (MINLP) formulation is utilized and further linearized into a mixed-integer linear program (MILP) to capture crucial system behaviors. The long-term model serves as the long-term layer within the three-layer

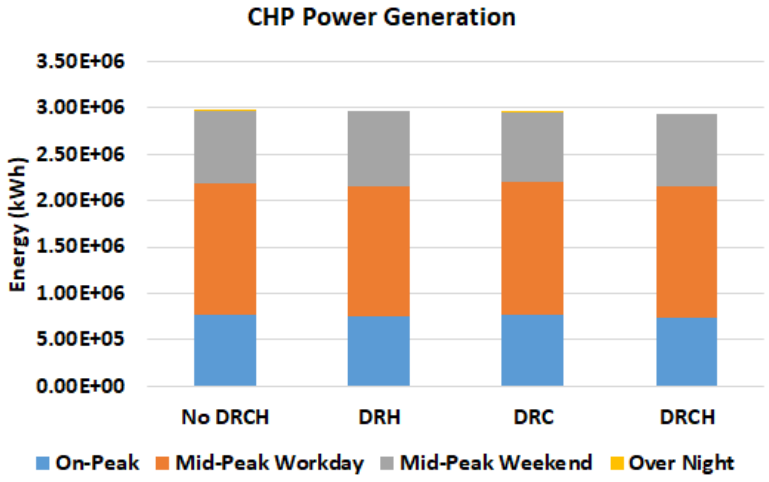

Figure 6.21: CHP Power Generation across Price Ranges and Scenarios

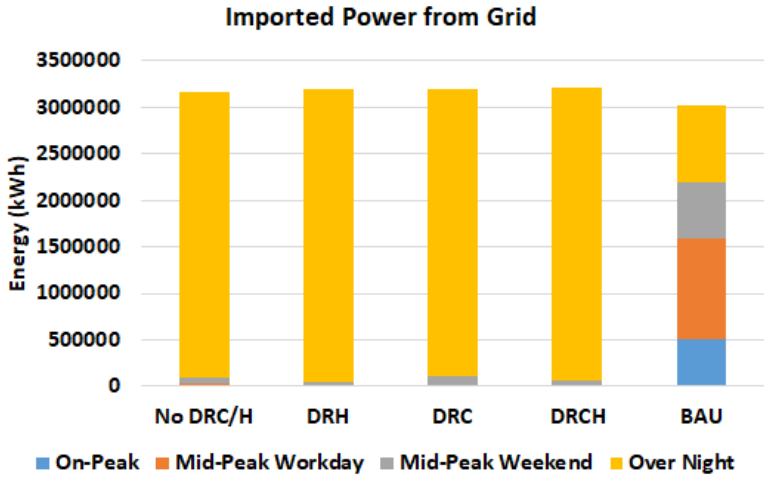

Figure 6.22: Imported Power Variation across Price Ranges and Scenarios

decision-making framework created for the energy management system of the ICE-Harvest. The simulation results demonstrate the effectiveness of the proposed strategy and offer valuable insights into optimizing the long-term operation of the system under DRH and DRC. The capabilities of the ICE-Harvest system, such as waste heat harvesting, demand response, and reducing reliance on fossil fuel power plants, are successfully demonstrated. Furthermore, the GBF displays seasonal charging and discharging patterns, discharging during winter until its state of charge (SOC) reaches zero and charging during summer until it reaches its maximum capacity.

Chapter 7

Conclusion and Future Work

7.1 Conclusion

The motivation behind this study stemmed from the pressing concerns of climate change and the need to decarbonize the energy sectors, particularly the building sector, which accounts for a significant portion of greenhouse gas emissions. This dissertation investigates the optimization and performance analysis of the Integrated Community Energy and Harvesting (ICE-Harvest) system. ICE-Harvest is designed to optimize energy utilization and promote sustainability in dense communities in cold climates. It comprises a single-pipe variable-temperature micro-thermal network, a micro-electrical network, and various distributed energy resources (DERs). The DERs, located in the energy generation center of the system, are combined heat and power (CHP) units, boilers, heat pumps, battery energy storage (BES), stratified hot water tank (SHWT), and a geothermal borehole field (GBF) as a long-term (seasonal) storage system. The objective of this research is to develop an optimal operation strategy for the system, considering the coordination of its components to realize its

full potential. Due to the specific configuration of the system with components that require short-term and long-term operation scheduling, a hierarchical decision-making framework is put forward in which three sequential layers are integrated. The three layers determine the long-term, short-term, and ultra-short-term optimal operation of the ICE-Harvest system. The layers are differentiated by their objective, planning horizon, time resolution, and optimization models.

For this aim, the study begins by formulating precise quasi-dynamic mathematical representations of the system, carefully considering the physical and operational limitations. These formulations capture the system's intricacies and serve as the foundation for optimization models.

In pursuit of this goal, the structure of the ICE-Harvest system is broken down into smaller pieces, and then the other parts of the system are gradually added to form the whole system. For this aim, at first, EGC, excluding the GBF and its correspondences, is directly connected to a building represented by electrical and thermal loads and equipped with water source heating and cooling HPs to form a building microgrid (BMG). A precise quasi-dynamic mathematical representation of BMG is developed considering physical and operational limitations, and the operation of the DERs together is studied.

Following that, an advanced version of the ICE-Harvest system is developed, incorporating single-pipe variable-temperature micro-thermal and micro-electrical networks. A detailed quasi-dynamic optimization model is introduced, considering electrical, thermal, and hydraulic constraints. To solve the resulting nonconvex mixed-integer nonlinear programming (MINLP) problem, a novel decomposition algorithm is proposed. It divides the problem into linear and nonlinear sub-problems, solved

successively. The linear sub-problem representing the short-term layer of the three-layer decision-making framework determines the binary variables, and the nonlinear sub-problem representing the ultra-short-term layer determines the optimal dispatch of the system. Additionally, to assess the significance and efficacy of detailed modeling in the optimization process, four other distinct mathematical models and dispatch strategies are created and extensively compared to the proposed dispatch strategy to evaluate the system's performance under each approach. Upon evaluating five dispatch strategies, it is enlightened that not considering thermal dynamics and heat transfer constraints will result in underestimating electricity and natural gas consumption. In contrast, if thermal pipeline capacity is not considered and mass flow and temperature are not manipulated, the system's capability will be underestimated.

Furthermore, a long-term optimization framework is developed for the ICE-Harvest system, specifically focusing on the geothermal borehole field (GBF). The problem is formulated as a mixed-integer nonlinear program (MINLP) and further linearized into a mixed-integer linear program (MILP) to capture essential system behaviors. This long-term model is represented as the long-term layer of the three-layer decision-making framework designed for the energy management system of the ICE-Harvest. Overall, the simulation results showcase the effectiveness of the proposed strategy and provide insights for optimizing long-term system operation. The capabilities of the ICE-Harvest system, including waste heat harvesting, demand response, and offsetting fossil fuel power plants, are demonstrated while emphasizing the importance of detailed modeling for accurate optimization and system evaluation. In addition, GBF exhibits seasonal charging and discharging patterns, discharging during winter until its state-of-charge (SOC) reaches zero and charging during summer until it reaches

maximum capacity.

In addition to operation optimization, a multi-objective approach is proposed for the optimal design of the ICE-Harvest system, focusing on component sizing. The resulting nonlinear optimization model is linearized, considering total annual cost (TAC) and greenhouse gas (GHG) emissions as criteria. Two approaches for assessing GHG emissions in energy systems are discussed: average emission factor (AEF) and marginal emission factor (MEF). AEF calculates emissions by dividing total CO2 emissions by total electricity generation, but it does not accurately reflect the effects of dispatchable demands on GHG emissions. MEF, on the other hand, tracks the marginal change in demand and provides a more accurate analysis of the actual emissions impact. The optimization process generates a Pareto front curve using the ϵ-constraint method, and a compromise solution is selected. The results demonstrate a trade-off between TAC and GHG emissions, with higher capital investment in CHP capacity associated with reduced emissions. The optimal configuration of the ICE-Harvest system involves the predominant involvement of CHP, SHWT, and BES. The study highlights the substantial amount of harvested energy (1072.409 MWh annually) that would otherwise be wasted in conventional district heating networks.

7.2 Future Work

The following areas are proposed as potential directions for future research:

- Integration of Renewable Energy Sources: Investigate the potential integration of additional renewable energy sources, such as solar photovoltaic (PV) systems or wind turbines, into the ICE-Harvest system. Assess the impact of these

sources on system performance, optimal operation strategies, and overall energy sustainability.

- Scalability and Replicability: Study the scalability and replicability of the ICE-Harvest system for different community sizes and geographical locations. Assess the system's performance and optimal design considerations when implemented in larger or smaller communities. Investigate the economic viability and potential barriers to widespread adoption of the ICE-Harvest system, considering factors such as initial investment costs, policy and regulatory frameworks, and stakeholder engagement.

- Life Cycle Assessment and Techno-Economic Analysis: Conduct a comprehensive life cycle assessment (LCA) and techno-economic analysis (TEA) of the ICE-Harvest system to evaluate its environmental impacts and economic feasibility. Consider the entire life cycle of the system, including manufacturing, installation, operation, and end-of-life considerations. Assess the system's overall sustainability, including its embodied energy, resource consumption, and potential for circular economy principles.

- Real-world Demonstration Projects: Collaborate with industry partners and local communities to implement real-world demonstration projects of the ICE-Harvest system. Monitor and evaluate the system's performance, energy savings, environmental benefits, and user satisfaction. Gather valuable feedback from stakeholders and occupants to further refine the system's design, operation strategies, and integration into existing energy infrastructure.

By addressing these future research directions, we can continue to advance the ICE-Harvest system, enhance its performance, and contribute to the transformation of the building sector towards more sustainable and energy-efficient communities.

Appendix A

Verificaiton Study

This appendix presents a comparative study that aims to compare and cross-validate the results obtained from ICE-Harvest system operation optimization in this study with an alternative modeling (control) approach. For this verification study, the results provided by the proposed optimization-based operation strategy are compared to the ICE-Harvest system simulated in Modelica software by [58].

Due to a lack of access to the actual Modelica simulation models, the comparison is limited to evaluating the ICE-Harvest system's performance in natural gas consumption and total electricity import using the data provided in [58]. It should be noted that operating the ICE-Harvest system with two different control strategies can lead to variations in primary energy consumption as it impacts how the system utilizes its energy resources, manages demand, and optimizes overall performance. This study uses an optimization approach that minimizes the cost to generate the system operation set points. In contrast, in [58], the set-points are pre-established and somehow fixed by prioritizing waste energy harvesting. Therefore, according to [58], it is expected that the electricity consumption to be greater than the proposed

optimization approach as there is no priority in the optimization approach other than minimizing the cost considered.

Fig. A.1 illustrates the electricity imported from the grid and total natural gas consumption of the ICE-Harvest system compared to the BAU. The natural gas consumption in the ICE-Harvest system includes two components: on-site natural gas consumption and the estimated natural gas consumed in natural gas-fueled power plants in the power system to meet the system's electricity demand. On-site Natural Gas Consumption refers to the total amount of natural gas consumed within the ICE-Harvest system's premises. It accounts for the energy used by the natural gas boiler (NGB) and the combined heat and power (CHP) units. The estimated natural gas consumed in the Natural Gas-Fueled Power Plants represents the quantity of natural gas required to produce the electricity supplied to the system. This component takes into account the energy losses, efficiency of power generation, and transmission losses associated with generating electricity from natural gas in power plants outside the ICE-Harvest system.

By considering both on-site and off-site natural gas usage, the assessment provides a more complete understanding of the system's overall reliance on natural gas and its implications for energy efficiency and environmental impact under different operation strategies. It is noteworthy that, based on the proposed optimization strategy, the ICE-Harvest system exhibits higher natural gas consumption but lower electricity consumption compared to the Modelica simulation. Furthermore, the figure presented below illustrates the imported electricity during peak hours. As anticipated, the optimization approach empowers the ICE-Harvest system to curtail its reliance on imported power during peak hours, effectively avoiding the higher electricity prices

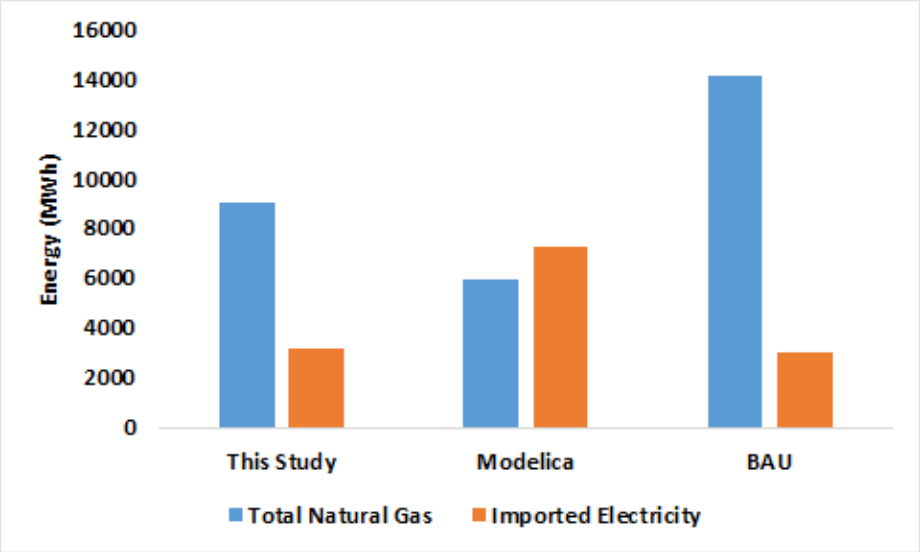

Figure A.1: Total Imported Electricity and Natural Gas of BAU Vs ICE-Harvest System

prevalent during that time period.

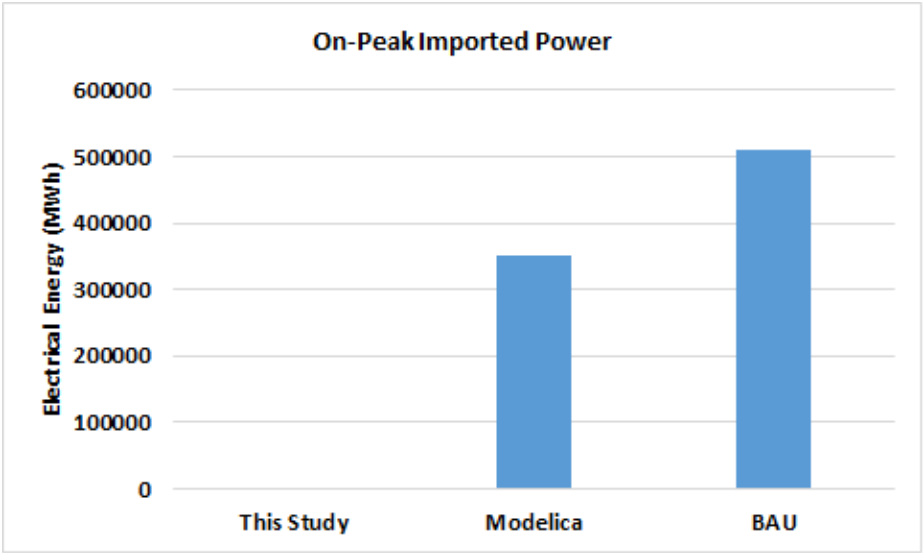

Figure A.2: On-Peak Imported Electricity by BAU Vs ICE-Harvest System

Bibliography

[1] IEA. Buildings. Available at urlhttp:// https://www.iea.org/reports/buildings (2022).

[2] Ardehali Lorestani and MM Ardehali. Optimal integration of renewable energy sources for autonomous tri-generation combined cooling, heating and power system based on evolutionary particle swarm optimization algorithm. *Energy*, 145:839–855, 2018.

[3] Mohamed Y. Abdelsalam, Kelton Friedrich, Saber Mohamed, Jorge Chebeir, Vickram Lakhian, Brendan Sullivan, Ahmed Abdalla, Jessica Van Ryn, Jeffrey Girard, Scott Lightstone, Marilyn F. Bucking, and James S. Cotton. Integrated community energy and harvesting systems: A climate action strategy for cold climates. Unpublished Manuscript, 2022.

[4] James Tetazoo. [independent electricity system operator. year-end data; 2017. Available at `https://www.ieso.ca/Corporate-IESO/Media/Year-End-Data/2017`.

[5] Ahmed Abdalla, Saber Mohamed, Friedrich Kelton, Scott Bucking, and James S Cotton. The impact of the thermal distribution network's operating temperature

and system design on different communities' energy profiles. *Sustainable Cities and Society*, page 104540, 2023.

[6] Akos Revesz, Phil Jones, Chris Dunham, Gareth Davies, Catarina Marques, Rodrigo Matabuena, Jim Scott, and Graeme Maidment. Developing novel 5th generation district energy networks. *Energy*, 201:117389, 2020.

[7] Henrik Lund, Poul Alberg Østergaard, Tore Bach Nielsen, Sven Werner, Jan Eric Thorsen, Oddgeir Gudmundsson, Ahmad Arabkoohsar, and Brian Vad Mathiesen. Perspectives on fourth and fifth generation district heating. *Energy*, 227:120520, 2021.

[8] B.V. Mathiesen, H. Lund, D. Connolly, H. Wenzel, P.A. Østergaard, B. Möller, S. Nielsen, I. Ridjan, P. Karnøe, K. Sperling, and F.K. Hvelplund. Smart energy systems for coherent 100% renewable energy and transport solutions. *Applied Energy*, 145:139–154, 2015.

[9] Thomas Lickleder er, Thomas Hamacher, Michael Kramer, and Vedran S Perić. Thermohydraulic model of smart thermal grids with bidirectional power flow between prosumers. *Energy*, 230:120825, 2021.

[10] McMaser Institute for Energy Studies. Ice harvest. Available at url-http://https://energy.mcmaster.ca/icepick/.

[11] Alireza Lorestani, Jorge Chebeir, Mehdi Narimani, and James S Cotton. Multi-objective optimization of integrated community energy and harvesting (ice-harvest) system based on marginal emission factor. In *2021 IEEE International Smart Cities Conference (ISC2)*, pages 1–7. IEEE, 2021.

[12] Energy Information Administration (EIA). Annual energy review. Available at https://www.eia.gov/totalenergy/data/annual/, 2021.

[13] Canada Energy Regulator. Canada's energy future data appendices. Available at https://doi.org/10.35002/zjr8-8x75, 2021.

[14] Dongfeng Yang, Yang Xu, Xiaojun Liu, Chao Jiang, Fanjie Nie, and Zixu Ran. Economic-emission dispatch problem in integrated electricity and heat system considering multi-energy demand response and carbon capture technologies. *Energy*, 253:124153, 2022.

[15] Ana Turk, Qiuwei Wu, Menglin Zhang, and Jacob Østergaard. Day-ahead stochastic scheduling of integrated multi-energy system for flexibility synergy and uncertainty balancing. *Energy*, 196:117130, 2020.

[16] Georgios Papaefthymiou, Bernhard Hasche, and Christian Nabe. Potential of heat pumps for demand side management and wind power integration in the german electricity market. *IEEE Trans. Sustain. Energy*, 3(4):636–642, 2012.

[17] Poul Alberg Østergaard and Anders N. Andersen. Booster heat pumps and central heat pumps in district heating. *Applied Energy*, 184:1374–1388, 2016.

[18] Xinyu Chen, Chongqing Kang, Mark O'Malley, Qing Xia, Jianhua Bai, Chun Liu, Rongfu Sun, Weizhou Wang, and Hui Li. Increasing the flexibility of combined heat and power for wind power integration in china: Modeling and implications. *IEEE Trans. Power Syst.*, 30(4):1848–1857, 2015.

[19] Yuanhang Dai, Lei Chen, Yong Min, Qun Chen, Junhong Hao, Kang Hu, and Fei Xu. Dispatch model for chp with pipeline and building thermal energy storage

considering heat transfer process. *IEEE Trans. Ind. Informatics*, 10(1):192–203, 2019.

[20] C. Shao, Y. Ding, J. Wang, and Y. Song. Modeling and integration of flexible demand in heat and electricity integrated energy system. *IEEE Trans. Sustain. Energy*, 9(1):361–370, 2018.

[21] Sayyed Faridoddin Afzali, James S Cotton, and Vladimir Mahalec. Urban community energy systems design under uncertainty for specified levels of carbon dioxide emissions. *Appl. Energy*, 259:114084, 2020.

[22] X. Lu, M.B. McElroy, W. Peng, S. Liu, C.P. Nielsen, and H. Wang. Challenges faced by china compared with the us in developing wind power. *Nat. Energy*, 1(6):16061, 2016.

[23] Mohammad Sameti and Fariborz Haghighat. Optimization of 4th generation distributed district heating system: Design and planning of combined heat and power. *Renew. Energy*, 130:371–387, 2019.

[24] Henrik Lund, Sven Werner, Robin Wiltshire, Svend Svendsen, Jan Eric Thorsen, Frede Hvelplund, and Brian Vad Mathiesen. 4th generation district heating (4GDH): Integrating smart thermal grids into future sustainable energy systems. *Energy*, 68:1–11, 2014.

[25] Guodong Liu, Tao Jiang, Thomas B Ollis, Xiaohu Zhang, and Kevin Tomsovic. Distributed energy management for community microgrids considering network operational constraints and building thermal dynamics. *Appl. Energy*, 239:83–95, 2019.

[26] Simone Buffa, Marco Cozzini, Matteo D'Antoni, Marco Baratieri, and Roberto Fedrizzi. 5th generation district heating and cooling systems: A review of existing cases in europe. *Renew. Sust. Energ. Rev.*, 104:504–522, 2019.

[27] Hongming Yang, Tonglin Xiong, Jing Qiu, Duo Qiu, and Zhao Yang Dong. Optimal operation of des/cchp based regional multi-energy prosumer with demand response. *Applied Energy*, 167:353–365, 2016.

[28] Pei Huang, Benedetta Copertaro, Xingxing Zhang, Jingchun Shen, Isabelle Löfgren, Mats Rönnelid, Jan Fahlen, Dan Andersson, and Mikael Svanfeldt. A review of data centers as prosumers in district energy systems: Renewable energy integration and waste heat reuse for district heating. *Applied Energy*, 258:114109, 2020.

[29] Lisa Brand, Alexandra Calvén, Jessica Englund, Henrik Landersjö, and Patrick Lauenburg. Smart district heating networks–a simulation study of prosumers' impact on technical parameters in distribution networks. *Appl. Energy*, 129:39–48, 2014.

[30] Hanne Kauko, Karoline Husevåg Kvalsvik, Daniel Rohde, Armin Hafner, and Natasa Nord. Dynamic modelling of local low-temperature heating grids: A case study for norway. *Energy*, 139:289–297, 2017.

[31] Haoran Li, Juan Hou, Tianzhen Hong, and Natasa Nord. Distinguish between the economic optimal and lowest distribution temperatures for heat-prosumer-based district heating systems with short-term thermal energy storage. *Energy*, 248:123601, 2022.

[32] Ryan Rogers, Vickram Lakhian, Marilyn Lightstone, and James S Cotton. Modeling of low temperature thermal networks using historical building data from district energy systems. In *Proceedings of the 13th International Modelica Conference, Regensburg, Germany, March 4–6, 2019*, number 157. Linköping University Electronic Press, 2019.

[33] Marwan Abugabbara, Saqib Javed, and Dennis Johansson. A simulation model for the design and analysis of district systems with simultaneous heating and cooling demands. *Energy*, 261:125245, 2022.

[34] Felix Bünning, Michael Wetter, Marcus Fuchs, and Dirk Müller. Bidirectional low temperature district energy systems with agent-based control: Performance comparison and operation optimization. *Appl. Energy*, 209:502–515, 2018.

[35] Ahmed Abdalla, Saber Mohamed, Scott Bucking, and James S Cotton. Modeling of thermal energy sharing in integrated energy communities with micro-thermal networks. *Energy Build.*, 248:111170, 2021.

[36] Marco Wirtz, Miguel Heleno, Hannah Romberg, Thomas Schreiber, and Dirk Müller. Multi-period design optimization for a 5th generation district heating and cooling network. *Energy and Buildings*, 284:112858, 2023.

[37] Justus von Rhein, Gregor P.Henzeb, Nicholas Long, and Yangyang Fu. Development of a topology analysis tool for fifth-generation district heating and cooling networks. *Energy Convers. Manag.*, 196:705–716, 2019.

[38] Ashreeta Prasanna, Viktor Dorer, and Nadège Vetterli. Optimisation of a district energy system with a low temperature network. *Appl. Energy*, 137:632–648, 2017.

[39] Marco Wirtz, Lukas Kivilip, Peter Remmen, and Dirk Müller. 5th generation district heating: A novel design approach based on mathematical optimization. *Appl. Energy*, 260:1–20, 2020.

[40] Paolo Gabrielli, Alberto Acquilino, Silvia Siri, Stefano Bracco, Giovanni Sansavini, and Marco Mazzotti. Optimization of low-carbon multi-energy systems with seasonal geothermal energy storage: The anergy grid of eth zurich. *Energy Conversion and Management: X*, 8:100052, 2020.

[41] Marco Wirtz, Lisa Neumaier, Peter Remmen, and Dirk Müller. Temperature control in 5th generation district heating and cooling networks: An milp-based operation optimization. *Appl. Energy*, 288:116608, 2021.

[42] Yichi Zhang, Pär Johansson, and Angela Sasic Kalagasidis. Feasibilities of utilizing thermal inertia of district heating networks to improve system flexibility. *Applied Thermal Engineering*, page 118813, 2022.

[43] Joshua Fitzpatrick, Alireza Lorestani, Jorge Chebeir, Mehdi Narimani, and James S Cotton. Multi-agent based control framework for an integrated community energy system. In *2022 IEEE International Smart Cities Conference (ISC2)*. IEEE, 2022. (in press).

[44] James Scott Cotton, Kelton Friedrich, Vick Lakhian, Saber Mohamed, Mohamed Yasser Abdelaslam, Jorge Chebeir, and Jeff Girard. Integrated community energy and harvesting system, October 21 2021. US Patent App. 17/301,907.

[45] Alireza Lorestani, Jorge Chebeir, Mehdi Narimani, and James S Cotton. Modeling and scheduling of an integrated thermal and electrical building microgrid.

In *2020 IEEE Power & Energy Society General Meeting (PESGM)*, pages 1–5. IEEE, 2020.

[46] Frank Kreith and Raj M Manglik. *Principles of heat transfer*. Cengage learning, 2016.

[47] Chenyu Wu, Wei Gu, Ping Jiang, Zhenyuan Li, Hongyi Cai, and Baoju Li. Combined economic dispatch considering the time-delay of district heating network and multi-regional indoor temperature control. *IEEE Trans. Sustain. Energy*, 9(1):118–127, 2018.

[48] M. Serna-Gonzáleza, J. M. Ponce-Ortegaa, and A. Jiménez-Gutiérrez. Minlp optimization of mechanical draft counter flow wet-cooling towers. *Chem. Eng. Res. Des*, 88:614–625, 2010.

[49] K.W. Li and A.P. Priddy. *Power Plant System Design*. John Wiley & Sons, New York, USA, 1 edition, 1985.

[50] M.H. Panjeshahi, A. Ataei, M. Gharaie, and R. Parand. Optimum design of cooling water systems for energy and water conservation. *Chem. Eng. Res. Des.*, 87(2):200–209, 2009.

[51] Eusiel Rubio-Castro, Medardo Serna-González, José María Ponce-Ortega, and Mahmoud M. El-Halwagi. Synthesis of cooling water systems with multiple cooling towers. *Appl. Therm. Eng.*, 50:957–974, 2013.

[52] Chenglin Zheng, Xi Chen, Lingyu Zhu, and Jiaqi Shi. Simultaneous design of pump network and cooling tower allocations for cooling water system synthesis. *Energy*, 150:653–669, 2018.

[53] Lingwen Gan, Na Li, Ufuk Topcu, and Steven H Low. Exact convex relaxation of optimal power flow in radial networks. *IEEE Transactions on Automatic Control*, 60(1):72–87, 2014.

[54] GAMS Development Corporation. *GAMS Documentation*. 2020.

[55] Mohit Tawarmalani and Nikolaos V Sahinidis. A polyhedral branch-and-cut approach to global optimization. *Mathematical programming*, 103(2):225–249, 2005.

[56] Wouter Schram, Ioannis Lampropoulos, Tarek AlSkaif, and Wilfried Van Sark. On the use of average versus marginal emission factors. In *SMARTGREENS 2019-Proceedings of the 8th International Conference on Smart Cities and Green ICT Systems*, pages 187–193. SciTePress, 2019.

[57] Vira Chankong and Yacov Y. Haimes. *Multiobjective decision making: theory and methodology*. Dover Publications, Inc., Mineola NY, 1 edition, 2008.

[58] Joshua Fitzpatrick. *Control of the ICE-Harvest System using an Advanced Multi-Agent Framework*. PhD thesis, 2022.